JIP1 REGULATES AXONAL TRANSPORT OF APP AND AUTOPHAGOSOMES VIA COORDINATION OF KINESIN AND DYNEIN MOTORS

Meng-meng Fu

A DISSERTATION

in

Neuroscience

Presented to the Faculties of the University of Pennsylvania

in

Partial Fulfillment of the Requirements for the

Degree of Doctor of Philosophy

2013

Supervisor of Dissertation

Signature _____
Erika L. F. Holzbaur
Professor of Physiology

Graduate Group Chairperson

Signature _____
Joshua Gold
Associate Professor of Neuroscience

Dissertation Committee:
Steven S. Scherer, Professor of Neurology
Dennis L. Kolson, Professor of Neurology
Virginia M.-Y. Lee, The John H. Ware 3rd Professor of Alzheimer's Research

JIP1 REGULATES AXONAL TRANSPORT OF

APP AND AUTOPHAGOSOMES

VIA COORDINATION OF KINESIN AND DYNEIN MOTORS

Meng-meng Fu

DEDICATION

This work is dedicated to my two grandmothers, who led very different lives from mine. Though they received little formal education, as were the norms for women at that time, their wisdom helped them to survive wars and famines and, perhaps most importantly, to raise my mother and father. Only as an adult have I realized the risks and hardships they endured to immigrate to a new country in order to give me the opportunities I have had. Perhaps as a result of my grandmothers' influence, my parents have raised me to be an independent and freethinking woman and continually encouraged my growth as a scientist.

ACKNOWLEDGMENT

First and foremost, I would like to thank my mentor, Dr. Erika Holzbaur, for her encouragement and support – in the best of times and in the worst of times. Erika is often my biggest cheerleader, but has also allowed me the opportunity to learn from my mistakes. She always has my best interests in mind and I know that she will continue to be my advocate in the years to come. Her unbridled enthusiasm and passion for science is contagious and constantly inspires our laboratory to explore new ideas and directions. In addition, I have had the privilege of getting to know her beautiful family (and little dog too!) and I hope that someday I will be as successful as she is both professionally and personally.

Next, I would like to thank the members of my thesis committee, Drs. Dennis Kolson, Virginia Lee, and Steve Scherer. Each of them has generously offered their time, expertise and invaluable and candid career advice. They are all formidable scientists (and clinicians) and inspire me to explore the overall implications of my research.

I would be remiss if I did not acknowledge past and current members of the Holzbaur Lab for making the lab a fun and collaborative place to work and for sharing lots of chocolate from around the world. In particular, Mariko Tokito, our lab manager, generated many of the constructs I used and taught me how to purify proteins. She is so fastidious in her experimental work that I often ask myself, particularly when learning a new protocol or technique, "What would Mariko do?" Dr. Eran Perlson taught me how to culture DRGs and Drs. Trey Schroeder and Adam

Hendricks taught me *in vitro* motility assays. Dr. Karen Wallace bred and maintained all mice used in my experiments. Every person in the lab has contributed in some way via helpful discussions and insightful comment throughout the progression of this project.

The laboratories of Drs. Carlos Dotti, Lawrence Holzman, Virginia Lee, Jacque Neefjes, Sarah Rice, Thomas Schwarz, and Kristen Verhey all provided constructs and their scientific generosity is appreciated.

Finally, my friends and family have kept me sane and provided countless hours of counsel and encouragement and I would not be who I am today without their support.

ABSTRACT

JIP1 REGULATES AXONAL TRANSPORT OF APP AND AUTOPHAGOSOMES VIA COORDINATION OF KINESIN AND DYNEIN MOTORS

Meng-meng Fu

Erika Holzbaur

Neurons are specialized cells that extend polarized processes called dendrites and axons in order to maintain synaptic connections over long distances. Consequently, neuronal homeostasis requires axonal transport of organelles, such as mitochondria, synaptic vesicles, and autophagosomes. The microtubule-based motors responsible for long-distance fast axonal transport are the anterograde kinesin motors and the retrograde dynein motors. Two cargos that exhibit robust axonal transport characterized by high speeds with few directional switches are APP- (amyloid precursor protein) positive vesicles and autophagosomes. While APP-positive vesicles transport occurs in both anterograde and retrograde directions, autophagosomes move unidirectionally in the retrograde direction. Here, we demonstrate that processive transport of both these cargos requires coordination of opposing motor activity by the scaffolding protein JIP1 (c-jun N-terminal kinase-interacting protein). We identify novel interactions between JIP1 and kinesin heavy chain (KHC), which are sufficient to relieve KHC autoinhibition and activate motor function in single molecule assays. In addition, the direct binding of the dynactin subunit $p150^{Glued}$ to JIP1 competitively inhibits KHC activation *in vitro* and disrupts the transport of APP in neurons. Together with coimmunoprecipitation results, these experiments support a model whereby JIP1 coordinates transport by switching between anterograde and retrograde motile complexes. Furthermore, we find that

mutations in the JNK-dependent phosphorylation site S421 in JIP1 alter both KHC activation *in vitro* and the directionality of APP and autophagosome transport in neurons. In knockdown and rescue experiments, the phosphomimetic JIP1-S421D promotes anterograde APP transport and disrupts retrograde autophagosome transport while the phosphodeficient JIP1-S421A promotes retrograde APP transport and rescues retrograde autophagosome transport. Thus, post-translational modification of a scaffolding protein can serve as a molecular switch that coordinates opposing motor activity in order to regulate the direction of vesicular transport of various organelles in the axon.

TABLE OF CONTENTS

LIST OF ILLUSTRATIONS

Figures in Chapter 2:

Figures in Chapter 3:

CHAPTER 1

Introduction

This chapter was written by Meng-meng Fu. Portions of this chapter will be adapted for an invited review for *Trends in Cell Biology*.

AXONAL TRANSPORT: A HISTORICAL PERSPECTIVE

More than a century ago, the 1906 Nobel Prize in Physiology or Medicine was jointly awarded to Camillo Golgi and Santiago Ramón y Cajal in recognition of their work on the structure of the nervous system. Though both these neuroanatomists used the silver impregnation method developed by Golgi to visualize neural tissues, they espoused very different views of how the nervous system functions. A proponent of reticular theory, Golgi believed that the nervous system consisted of a contiguous network of interconnected cells that function in a synchronous manner. On the other hand, Ramón y Cajal advanced the neuron theory, in which individual neurons function as autonomous entities. Moreover, he proposed that impulses in the nervous system travel from dendrites to the cell body and continue along the axon. Today, neuroscientists accept many tenets of the neuron theory as dogma, but definitive proof for the neuron theory did not arise until well after Ramón y Cajal's lifetime, when advances in electron microscopy (EM) in the 1950's allowed visualization of the synapse as a distinct space between neurons.

Ramón y Cajal also believed that the neuronal cell body or soma provided nutrition and support for dendrites and axons. As early as the 1850's, the British physiologist Augustus Volney Waller conducted nerve severing experiments in frogs and recorded distal nerve atrophy and nerve ending disintegration, stereotyped responses that are still known today as Wallerian degeneration. In 1909, Ramón y Cajal performed similar experiments on rabbit sciatic nerve and in addition to distal nerve atrophy, also observed accumulation of axoplasm at the cut site. He concluded from these experiments that the transfer of materials from the cell body is essential for axon survival (Reviewed in (Fishman, 2007).

Observations from the 1950's to 1960's fueled a debate over the nature of axonal transport – whether it was a slow process or a fast process. In 1948, in nerve constriction experiments in rats, Paul Weiss and Helen Hiscoe observed accumulations along the proximal nerve, which they called balloons and beads. Release of the constriction led to clearance of these nerve swellings with an estimated rate of 1-2 millimeters (mm) per day; thus, Weiss and Hiscoe posited that axoplasm moves via slow bulk flow, similarly to toothpaste that is squeezed through a tube (Weiss and Hiscoe, 1948). This predicted speed was consistent with isotope labeling experiments performed by Samuels and colleagues in 1951 demonstrating that ^{32}P injected in the spinal cord of guinea pigs appeared several days later in the sciatic nerve with an estimated rate of 3 mm/day (Samuels et al., 1951).

However, subsequent experiments suggested that axonal transport occurs much more quickly. In 1964, the Polish physiologist Liliana Lubinska and colleagues performed a series of elegant double transection experiments in dog sciatic nerve. At various time points of hours to days after nerve transection, the proximal stump, the isolated nerve segment, and the distal stump were all chopped into smaller pieces and analyzed for acetylcholinesterase (AChE) activity. They observed that AChE activity peaked at the most distal and proximal pieces of all three nerve segments just hours after transection, leading to two important conclusions – that AChE-containing particles move quickly along the axon with estimated speed of ~200 mm/day and that they move in both anterograde and retrograde directions (Lubinska et al., 1964). Nevertheless, the prevailing opinion favored slow transport and Lubinska's data was not readily accepted and hotly debated (Dahlstrom, 2010)

Several years later, Jirina Zelena, in collaboration with Lubinska, identified using light and electron microscopy that the transported material in these nerve transection experiments also includes organelles, such as mitochondria and ribosomes (Zelena, 1970; Zelena et al., 1968). Moreover, in 1967, Raymond Lasek repeated the Samuels experiment, but rather than evaluating at time points of days and weeks, he observed just hours after isotope injection, movement of materials with estimated speeds of several hundred millimeters per day (Lasek, 1967).

The following decades brought acceptance of the coexistence of both slow and fast axonal transport and a classification system that is still used today. Lasek and colleagues assessed accumulation of injected isotopes in guinea pigs at both short (3 hours) and long (15 days) time periods post-injection. This allowed delineation of fast component (FC) transport at speeds of ~300-400 mm/day (~3-4 μm/s) from slow transport, which was subdivided into slow component a (SCa), with speeds of 0.3 to 1.0 mm/day (~0.003-0.01 μm/s), and slow component b (SCb), with speeds of 2 to 4 mm/day (~0.02-0.04 μm/s). Cytoplasmic proteins identified as slow transport cargos include tubulin and neurofilaments in SCa and actin and clathrin in SCb (Tytell et al., 1981).

Whereas *in vivo* radiolabelling allows bulk protein transport to be measured, advances in fluorescent microscopy as well as primary neuron cultures in the late 1990's allowed selective labeling of vesicular cargos using fluorescently tagged proteins, such as green fluorescent protein (GFP). Primary neurons in culture expressing GFP-tagged endosomal markers, such as TrkA, or synaptic vesicle markers, such as SNAP-25, exhibited fast axonal transport with speeds ~1-2 μm/s

(Nakata et al., 1998). More recently, expression in primary neurons of classical cytosolic slow transport proteins, such as synapsin, tagged with photoactivatable GFP (PAGFP), has been used to measure slow transport. Long-term imaging of PAGFP-synapsin localization showed an anterograde directional bias with calculated drift speeds of ~0.008-0.01 μm/s (Scott et al., 2011), consistent with earlier *in vivo* radiolabeling SCa speeds. Though the specific mechanisms of slow transport remain unclear, the current view accepts both slow and fast transport occurrence in the axon.

MICROTUBULE TRACKS

Long-range fast axonal transport is dependent on the microtubule cytoskeleton. Experiments performed in the late 1960's demonstrated that injection of the microtubule depolymerizing drug colchicine disrupted accumulation of AChE in a dose-dependent manner (Kreutzberg, 1969). In addition to axonal transport, microtubules also have other important functions in eukaryotic cells, such as maintenance of cell shape as well as regulatory roles in cell division.

Structurally, microtubules exist as hollow tubes that are about 25 nanometers (nm) in diameter and formed from 13 radially arranged protofilaments. Each protofilament is composed of polymerized α- and β-tubulin heterodimers that are aligned in a head-to-tail manner; in other words, α and β monomers alternate longitudinally along a single protofilament. This orientation of α- and β-tubulin determines the polarity of the microtubule, with α-tubulin facing the stable minus end and β-tubulin facing the dynamic plus end.

In addition to the longitudinal contacts, lateral contacts between neighboring protofilaments sustain the cylindrical structure of microtubules. Usually, these lateral interactions occur between one α-tubulin with another adjacent α-tubulin or one β-tubulin with another β-tubulin. This lateral alignment of tubulin monomers follows a left-handed helical shape with an inclination angle ~13-15°. However, on each microtubule, along a single longitudinal interface between two juxtaposed protofilaments is a helical discontinuity or "seam" formed via lateral interactions of adjoining α-tubulins with β-tubulins (Mandelkow et al., 1986).

In vitro, microtubule polymerization is characterized by an early slow lag phase in growth. Cells have evolved specialized nucleation sites called microtubule-organizing centers (MTOCs) to overcome this slow growth phase. MTOCs are composed of γ-tubulin, a homologue of α- and β-tubulin, and γ-tubulin complex proteins (GCPs), which collectively form a nucleating complex with a classic ring structure. In animal cells, the MTOC is the centrosome, a perinuclear structure composed of two centrioles, from which a polarized microtubule array emanates (Kollman et al., 2011). Interestingly, plants are acentrosomal and nucleation is thought to occur off of pre-existing microtubules (Wasteneys and Ambrose, 2009).

Microtubules alternate between periods of slow growth and rapid shrinking or catastrophe; this molecular phenomenon is known as dynamic instability. Each monomer of tubulin contains a guanine nucleotide binding site, but only the site on β-tubulin is exchangeable as α-tubulin remains in the guanosine triphosphate (GTP) bound state. Soluble tubulin heterodimers are typically GTP-bound; however, polymerization onto the plus-end of the microtubule allows the GTP on β-tubulin to be hydrolyzed to guanosine diphosphate (GDP). In the GDP-bound state, tubulin heterodimers are more likely to dissociate from the microtubule lattice, thus leading to shrinking of the microtubule, or catastrophe. Recent high-resolution images acquired via atomic force microscopy (AFM) indicate that this is likely due to increased curvature of the GDP-bound protofilaments, which are predicted to lead to unraveling of the microtubule lattice (Elie-Caille et al., 2007). In contrast, tubulin heterodimers that remain GTP-bound are more stable and resist depolymerization (Howard and Hyman, 2009).

Microtubule Organization in Neurons

After decades of research, the cytoskeletal architecture of neurons is still a mystery. Classic EM experiments predicted that microtubules in the axon have lengths exceeding 100 μm (Bray and Bunge, 1981; Letourneau, 1982). However, caveats of these experiments must be considered when interpreting the results. One experiment counted the number of microtubule "starts" and "stop" in serial transverse sections of axons in a nerve bundle, but had limited total observational length of ~13 μm and average thickness of ~67 nm per slice (Bray and Bunge, 1981). Another experiment using detergent-extracted neurons noted that microtubules were bundled, thus obscuring estimations of microtubule length (Letourneau, 1982).

Microtubules have regionally distinct organization in the neuron. Early determination of microtubule polarity used the "hooking" technique, in which tubulin polymerization in the presence of a special buffer proceeds via addition of protofilament sheets onto the surface of pre-existing microtubules. In cross-sectional EM, microtubule plus ends appear as clockwise hooks or barbs while minus ends appear as counterclockwise hooks. In the axon, microtubules are uniformly oriented with >90-95% of plus ends directed away from the soma; in dendrites, microtubules have mixed polarity with ~55% of plus ends directed away from the soma (Baas et al., 1988; Burton and Paige, 1981). Subsequently, the popularization of fluorescently tagged plus-end microtubule-binding proteins, such as EB1 or EB3, as indicators of microtubule polarity in cells confirmed the hooking results for dendritic and axonal microtubule polarity in live-cell imaging experiments (Stepanova et al., 2003).

Recent experiments indicate that nucleation of axonal microtubules do not require centrosomes. Laser ablation of the centrosome in primary hippocampal neurons does not deter axon extension, suggesting that acentrosomal microtubule nucleation occurs in the axon (Stiess et al., 2010). Another study showed that in dendrites of *Drosophila* neurons, Golgi outposts serve as sites of acentrosomal microtubule nucleation in a γ-tubulin-dependent manner (Ori-McKenney et al., 2012). However, acentrosomal microtubule nucleation has not been demonstrated in axons though this is a likely possibility.

THE KINESIN FAMILY OF ANTEROGRADE MOTORS

By the 1980's, fast axonal transport was attributed to organelle movement, which could be observed in the extruded axoplasm of giant squid axons (Gilbert et al., 1985; Vale et al., 1985c). Electron micrographs gave the first indication that vesicular axonal transport is likely driven by "crossbridging filaments", or motor proteins that bind to microtubules (Gilbert et al., 1985). The observation that organelle movement depends on ATP led to the hypothesis that motor proteins are ATPases (Vale et al., 1985d). Shortly thereafter, kinesin was purified from giant squid axoplasm and bovine brain and confirmed as the motor protein, or "translocator" that is responsible of organelle movement (Vale et al., 1985a). In the years following this initial discovery, multiple kinesin genes were cloned from various eukaryotic organisms.

The current count of murine or human kinesins is 45 (Hirokawa and Takemura, 2005); these kinesins have been categorized into 14 subfamilies following a commonly accepted nomenclature system (Lawrence et al., 2004). For the kinesin neophyte, this nomenclature is very confusing and numberings across individual kinesin genes/proteins and families often conflict with each other. For example, "conventional kinesin", or Kinesin-1, was the first identified kinesin and includes KIF5A, KIF5B and KIF5C. This is not to be confused with KIF1, which is a member of the Kinesin-3 family, which also includes KIF13.

Kinesins can be further classified as N-kinesins, M-kinesins, C-kinesins, which refers to the locations of their motor domains (N-terminus, middle, or C-terminus, respectively). Remarkably, the position of kinesin motor domains correlates with

their directional bias toward either plus-ends or minus-ends of microtubules. The majority of kinesins have N-terminal domains, move toward the plus-ends of microtubules and play a role in anterograde intracellular trafficking. C-kinesins, such as Kinesin-14, move toward the minus-end of microtubules and play a role in spindle pole alignment during mitosis. M-kinesins include the Kinesin-13 family, which is also known as mitotic centromere-associated kinesin (MCAK), and depolymerizes microtubules (Hirokawa and Takemura, 2005).

The majority of kinesins form homodimers, though Kinesin-2's (KIF3A and KIF3B) heterodimerize. Dimerization underlies the stepping mechanism of kinesin, with each motor domain responsible for a step. For example, Kinesin-3 was historically thought to be a monomer that displays diffusive movement (Okada et al., 1995), but was subsequently shown to be motile as a dimer (Klopfenstein et al., 2002). The elegant geometry of the microtubule structure is intricately connected to the motor properties of kinesins. Each monomer of α- and β-tubulin has a longitudinal length of 4 nm; kinesins have a uniform step size of 8 nm, which corresponds to alternate binding of each motor domain with each successive β-tubulin. Moreover, each longitudinal protofilament forms a straight track and kinesins step along a single protofilament, which effectively restricts its motility to one face of the microtubule.

Single molecule experiments demonstrate that kinesins exhibit high speeds and high stall forces *in vitro*. Kinesins from different families do not have uniform speed *in vitro* and these values range from ~0.15–0.8 μm/s. Kinesin speed directly correlates with the rate of ATPase hydrolysis, as each step corresponds one ATP hydrolysis event (Friel and Howard, 2012). Single molecule kinesins have stall forces ~5–7 pN (Twelvetrees et al., 2012), meaning that they are particularly efficient at organelle

transport. These measurements indicate that one kinesin motor may be sufficient to generate high forces and efficiently tow cargos and indeed only 1–2 kinesins are estimated to be associated to a single endosome or lysosome (Hendricks et al., 2010).

Multiple families of kinesins play a role in axonal transport of diverse cargos. Of the conventional Kinesin-1 family, KIF5B is ubiquitously expressed, but KIF5A and KIF5C are upregulated in neurons (Kanai et al., 2000). Kinesin-1 transports mitochondria, endosomes, lysosomes, RNA granules, APP-positive vesicles, and synaptic vesicles, including those containing AMPA receptors and GABA receptors. Kinesin-2 transports lysosomes and synaptic vesicles containing NMDA receptors. Kinesin-3 also plays a role in transporting mitochondria and synaptic vesicles, including those containing NMDA receptors (Hirokawa et al., 2010). Though various kinesins may cooperate to transport a single cargo, this idea has not been extensively explored for axonal transport.

The specific interplay between kinesins and cargos relies on adaptor proteins or scaffolding proteins, which serve as links between vesicular proteins and motors. I will discussed their relationships and regulatory schemes in a later section. One exception, however, is Kinesin-3, which contains a C-terminal pleckstrin homology (PH) domain that underlies its ability to specifically associate with phospholipids. Experiments with *C. elegans* KIF1A shows that its PH domain preferentially associates with liposomes containing phosphatidylinositol(4,5)bisphosphate (PIP2) or cholesterol/sphingomyelin in a concentration-dependent manner (Klopfenstein et al., 2002).

Kinesin Autoinhibition

In the cell, kinesin that is not associated with cargo does not display motor activity or is autoinhibited; cargo association to KHC relieves this autoinhibition and activates motor activity. Kinesin autoinhibition likely has two essential cellular functions – to prevent the unnecessary crowding of kinesins on the microtubule (i.e. traffic jams) and to prevent wasteful hydrolysis of ATP in the absence of cargo association (Verhey and Hammond, 2009).

The non-motor regions of kinesin play an important role in regulating motor ATPase activity. For Kinesin-1, commonly referred to as KHC, the N-terminal motor domain precedes a neck linker region important in coordinating motor activity of the two heads, a flexible hinge or stalk region, and a C-terminal tail. In early micrographs of KHC, the tail appeared to fold back onto the motor head via bending of the stalk (Hirokawa et al., 1989). Subsequent *in vitro* motility experiments determined that full-length KHC has little motor activity, whereas a constitutively active KHC containing only the motor head and neck linker region (AA 1-560) displayed tenfold higher run frequency. Deletions of either the "hinge 2" stalk region or the tail region resulted in KHCs that also displayed robust motility, leading to the conclusion that both the stalk and tail are pivotal for the autoinhibition of soluble KHC motor activity (Friedman and Vale, 1999).

The biochemistry underlying the autoinhibitory binding between KHC tail and head is well characterized. A highly basic region of KHC tail containing a conserved basic IAK motif is sufficient to confer head binding (Stock et al., 1999). Full length KHC containing the IAK motif has 140-fold inhibition of ATPase activity compared to

truncated KHC head (Hackney and Stock, 2000) and this led to the initial suggestion that KHC tail may bind directly to the ATPase domain of KHC head (Dietrich et al., 2008). However, subsequent experiments demonstrated that one KHC tail is sufficient to autoinhibit the KHC head dimer (Hackney et al., 2009) and this predicted 1:2 stoichiometry of tail:head was validated by the 2.2-Angstrom crystal structure of KHC head with the a 16-AA peptide containing the IAK motif, which elegantly demonstrated that the KHC tail peptide binds to the cleft between the two motor heads where it likely prevents ADP release by restricting the movement of the motor domains (Kaan et al., 2011).

This "double lockdown" model has the important cellular implication that relief of KHC autoinhibition must prevent both KHC tails from binding to KHC head. Indeed, organelle-associated scaffolding proteins that are able to activate KHC motility *in vitro* via stalk and/or tail binding can exist as dimers (Fu and Holzbaur, 2013; Sun et al., 2011).

The majority of soluble KHC is thought to exist in an inactive state where it binds to kinesin light chain (KLC) in a heterotetrameric complex. KLC binds to a region from AA 682–810 encompassing the stalk and tail of KHC (Verhey et al., 1998). Experiments with full-length KHC and full-length KLC demonstrate that tetrameric KHC/KLC is autoinhibited. In fact, addition of full-length KLC to KHC leads to ~30% decrease in run frequency and velocity and ~60% decrease in run length (Friedman and Vale, 1999). Moreover, full-length KHC/KLC heterotetramers have decreased microtubule-binding ability compared to KHC homodimers (Verhey et al., 1998). Thus, the function of KLC may be to keep soluble KHC in an inactive state.

In contrast, a subsequent paper advanced the opposing idea that KLC binding to KHC relieves autoinhibition; however, these *in vitro* experiments used truncated proteins instead of full-length ones and interpretation of the results may have additional caveats. A key experiment in this paper showed that addition of KHC tail (AA 790–975) decreased KHC head ATPase activity in a concentration dependent manner, consist with previous work on the mechanism of autoinhibition. However, addition of KLC to this system resulted in increased KHC head ATPase activity (Wong et al., 2009), suggesting that KLC decreases the autoinhibitory ability of KHC tail. An alternative interpretation is that addition of a third protein, KLC, to the system altered binding kinetic and decreased the amount of KHC tail that was available for binding to KHC head.

Classic sucrose density gradient centrifugation of brain-derived kinesin shows that three separate pools of KLC and KHC exist – a low-density pool containing only KLC, a high-density pool containing KHC and KLC, and a higher-density pool containing KHC alone (Hackney et al., 1992). Consistent with this result, recent experiments also found that KHC can exist in the absence of KLC in high-density sucrose gradient fractions (Sun et al., 2011). Indeed, these observations support the idea that activated KHC that is bound to cargo-associated scaffolding protiens may exist independently of KLC.

Interestingly, KLC has been suggested to act as an adaptor protein as well. Phosphorylation of KLC facilitates anterograde transport of the cargo calsyntenin and a phosphodeficient KLC is unable to sustain robust anterograde calsyntenin transport (Vagnoni et al., 2011). It is unclear whether KLC directly associates with calsyntenin or whether another scaffolding protein may mediate the interaction between KLC and

calsyntenin. Moreover, phosphorylation of KLC may alter the accessibility of KHC to access scaffolding proteins that would relieve its autoinhibition. Nevertheless, phosphorylation of KLC likely underlies its ability to associate with cargos.

Thus, I suggest a model for KLC to function as a clamp that facilitates autoinhibition of KHC in the soluble heterotetrameric kinesin complex. Consistent with pools of KLC in the absence of KHC (Hackney et al., 1992), concentrations of soluble KLC likely exceed those of soluble KHC to ensure the fidelity of autoinhibition. Phosphorylation of KLC may be a priming step for relieving KHC autoinhibition via binding to scaffolding proteins. Finally, once associated with cargos, KHC homodimers may not require KLC association when directly activated by scaffolding proteins.

THE RETROGRADE MOTOR CYTOPLAMSIC DYNEIN

In the same year that kinesin was identified, the same group of researchers observed that a different protein was responsible for generating motion toward the microtubule minus-end (Vale et al., 1985b). We now know that this motor is cytoplasmic dynein, which is distinct from axonemal dynein that is necessary for ciliary and flagellar movement.

In contrast to the plethora of kinesins, cytoplasmic dynein is the only minus-end directed microtubule motor and is responsible for retrograde axonal transport. In contrast to kinesins, which achieve functional diversity through many different motors, dynein achieves functional diversity through its many binding partners. Indeed, dynein itself refers to an enormous ~1.5 megadalton (MDa) complex of proteins that includes two motor dynein heavy chains (DHC; ~500 kDa each), two dynein intermediate chain (DIC; ~74 kDa each), two light intermediate chains (DLIC; ~33–59 kDa), and several dimers of light chains (DLC also known as LC7/roadblock, LC8, and TcTex1; ~10–14 kDa). In each dynein complex, a dimer of two DHCs bind to two DLICs and two DICs; DLCs bind to DICs.

The DHC motor is a member of the AAA family of ATPases, which contain hexamers of ATPase domains that assemble into a large ring-like protein. The dynein ring structure is asymmetric, with a 10-nm antiparallel coiled-coil stalk domain extending out from AAA4. The end of this stalk contains the microtubule binding region of DHC, which is effectively distant from the site of ATP hydrolysis. The recently solved 6-Angstrom structure of yeast DHC reveals that a buttress between AAA5 and AA6

conducts conformational changes during the ATPase hydrolysis to the stalk domain (Carter et al., 2011).

Single molecule studies show that dynein is weak motor with ~1pN stall force and variable step size of 8–24 nm. Unlike kinesin, it can sidestep or move laterally onto adjacent protofilaments. Interestingly, the *in vitro* behavior of mammalian dynein greatly differs from that of yeast dynein; whereas yeast dynein is robustly minus-end directed, mammalian dynein moves bidirectionally in a back-and-forth manner both toward the minus and plus ends (Ross et al., 2006).

Dynein Activators

Early experiments with purified dynein noted that the motor bound to microtubules, but failed to move. Sedimentation and ion exchange chromatography experiments determined that certain purified components could activate dynein and increase motility (Schroer and Sheetz, 1991). This activating factor was identified to be the large complex of proteins known as dynactin. The first subunit of dynactin cloned was $p150^{Glued}$, which was named for its size (~150 kDa) and its homology to the *Drosophila* Glued gene (Holzbaur et al., 1991), which when mutated leads to defects in retinal organization and retinal projection to the optic tectum. A subsequent paper also cloned $p150^{Glued}$, but sequencing missed the first ~200 amino acids (AA) that is homologous to *Drosophila* Glued and so it was independently named dynactin, for dynein activator (Gill et al., 1991). Current convention uses the term dynactin to denote the complex of proteins whereas the term $p150^{Glued}$ denotes one protein in the dynactin complex.

Dynactin is a large ~1-MDa complex of proteins that has two structural components – a ~ 10-nm x 40-nm rod and a ~25–50-nm projecting arm. The rod is composed of polymers of actin-related protein 1 (Arp1) as well as Arp11, conventional actin-capping protein (CapZ), p62, p27, and p25. The projecting arm of dynactin consists of the N-terminus of the $p150^{Glued}$ dimer, which is connected to the rod via its C-terminus and supported by p50 dynamitin and p24 (Schroer, 2004). Dynactin associates with dynein via binding between the first coiled coil (CC1) domain of $p150^{Glued}$ and DIC (Karki and Holzbaur, 1995).

The $p150^{Glued}$ subunit of dynactin contains several distinct domains. At the N-terminus is the microtubule-binding CAP-Gly domain (AA 1-110), followed by the CC1 domain (AA 217-548) that binds to DIC. Toward the C-terminus, is another coiled coil domain (CC2, AA 926-1049), which connects to the dynactin complex via binding to Arp1 (Waterman-Storer et al., 1995). At the extreme C-terminus of $p150^{Glued}$ is a cargo-binding domain (~AA 1049-1278) that binds to various vesicular adaptors, such as Rab7-interacting lysosomal protein (RILP(Johansson et al., 2007)), huntingtin-associated protein 1 (HAP1(Engelender et al., 1997)), the retromer sortin nexin 6 (SNX6(Hong et al., 2009; Wassmer et al., 2009)), and JIP1 (Fu and Holzbaur, 2013).

In the cell, dynein also associates with various other activator complexes, including Bicaudal D (BicD) as well as the complexes of lissencephaly 1 (Lis1) and nuclear distribution protein E (NudE) or NudE-like (NudEL). Rather than individually associating with dynein, these activators can act in concert with each other for efficient retrograde transport.

REGULATION OF TRANSPORT

Regulation of axonal transport can occur at three levels – at the level of the microtubule tracks, at the level of kinesin or dynein motors, or at the level of adaptors or scaffolding proteins that mediate the association of motors to cargos. Microtubules can undergo post-translational modifications, such as acetylation and tyrosination, which can aid or hinder motor processivity. Both kinesin and dynein motors can directly undergo site-specific phosphorylation, which has been suggested to alter motor processivity. Finally, at the cargo level, scaffolding proteins and adaptor complexes, which are a diverse class of motor-associated proteins, can be regulated via various post-translational modifications, calcium binding, and proteolysis.

Microtubule Modifications and Microtubule Associated Proteins

Various proteins are capable of associating with specific regions along the microtubule. These include plus-end binding proteins, minus-end binding proteins, and other microtubule-associated proteins (MAPs) that bind along the length of the microtubule. Moreover, α- or β-tubulin can undergo post-translational modifications, such as acetylation, glutamylation, amination, and tyrosination. Interestingly, many of these modifications occur on the last amino acids of C-terminal tubulin, which are exposed on the surface of the polymerized microtubule where they are thought to alter interaction with motors, and other microtubule interacting proteins (Janke and Bulinski, 2011).

Quick-freeze, deep-etch electron microscopy first showed that microtubules in neurites are crosslinked by filamentous structures, which were later identified to be MAPs. In neurons, MAP association has been implicated in the spatial distribution of microtubules. MAP2 binds to dendritic microtubules, which have spatial resolution of ~20 nm while tau binds to axonal microtubules, which are spaced ~65 nm. Little is known about how this difference in microtubule spacing might affect transport though high-resolution imaging has shown that cargos can switch tracks in the axon.

In particular, the effect of tau has distinct effects on single molecule motor processivity. *In vitro* motility experiments show that when motors encounter patches of tau on microtubules, kinesin tends to detach whereas dynein tends to switch directions. Moreover, kinesin inhibition occurs at about one tenth the concentration of tau that inhibited dynein. This selective sensitivity of kinesin led to the proposal of that tau forms a gradient in the axon with high distal concentrations to facilitate dissociation of kinesin without affecting dynein binding (Dixit et al., 2008). Moreover, tau patches on microtubules also affect *in vitro* cargo-associated kinesins that function in tandem (Vershinin et al., 2007).

Direct Regulation of Kinesin and Dynein

Post-translational modification of kinesin has been suggested as a mechanism for regulation of axonal transport. In spinal and bulbar muscular atrophy, the polyglutamine region of androgen receptor (PolyQ-AR) is expanded. Overexpression of PolyQ-AR in cells reduces KHC binding to microtubules and increases KHC phosphorylation. Moreover, addition of PolyQ-AR peptides to extruded giant squid axoplasm decreases anterograde movement of particles on the timescale of 20–50

minutes. These effects from PolyQ-AR addition are thought to be mediated via activation of JNK (c-jun N-terminal kinase), which was demonstrated to phosphorylate KHC motor head *in vitro* (Morfini et al., 2006). A follow-up paper suggested that the pathogenic polyglutamine repeat expansion in huntingtin protein (PolyQ-Htt) also leads to aberrant activation of the neuronal specific JNK3, which phosphorylates KHC. *In vitro* phosphorylation assays of KHC head with recombinant JNK and subsequent mass spectrometry analysis identified the S176 phosphorylation site (Morfini et al., 2009).

These findings are controversial for several reasons. Huntingtin is a known scaffolding protein that interacts with both anterograde and retrograde motors (Caviston et al., 2007; Engelender et al., 1997; McGuire et al., 2006), yet these authors show that huntingtin in brain homogenates does not bind to KHC, KLC, DIC, or DHC. Moreover, *in vitro* phosphorylation assays are likely to identify nonphysiological targets; an alternative approach is to add recombinant JNK to a cell lysate or brain homogenate and then look for phosphorylated KHC. Finally, though giant squid axoplasm assays were pivotal in the identification of kinesin and cytoplasmic dynein nearly thirty years ago, they are no longer state-of-the-art; transport measures essentially track the decay of directed movement of unidentified organelles or particles over timescales of up to an hour or more with no subsequent statistical analyses. However, this does not mean that the KHC-S176 phosphorylation site is irrelevant; rather, *in vitro* motility assays need to be performed to determine its effect on KHC motor activity and more precise experiments need to determine its physiological relevance.

Recently, phosphorylation of DIC has been implicated in the trafficking of signaling

endosomes in the neuron. Trafficking of growth factors such as neurotrophic growth factor (NGF) or brain-derived neurotrophic factor (BDNF) from the distal axon back to the soma proceeds via the endosomal pathway, maturing from Rab5-positive early endosomes to Rab7-positive late endosomes (Deinhardt et al., 2006). One downstream effector of the NGF receptor TrkB is extracellular signal-regulated kinase (ERK1/2). NGF binding to TrkB receptors is thought to trigger downstream via ERK1/2, which may directly phosphorylate DIC at the S80 site to efficiently recruit dyneins for the retrograde transport of signaling endosomes (Mitchell et al., 2012). Clarification of how phosphorylation of DIC at S80 enhances dynein recruitment is an important next step in solidifying this model.

SCAFFOLDING PROTEINS COORDINATE MOTOR ACTIVITY

Multiple models of transport regulations have sought to explain the determination of direction of microtubule-based transport from a molecular level (Gross, 2004; Welte, 2004). In one model, only anterograde or retrograde motors can bind to a cargo at any given time. However, this unlikely as both *in vitro* and cellular studies suggest that opposing motors can bind simultaneously to cargos (Encalada et al., 2011; Hendricks et al., 2010; Maday et al., 2012; Soppina et al., 2009). Cargo-associated motors may not all be active at the same time though. Indeed, autophagosomes associate with both kinesins and dyneins yet undergo robust unidirectional retrograde axonal transport (Maday et al., 2012). Though it is unclear why opposing motors are found on the same cargo, it is possible that by avoiding the additional step of recruiting motors onto vesicles, the readily available pool of vesicular motors may allow for quick transitions, perhaps to avoid roadblocks or traffic jams or in response to changes in the local cellular environment.

Thus, a second tug-of-war model predicts that the opposing motors kinesin and dynein can bind simultaneously to a given cargo and drive motility toward either the microtubule plus- or minus-end in a stochastic and unregulated manner (Hendricks et al., 2010; Muller et al., 2008). In this model, net direction of transport is determined by which set of motors exerts the most force at any given time; frequent directional switches are predicted, consistent with the motility of bidirectional cargos. These predicted motor properties would be disadvantageous for axonal transport, which necessitates the ability to quickly deliver cargo across vast cellular distances.

In contrast, the third coordination model proposes that a cargo-bound adaptor regulates the activity of one or both motors, leading to processive motility along the microtubule, with few directional changes. Importantly, the contribution of scaffolding proteins likely underlies the difference in run lengths observed for single molecule motors *in vitro* (~1–2 μm for Kinesin-1 and Kinesin-2) versus organelle transport in cells.

In eukaryotic cells, diverse scaffolding proteins serve as adaptors that link motors to cargos. Scaffolding proteins often exist in large complexes and form redundant interactions with other adaptors as well with motors. Regulation of transport at the cargo level via scaffolding proteins can either alter cargo association or motor activation. Though many adaptors have been identified for different vesicular organelles as well as proteinaceous or RNA cargos, I will focus on several scaffolding complexes that have well-characterized protein interactions and regulatory schemes.

RILP Complex

The scaffolding protein RILP (Rab7-interacting lysosomal protein) facilitates retrograde transport of late endosomes and lysosomes via direct binding to the C-terminus of the $p150^{Glued}$ subunit of dynactin (Jordens et al., 2001). In addition, it forms a large tripartite complex with Rab7 and ORP1L in a GTP-dependent manner. Activated GTP-bound Rab7 facilitates the step-wise recruitment of RILP then ORP1L to the late endosome. ORP1L then transfers the complex onto vesicular βIII-spectrin (Johansson et al., 2007), which associates with the vesicular membrane and also is capable of an additional interaction with dynactin via binding to the Arp1 subunit (Holleran et al., 2001). The oxysterol-binding protein ORP1L was subsequently

shown to be a cholesterol sensor that facilitates RILP/p150^{Glued} binding in peripheral lysosomes but recruits ER proteins which leads to dissociation of p150^{Glued} in nonperipheral lysosomes (Rocha et al., 2009).

The idea that lipid sensing may play a role in adaptor association is not unique to ORP1L. SNX6 is a protein in the retromer complex that mediates direct binding to C-terminal p150^{Glued} (Hong et al., 2009; Wassmer et al., 2009). Retromers facilitate the return of cargos to the trans-Golgi network (TGN) where lipid composition plays a role in release of the retrograde motor. Phosphotidylinositol-4-phosphate (PI4P), a Golgi-enriched phosphoinositol, facilitates the dissociation of p150^{Glued} from SNX6 (Niu et al., 2013). Regulation of motor association via membrane lipid composition is emerging as an important yet understudied facet of vesicular transport.

The stoichiometry of RILP association has been suggested to play an important role in recruiting teams of dyneins to lysosomes. In optical trapping experiments in intact cells, phagosomes in rodent macrophage cell lines exhibit bidirectional movement with measurable forces generated by both kinesin and dynein. However, highly processive retrograde runs have high stall forces that cluster around even values of 2 pN, 4 pN, 6 pN and so forth (Hendricks et al., 2012; Rai et al., 2013). Since mammalian dynein has a unitary stall force of 1pN, these results suggest that teams of 4-10 dyneins are recruited onto vesicles in pairs. It is possible that because Rab7 recruits RILP in pairs (Jordens et al., 2001), that this could a molecular determinant underlying the pairwise association of dynein on these phagosomes.

Mitochondrial Scaffolding Proteins Milton/Miro

In axons, the majority of mitochondria (~60%) are stationary, but the remainder move robustly in both anterograde and retrograde directions with speeds ~0.4-1.0 μm in primary rodent neurons (MacAskill and Kittler, 2010). The mitochondrial Milton/Miro complex mediates the binding of microtubule-based motors to mitochondria. Miro (Mitochondrial Rho GTPase) contains a transmembrane domain that is responsible for its association with the outer mitochondrial. Miro recruits Milton, which binds directly to Kinesin-1 via KHC in a KLC-independent manner (Glater et al., 2006). Whereas *Drosophila* has one gene that encodes Milton, mammals have two copies of the Milton homologues TRAK1 and TRAK2.

High calcium levels disrupt the association of KHC to mitochondria, consistent with high calcium levels in at synapses, which have high local energetic demands. Miro contains two calcium-sensing EF hand domains and two molecular mechanisms have been proposed to explain the calcium-dependent regulation of Milton/KHC association. In the Schwarz Model, high levels of calcium lead to association of KHC motor head to Miro, effectively preventing the head from processing along microtubules (Wang and Schwarz, 2009). In the Kittler Model, calcium binding to Miro results in the release of KHC from Milton, likely by altering the binding of Milton and Miro (Macaskill et al., 2009). Both groups show that N-terminal Milton binds to Miro, but while the Schwarz group showed that this interaction occurs on C-terminal Miro, the Kittler group showed that this interaction occurs on N-terminal Miro. Moreover, experimental concentrations of calcium differ greatly.

Recently, Milton was also shown to bind to retrograde motors via the $p150^{Glued}$

subunit of dynactin (van Spronsen et al., 2013). However, it is unclear how an additional interaction with the retrograde motor may affect mitochondrial motility from a molecular level.

To further complicate the regulation of mitochondrial transport, the stationary pool of mitochondria is thought to be anchored to microtubule via the mitochondrial docking protein syntaphilin. Depletion of syntaphilin leads to dramatic decreases in the percentage of stationary mitochondria (Kang et al., 2008). Consistent with the idea that mitochondrial capture occurs at sites of high energetic demand, a recent paper showed that the LKB1/NUAK1 pathway, which is necessary for axon branching, regulates mitochondrial capture at presynaptic sites via syntaphilin (Courchet et al., 2013). Though syntaphilin contains 12% serines and multiple phosphorylation sites (Sheng and Cai, 2012), it has not been established whether the LKB1/NUAK1 kinase pathways may modify syntaphilin directly via phosphorylation or indirectly via intermediate effectors.

In addition to regulating mitochondrial docking, syntaphilin has recently been shown to bind the tail of KHC. Unlike other adaptor proteins that also bind to KHC tail and activate KHC activity by relieving autoinhibition, binding of syntaphilin to KHC tail competes against its binding to Milton. Effectively, at high concentrations of calcium, consistent with the Kittler model, KHC tail dissociates from Milton and binds to syntaphilin where it is unable to hydrolyze ATP efficiently (Chen and Sheng, 2013). Unlike other proteins that bind to KHC tail to activate KHC motor activity, syntaphilin binding has the opposite effect yet it is unclear how KHC that is unfolded via syntaphilin remains autoinhibited. Interesting, this model does not occlude the

Schwarz Model and likely syntaphilin-bound KHC may be hindered from binding to microtubules via interaction between KHC motor head and Miro.

Huntingtin Complex

The large 350-kDa huntingtin is a bidirectional scaffolding protein with the ability to bind to both anterograde and retrograde motors. Originally shown to bind to $p150^{Glued}$, it was subsequently shown to interact directly with DIC (Caviston et al., 2007). In addition, huntingtin also binds to the adaptor protein HAP1, which itself can associate with anterograde motors via KLC (McGuire et al., 2006) and KHC (Twelvetrees et al., 2010); HAP1 also interacts with $p150^{Glued}$ (Engelender et al., 1997), thus forming a secondary interaction between the huntingtin complex and retrograde motors.

Finally, huntingtin may coordinate actin-based transport via its ability to bind to the myosin VI adaptor optineurin (Sahlender et al., 2005). The ability of huntingtin to integrate adaptors for both microtubule-based motors as well as for an actin based motor is consistent with knockdown experiments in HeLa cells suggesting that hungtingtin is necessary for the transition of endosomes and lysosomes from actin tracks to microtubule tracks in the cell periphery (Caviston et al., 2011). Yet another huntingtin adaptor may play an important role in the maturation of early to late endosomes. The HAP40 protein binds to both huntingtin as well as to Rab5; thus it has been proposed that huntingtin alternates between two states – a HAP40/optineurin complex that facilitates actin-based motility of the Rab5-positive early endomes and a HAP1/kinesin/dynein complex that facilitates microtubule-based transport (Caviston and Holzbaur, 2009).

The huntingtin complex has been implicated in transport of a plethora of cargos, including signaling endosomes and lysosomes (Caviston et al., 2007), APP-positive vesicles (Yang et al., 2012), RNA (Ma et al., 2011), and GABA receptors (Twelvetrees et al., 2010). Recently, the association of vesicular huntingtin with the glycolytic enzyme GAPDH has been suggested to supply "on-board" ATP for axonal cargos (Zala et al., 2013). However, it is unclear how the huntingtin/HAP1 transport complex, which could easily exceed 1 megadalton (MDa), associates with cargos since a direct link between huntingtin and any transmembrane or vesicular associated proteins has yet been demonstrated.

Phosphorylation of huntingtin at S421 by the kinase Akt may act as a switch between anterograde versus retrograde motor association. Phosphorylation of huntingtin promotes anterograde transport of BDNF-positive vesicles, as expression of phosphomimetic huntingtin-S421D doubles the ratio of anterograde to retrograde flux of BDNF-positive vesicles, concurrent with ~20% increase in anterograde speed (Colin et al., 2008).

Another bidirectional scaffolding protein is the RNA-binding protein La, which facilitates the binding of anterograde and retrograde motors to RNA granules. La can be covalently modified at the K41 site by addition of small ubiquitin-like modifying polypeptides (SUMO). Sumoylated La associates with DIC but not with KHC, suggesting that sumoylation of La may preferentially promote retrograde RNA transport. Indeed live-cell imaging of wildtype La-GFP displays both anterograde and retrograde movement in axons whereas La-GFP containing a K41R mutation showed only anterograde transport, indicative of failure to associate with dynein in the

absence of sumoylation. Importantly, these results also imply that SUMO ligases must be enriched or have enhanced activation in the distal axon (van Niekerk et al., 2007), a process that is not well understood. Nevertheless, this was one of the first clear demonstrations of a post-translational modification affecting a switch in transport direction in support of the coordination model.

JIP1 and JIP3

JNK-interacting proteins (JIPs) were originally characterized based on their ability to bind to multiple kinases in the c-jun N-terminal kinase (JNK) pathway. The mammalian JIP family consists of four members: JIP1, JIP2, JIP3, and JIP4. Though they have similar names, JIP1 and JIP2, which share homology, are structurally distinct from JIP3 and JIP4, which share homology (Whitmarsh, 2006). Though both JIP1 and JIP3 are both known motor scaffolding proteins, they do so through very different mechanisms.

The scaffolding protein JIP1 has been implicated in transport of mitochondria and synaptic vesicles (Horiuchi et al., 2005), as well as APP-positive vesicles (Muresan and Muresan, 2005b). JIP1 binds directly to the transmembrane cargo protein APP (Matsuda et al., 2001; Scheinfeld et al., 2002), as well as to the motor components KLC (Verhey et al., 2001). In addition, the KHC-binding protein FEZ1, which is found in a complex with JIP1, is necessary for activating KHC in the presence of KLC (Blasius et al., 2007).

JIP3 was originally identified as Sunday Driver, a mutation in flies and subsequently characterized as an adaptor that associates with dynactin in the transport of axonal

injury signals (Cavalli et al., 2005). Mass spectrometry of isolated JIP3-positive vesicles identified two classes of JIP3 vesicles – an endocytic population of large vesicles likely involved in initial retrograde injury signaling to the cell body and a pool of small vesicles containing synaptic proteins suggested to play a role in axonal outgrowth and guidance (Abe et al., 2009).

The recent characterization of direct binding between JIP3 and Kinesin-1 via the tail domain of KHC has cemented JIP3 as a bidirectional scaffolding protein. Indeed, JIP3 binding to KHC tail relieves its autoinhibition and is sufficient to activate KHC in single molecule motility assays (Sun et al., 2011). Moreover, the JIP3 homologue in *C. elegans*, UNC16, has also been demonstrated to bind to both Kinesin-1 as well as to dynein via DLIC (Arimoto et al., 2011).

JIP3 and JIP4 are effectors of the endosomal membrane protein ADP-ribosylation factor 6 (ARF6). GTP-ARF6 binds directly to the LZII (leucine zipper II) region of JIP3, where it interferes with JIP3's association with the TPR domain of KLC and favors binding to dynactin. This competitive binding is thought to facilitate trafficking of recycling endosomes (Montagnac et al., 2009). Because this paper preceded publication of the result that direct binding of JIP3 to KHC tail activates KHC motor, the question of whether ARF6 binding to JIP3 may perturb its ability to bind KHC tail.

JIP1 can homodimerize via its SH3 (src homology) domain (Kristensen et al., 2006) and additionally can heterodimerize with JIP2 and JIP3. It is unclear if JIP1 and JIP3 binding forms a heterodimer or a heterotetramer, but this complex of JIP1 and JIP3 is co-transported (Hammond et al., 2008) and functionally relevant in the transport

of APP. In immunostaining and coimmunoprecipitation experiments, JIP1 is necessary for the anterograde and retrograde transport of amyloid precursor protein (APP) and preferentially associates phosphorylated APP (Muresan and Muresan, 2005b). The additional association of JIP3 on this complex may sustain phosphorylation of APP, which in turn facilitates its binding to the JIP1-mediated transport complex (Muresan and Muresan, 2005a).

However, many questions remain about the role of scaffolding proteins in transport regulation. In particular, it is unclear whether bidirectional scaffolding proteins that are able to bind to both anterograde and retrograde motors simultaneously or alternating associate with each motor type. Moreover, if post-translational modifications are responsible for directional shifts, as is the case for huntingtin and La, then how does the scaffolding protein transduce these modifications into altered motor association and subsequent cellular changes in transport?

In the next chapter of this thesis, I will first show that JIP1 is essential for anterograde and retrograde axonal transport of its direct cargo, APP. Then, I will establish JIP1 as a bidirectional scaffolding protein that directly binds to both KHC and dynactin. I will present biochemical, biophysical, and cellular evidence in support of a model whereby JIP1 exists in two mutually exclusive states – either as an anterograde motor complexes or as a retrograde motor complex. Moreover, I will probe the cellular pathways underlying the direction of APP transport by evaluating JIP1 phosphomutants. Collectively, these experiments demonstrate that a cargo-associated scaffolding protein can coordinate transport by regulating kinesin activity and dynein association and that post-translational modification of this bidirectional scaffolding protein results in directional change in axonal transport.

In the subsequent chapter, I will address an additional ability of JIP1 to regulate the unidirectional retrograde transport of autophagosomes in axons. Though knockdown of JIP1 does not affect formation of autophagosome in the distal axon tip, it does disrupt retrograde transport in the mid-axon. Rescue with our phosphorylation mutants show that the phosphodeficient rescues retrograde autophagosome transport robustly while the phosphomimetic actually causes many observations of aberrant anterograde autophagosome motility. In addition, I will discuss preliminary evidence indicating that different regions of JIP1 may play important roles in the ability of JIP1 to associate with autophagosomes.

Together, our work suggests that axonal transport is highly regulated and that modification of cargo-associated proteins is an efficient mechanism for the transduction of directional transport changes.

CHAPTER 2

JIP1 Regulates Axonal Transport of APP via Coordination of Kinesin and Dynein Motor Activity

This chapter is adapted from:

Fu, MM and ELF Holzbaur (2013). JIP1 regulates the directionality of APP axonal transport by coordinating kinesin and dynein motors. *J. Cell Biol.* 202(3): 495-508.

ABSTRACT

Regulation of the opposing kinesin and dynein motors that drive axonal transport is essential to maintain neuronal homeostasis. Here, we examine coordination of motor activity by the scaffolding protein JNK-interacting protein 1 (JIP1), which we find is required for long-range anterograde and retrograde amyloid precursor protein (APP) motility in axons. We identify novel interactions between JIP1 and kinesin heavy chain (KHC) that relieve KHC autoinhibition, activating motor function in single molecule assays. The direct binding of the dynactin subunit $p150^{Glued}$ to JIP1 competitively inhibits KHC activation *in vitro* and disrupts the transport of APP in neurons. Together, these experiments support a model whereby JIP1 coordinates APP transport by switching between anterograde and retrograde motile complexes. We find that mutations in the JNK-dependent phosphorylation site S421 in JIP1 alter both KHC activation *in vitro* and the directionality of APP transport in neurons. Thus phosphorylation of S421 of JIP1 serves as a molecular switch to regulate the direction of APP transport in neurons.

INTRODUCTION

Targeted long-distance transport of proteins and organelles is critical in neurons, which extend polarized axons of up to one meter long in humans. In axons, the family of anterograde kinesin motors and the retrograde dynein motor transport cargos on microtubule tracks of uniform polarity. These cargos include synaptic vesicles, signaling endosomes, lysosomes, RNA granules, and mitochondria (Hirokawa et al., 2010).

Constitutive transport of axonal cargos can either be bidirectional, characterized by saltatory or frequent back and forth movement, or highly processive, characterized by long run lengths and high speeds. For example, mitochondria (Morris and Hollenbeck, 1993) and late endosomes/lysosomes (Hendricks et al., 2010) often move bidirectionally along axons, with short runs in either direction punctuated by frequent directional switches. In contrast, autophagosomes display highly processive and unidirectional retrograde motility along axons (Maday et al., 2012).

Three models have been proposed to explain how net direction of microtubule-based transport is determined at a molecular level (Gross, 2004; Welte, 2004). In the first model, only anterograde or retrograde motors can bind to a cargo at any given time. However, both *in vitro* and cellular studies suggest that opposing motors can bind simultaneously to cargos (Encalada et al., 2011; Hendricks et al., 2010; Maday et al., 2012; Soppina et al., 2009). In a tug-of-war model, opposing kinesin and dynein motors can bind simultaneously to cargo and drive motility toward either the microtubule plus- or minus-end in a stochastic and unregulated manner (Hendricks et al., 2010; Muller et al., 2008). In this model, net direction of transport is

determined by which set of motors exerts the most force at any given time; frequent directional switches are predicted, consistent with the motility of bidirectional cargos. In contrast, in the third, coordination model, a cargo-bound adaptor regulates the activity of one or both motors, leading to processive motility along the microtubule, with few directional changes.

To understand how the activity of opposing kinesin and dynein motors may be coordinated during axonal transport, we turned to the vesicular transmembrane protein APP (amyloid precursor protein). Axonal transport of APP is highly processive, with fast velocities and long run lengths in both anterograde and retrograde directions (Kaether et al., 2000). Impaired axonal transport of APP correlates with increased production of amyloid-b (Ab), an APP cleavage product that aggregates to form senile plaques in Alzheimer's Disease (Stokin et al., 2005). Despite this relationship between dysfunctional APP trafficking and disease pathology, the molecular mechanisms that regulate APP transport in neurons are not yet understood.

Anterograde APP transport is mediated via direct binding (Matsuda et al., 2001; Scheinfeld et al., 2002) to the scaffolding protein JIP1 (JNK-interacting protein; Muresan and Muresan, 2005b). JIP1 was originally identified for its ability to recruit multiple kinases in the JNK (c-jun N-terminal kinase) pathway (Dickens et al., 1997). Genetic studies suggest that JIP1 regulates constitutive axonal transport (Horiuchi et al., 2005) whereas the structurally unrelated scaffolding protein JIP3 (Koushika, 2008; Whitmarsh, 2006) plays a role in injury signaling (Abe et al., 2009; Cavalli et al., 2005).

Conventional Kinesin-1 is a heterotetramer consisting of the adaptor protein kinesin light chain (KLC) and the motor protein kinesin heavy chain (KHC or KIF5). JIP1 directly binds to KLC via a conserved 11-amino-acid motif at the C-terminus (Verhey et al., 2001). However, this binding domain is insufficient to activate KHC-mediated anterograde transport (Kawano et al., 2012), suggesting that additional interactions may be responsible for KHC activation in APP transport. Furthermore, though axonal transport of APP occurs in both anterograde and retrograde directions, neither the mechanism underlying its retrograde transport nor the switch regulating its directionality are currently known.

Here, we show that knockdown of JIP1 leads to severe deficits in both anterograde and retrograde axonal transport of APP in primary neurons. We identify novel, KLC-independent interactions between JIP1 and KHC and show via single molecule motility assays that JIP1 binding activates KHC motility *in vitro*. Furthermore, we identify another novel JIP1 interactor, $p150^{Glued}$, a subunit of the retrograde dynein/dynactin complex. $p150^{Glued}$ competitively inhibits the JIP1-mediated enhancement of KHC processivity *in vitro* and disrupted anterograde APP axonal transport. Furthermore, mutations at a JNK-dependent phosphorylation site in JIP1 (S421) alter KHC activation *in vitro* and the directionality of APP transport in neurons. Together, these experiments establish JIP1 as a coordinator of anterograde and retrograde motor activity whose regulation by phosphorylation determines the directionality of the axonal transport of APP.

METHODS AND MATERIALS

Cell culture and transfection

Dissected adult mouse dorsal root ganglion (DRGs) were treated with papain, collagenase, and dispase II then centrifuged through a 20% Percoll gradient (Perlson et al., 2009). Isolated DRGs were transfected using Amaxa Nucleofector SCN Program 6 (Lonza) and plated on glass-bottom microwell dishes (FluoroDish, World Precision Instruments) that were pre-coated with poly-L-lysine and laminin. DRGs were maintained in F-12 media (Invitrogen) with 10% FBS, 2 mM L-glutamine, 100 U/ml penicillin, and 100 µg/ml streptomycin. For knockdown experiments, DRGs were transfected with fluorescent red DY-547-conjugated siRNA (Dharmacon) and either APP-YFP or EGFP-Rab7. For $p150^{Glued}$-CBD overexpression experiments, neurons were transfected with APP-DsRed and pBI-CMV2(AcGFP)-FLAG-$p150^{Glued}$-CBD. For JIP1 knockdown and rescue experiments, neurons were transfected with DY-547-conjugated siRNA, APP-YFP, and pBI-CMV2(BFP)-JIP1(WT, S421A, or S421D).

Live-cell imaging

Cultured DRGs were imaged at 2 DIV in Hibernate A low-fluorescence medium (Brain Bits) inside a 37°C imaging chamber. Double- or triple-fluorescent neurons were observed at 63x using a Leica DMI6000B microscope with a CTR7000 HS control box run by Leica AF6000 software and a Hamamatsu C10600 Orca-R2 camera. Images of APP transport were acquired at 250 ms per frame for 1 minute.

Vesicle tracking and analysis

APP-positive vesicles were analyzed by generating 50-µm kymographs (at least 200

μm proximal of the soma) using Metamorph software. Motile particles (e.g. anterograde or retrograde) were defined as particles with net displacement greater than 1 μm. Individual runs were defined as a run with constant velocity; in other words, one vesicle can have several runs within the duration of a movie if it pauses or changes speed or direction. F-tests confirmed that neurons in different dishes are not significantly different; thus the neuron was defined as the biologically relevant unit and motility parameters were averaged for each neuron and subject to subsequent statistical analysis.

Co-immunoprecipitations

COS7 cells transfected using Fugene6 (Roche) according to manufacturer's instructions were harvested 18-24 hours post-transfection and lysed using 0.5% Triton X-100 (in HEM buffer). Lysates were incubated with Protein-G Dynabeads (Invitrogen) and co-immunoprecipitations were performed following manufacturer's instructions using the following antibodies: anti-JIP1 (Santa Cruz B7), anti-$p150^{Glued}$ (BD Transduction), anti-KHC (Chemicon 1614), anti-FLAG (Sigma), anti-GFP (Clontech), anti-HA (Covance), and anti-myc (Invitrogen). All coimmunoprecipitations represent at least 3 independent experiments.

Recombinant protein binding assays

For KHC stalk binding assays, mouse KIF5C stalk (AA560-682) was subcloned into the pGEX6p-1 vector (GE Healthcare), expressed in BL21 (DE3) *E. coli* (Novagen) and induced at ~OD_{600} of 0.6 for 2 hours with 0.4mM IPTG. *E. coli* were lysed with lysozyme and treated with DNAase I and RNase A and the resulting supernatant was purified by binding to glutathione Sepharose-4B (GE Healthcare). For KHC stalk binding experiments, pRSETA-His-JIP1 (Nihalani et al., 2003) was expressed in BL21

E. coli and purified using His-Bind Resin (Novagen) under denaturing conditions using urea as previously described (Karki and Holzbaur, 1995). Glutathione beads bound with either GST or GST-KHC-stalk[560-682] were incubated for 30 minutes at room temperature with purified His-JIP1, washed then eluted with denaturing buffer.

For KHC tail binding assays, His-JIP1 and His-KHC-tail[823-944] (Dietrich et al., 2008) were expressed in Rosetta *E. coli* and purified using His-Bind Resin following manufacturer's protocol. Purified His-KHC-tail[823-944] with or without purified His-JIP1 was incubated with Protein-G Dynabeads bound to anti-JIP1 antibody, washed then eluted with denaturing buffer.

For p150^{Glued} binding assays, MBP-p150^{Glued}[1049-1278] (Johansson et al., 2007) was expressed in Rosetta *E. coli*, purified using amylose resin (NEB) following manufacturer's protocol. Purified His-JIP1 (from Rosetta *E. coli*) and MBP-p150^{Glued}[1049-1278] were buffer-exchanged into HEM buffer with 25mM NaCl using PD10 columns (GE Healthcare). His-Bind resin bound to His-JIP1 was incubated for 30 minutes at room temperature with purified MBP or MBP-p150^{Glued}[1049-1278], washed then eluted with denaturing buffer. All binding assays were performed at least 2 times.

In vitro COS7 lysate motility assay

This assay was adapted from Blasius et al. (2007). Transfected COS7 cells expressing KHC-head-Halo (KIF5C[1-560]) or KHC-Halo were incubated with TMR ligand (Promega) following manufacturer's instructions. COS7 cells were lysed in P12 buffer (12mM PIPES, 2mM MgCl2, 1mM EGTA, pH 6.8) with 0.1% Triton X-100

and cleared by centrifugation at 1000g then 100,000g. Flow chambers were constructed using two strips of double-sided tape between a slide and a cover slip and lined with vacuum grease to yield a chamber volume of ~10 mL. Four solutions were flowed sequentially into the chamber and incubated at room temperature for 5 minutes each: 1) anti-tubulin antibody (Clontech), 2) Pluronic F-127 (50mg/mL), 3) Taxol-stabilized fluorescent microtubules (HiLyte 488 tubulin, Cytoskeleton) and 4) COS7 cell lysates in activation buffer (Cai et al., 2007). For each set of experiments, we conducted at least three independent trials, each with fresh lysate. To minimize variation between chambers, each chamber contained equal amounts of microtubules, KHC-Halo lysate and total lysate (by adding nontransfected lysate).

For each condition, we acquired multiple movies for each trial. Movies were acquired at 3 frames per second for 1 minute at room temperature using an Ultraview Vox spinning disk TIRF system (PerkinElmer) on an inverted Nikon Ti microscope with the 100x objective and a Hamamatsu ImagEM C9100-13 camera controlled by Volocity software. Kymographs of microtubules with lengths greater than 10 mm were analyzed for stationary binding events and runs. Run frequency measurements were normalized with respect to microtubule length. Individual runs were measured at the level of each motile particle (i.e. each particle has one run length or net displacement and one speed measurement).

Statistical analysis

Statistical analysis was performed using Student's t-test or one-way ANOVA with post-hoc Tukey's test. For JIP1 mutant experiments, we used post-hoc Dunnett's Test, comparing against the control wildtype JIP1 rescue condition. Bar graphs were

plotted as mean ± SEM and the following denotations for statistical significance were used: * $p<0.05$, ** $p<0.01$, *** $p<0.001$, n.s. (not significant).

RESULTS

JIP1 Knockdown Disrupts Both Anterograde and Retrograde Axonal Transport of APP

To probe the role of JIP1 in the regulation of axonal transport, we depleted JIP1 expression using targeted siRNA. Because primary neurons have low levels of transfection, we first tested the efficiency of our siRNA in the CAD mouse neuronal cell line, whose ability to extend long neurites upon differentiation by serum deprivation has been exploited to study polarized neuronal transport (Blasius et al., 2007). At 48 hours after transfection, our siRNA depleted endogenous JIP1 by more than 90% when assessed by immunostaining and Western blotting, with no compensatory changes in motor protein expression (Fig. 1A and 1B). In addition, a sequence-specific scrambled siRNA had no off-target effects on APP transport (Fig. 1C).

Next, we knocked down JIP1 in primary mouse dorsal root ganglion (DRG) sensory neurons that extend elongated axons with uniform microtubule polarity and have been previously used to study APP function (Nikolaev et al., 2009). Using fluorescent siRNA to identify JIP1-depleted cells, we imaged APP-YFP-positive axons and observed a striking ~60% decrease in the number of APP-positive vesicles (Figs. 2A and 2B). This dearth of APP-positive vesicles likely represents the cumulative effect of a shift in the steady state of vesicles entering or exiting the axon, perhaps resulting from changes in anterograde and retrograde transport.

Next, using kymograph analysis, we classified APP-positive vesicles as anterograde, retrograde, or non-motile. While control neurons exhibited robust APP transport, JIP1-depleted neurons displayed decreases of more than 50% and 30% in anterograde and retrograde APP motility, respectively, with a doubling of the percentage of non-motile vesicles (Fig. 2C and 2D). CAD cells depleted of JIP1 also showed similar changes in APP motility (Fig. 1D). Importantly, these alterations in APP transport are a targeted and specific effect of endogenous mouse JIP1 knockdown as both anterograde and retrograde motility are fully rescued by a bicistronic construct co-expressing siRNA-resistant human JIP1 and the transfection marker BFP (Fig. 2D). In addition, APP-positive vesicles that remain motile in JIP1-knockdown neurons exhibited decreases in both anterograde and retrograde run length and speed (Figs. 2E and 2F). The commensurate shift to arrested motility as well as decreases in speed and run length in JIP1-depleted neurons indicate that APP-positive vesicles are impaired in their ability to sustain processive runs in the absence of JIP1.

Direct Binding of JIP1 to KHC Stalk and Tail is Independent of KLC

The transport changes that we observed upon JIP1 depletion were consistent with a role for JIP1 in the formation and maintenance of a functional transport complex. Interestingly, recent experiments suggest that binding of KLC to JIP1 is insufficient for transport initiation (Kawano et al., 2012). Thus, we tested for additional interactions between JIP1 and Kinesin-1 by performing co-immunoprecipitations using mouse brain homogenate. An anti-JIP1 antibody coimmunoprecipitated KHC and a monoclonal anti-KHC antibody that recognizes the KHC head region robustly coimmunoprecipitated JIP1 (Fig. 3A). Interestingly, the anti-KHC

immunoprecipitation concentrated a ~120-kDa JIP1 band, which is found at very low levels in the brain homogenate and may represent a post-translationally modified form of JIP1.

To map the KHC domains that interact with JIP1, we co-transfected full-length myc-JIP1 along with GFP-KHC fragments (Konishi and Setou, 2009) into COS7 cells. Of the three mammalian KHCs, KIF5B is ubiquitously expressed whereas KIF5A and KIF5C are enriched in neurons (Kanai et al., 2000); thus we used KIF5C constructs in this study. Immunoprecipitations revealed that both KHC stalk and tail regions can bind independently to JIP1 while the KHC head region containing the motor domain does not (Figs. 3B and 3C). Using purified recombinant proteins, we demonstrated these interactions are direct, and further refined the KHC binding domains. Full-length His-JIP1 (Fig. 4A) binds independently to both GST-KHC-stalk (AA560-682) and His-KHC-tail (AA823-944; Figs. 3B, 3D and 3E). Moreover, neither of the recombinant KHC stalk or tail constructs include the KLC-binding domain of KHC (AA682-810; (Verhey et al., 1998), further indicating that the binding of JIP1 to KHC is independent of KLC.

To map the KHC binding sites within JIP1, we transfected either GFP-KHC-stalk or tail along with myc-JIP1 fragments into COS7 cells. Immunoprecipitations against myc-JIP1[307-700], a truncated JIP1 construct missing the 11-amino-acid C-terminal KLC-binding domain (KLC-BD), demonstrate robust binding to both KHC stalk and tail (Figs. 3F and 3G), confirming that KHC binds JIP1 independently of KLC. In addition, GFP-KHC-stalk bound to myc-JIP1[554-711], a C-terminal JIP1 fragment containing the phosphotyrosine binding (PTB) domain (Fig. 3F) while GFP-KHC-tail bound to myc-JIP1[285-440] (Fig. 3G). Further experiments with a N-

terminal fragment, JIP1[1-390], demonstrated no binding (Fig. 4B), which effectively restricts the minimal KHC-tail binding domain to AA391-440. These distinct binding sites confirm that KHC stalk and tail interact with separate regions of JIP1 and suggest that dual interactions may function to enhance the association of JIP1 to KHC.

Binding of JIP1 Relieves KHC Autoinhibition and Activates KHC Motility *in vitro*

In the cell, KHC tail binds to the KHC motor head domain to autoinhibit its ATPase activity, which likely prevents wasteful ATP hydrolysis and microtubule track congestion (Verhey and Hammond, 2009). This well-characterized interaction occurs via hydrogen bonding between the basic IAK motif in the tail and acidic residues on the motor head (Kaan et al., 2011). Interestingly, the minimal KHC-tail binding domain in JIP1 (AA391-440) contains 22% acidic residues (Fig. 4C) and may compete against KHC head for binding to KHC tail. Hence, we hypothesized that binding of KHC tail to JIP1 relieves KHC autoinhibition and activates KHC motility.

To test this idea functionally, we utilized an *in vitro* single molecule motility assay (Blasius et al., 2007). COS7 cells transfected with full-length KHC containing a C-terminal HaloTag (KHC-Halo) were incubated with membrane-permeable red TMR-conjugated HaloTag ligand and lysed. When applied to flow chambers containing immobilized green microtubules, fluorescent KHC-Halo from COS7 lysates can be visualized by TIRF (total internal reflection fluorescence) microscopy (Figs. 5A-5C). Consistent with the established mechanism of full-length KHC autoinhibition, KHC-Halo alone showed only rare non-motile microtubule binding events and runs (Figs.

5D and 5E), which may be attributed to stochastic KHC unfolding or activation by endogenous KHC-binding adaptors that are present at low levels in the cell lysate. As a positive control, we also imaged the motility of KHC-Head-Halo (AA1-560), which exhibited an average run length of ~2.5 μm and average speed ~0.55 μm/s (Figs. 5F and 5G), values comparable to those of recombinant KHC head (Dixit et al., 2008).

When combined with myc-JIP1 lysate, the frequency of KHC-Halo processive runs increased by more than 5-fold (Fig. 5D). Addition of myc-JIP1 also significantly increases the number of stationary binding events (Fig. 5E), indicating that JIP1 binding increased the probability of KHC unfolding. Moreover, KHC-Halo runs in the presence of myc-JIP1 were significantly faster and had longer run lengths, which doubled to approximately 5 μm (Fig. 5F and 5G) with ~15% of motile events reaching run lengths greater than 8 μm (Fig. 6).

In order to explore the functional consequence of distinct JIP1 interactions with KHC stalk and tail, we tested the effects of JIP1-TBD (tail-binding domain, AA285-440) or JIP1-SBD (stalk-binding domain, AA554-711) on KHC motility. Addition of JIP1-TBD or JIP1-SBD increased the number of motile KHC runs (Fig. 5D), indicating that either fragment is sufficient to activate KHC runs. Interestingly, when compared to the KHC-Halo alone, addition of JIP1-TBD increased the number of non-motile microtubule binding events, but JIP1-SBD did not (Fig. 5E), suggesting that a greater percentage of KHC unfolding events are converted into runs in the presence of JIP1-SBD.

However, neither JIP1-TBD nor JIP1-SBD was able to fully recapitulate the processive properties of KHC-Halo in the presence of full-length JIP1. Though addition of either JIP-TBD or JIP1-SBD increased KHC-Halo run length relative to the condition lacking JIP1, run lengths in the presence of JIP1-SBD were significantly shorter (by ~12%) than those in the presence of full-length JIP1 (Fig. 5F). Histograms of run length distribution indicate that this lower average is due to a higher proportion of short runs (<2 μm) and not due to an inability of JIP1-SBD to sustain long runs (Fig. 6). Moreover, though addition of JIP1-SBD, but not JIP1-TBD increased KHC-Halo speed relative to KHC alone (Fig. 5G), suggesting that binding of KHC stalk to JIP1 may function to enhance KHC speed. Thus, though either JIP1-SBD or JIP1-TBD is sufficient to activate KHC motility *in vitro*, binding of JIP1 to both KHC stalk and tail likely amplifies the fidelity of the JIP1-KHC interaction, allowing KHC to remain unfolded and process along the microtubule more quickly and for longer run lengths.

JIP1 Associates with Retrograde Motors via Direct Binding to the p150^{Glued} Subunit of Dynactin

The ability of JIP1 to activate KHC motility is consistent with the observed disruption of anterograde APP transport upon JIP1 depletion in DRGs (Figs. 2D-2F), but these knockdown results also induced deficits in retrograde APP transport. To investigate whether JIP1 associates with the retrograde motor complex, we performed coimmunoprecipitations using mouse brain homogenate and detected an interaction between JIP1 and the p150^{Glued} subunit of the dynein activator dynactin. An anti-p150^{Glued} antibody coimmunoprecipitates both 110-kDa and 90-kDa bands of JIP1; an anti-JIP1 antibody also coimmunoprecipitates p150^{Glued}, although to a lesser extent (Fig. 7A), perhaps due to the additional non-motor scaffolding functions of

JIP1 in the JNK signaling pathway (Dickens et al., 1997). In addition to this biochemical interaction, both JIP1 and p150^{Glued} are enriched at the distal axon tip (Dajas-Bailador et al., 2008; Moughamian and Holzbaur, 2012).

To further define the interaction between p150^{Glued} and JIP1, we performed a series of coimmunoprecipitations using lysates from COS7 cells co-transfected with full-length JIP1 and truncated p150^{Glued}. These experiments revealed that JIP1 does not bind to an N-terminal p150^{Glued} fragment (AA1-880) containing both the microtubule-binding CAP-Gly domain and the dynein-binding CC1 domain. Rather, JIP1 bound robustly to a C-terminal p150^{Glued} construct containing AA880-1278 (Fig. 7B), which will henceforth be referred to as the p150^{Glued} cargo-binding domain (p150^{Glued}-CBD). We further refined this binding domain using recombinant purified full-length His-JIP1 and a C-terminal p150^{Glued} fragment that excludes the CC2 region (AA 1049-1278; Fig. 7D). When applied to a column with bound His-JIP1, MBP did not bind to His-JIP1 while MBP-p150^{Glued}[1049-1278] was specifically retained (Fig. 7C). Interestingly, smaller co-purifying fragments of MBP-p150^{Glued}[1049-1278] (Fig. 7C, Lane 2) did not bind to His-JIP1 (Lane 4), suggesting that the last ~100AA of the C-terminus of p150^{Glued} are essential for JIP1 binding.

C-terminal p150^{Glued} also associates with other cargo adaptors, including HAP1 (huntingtin-associated protein 1; (Engelender et al., 1997), RILP (Rab7-interacting lysosomal protein; (Johansson et al., 2007), Sec23p (Watson et al., 2005), and the retromer subunit SNX6 (Hong et al., 2009; Wassmer et al., 2009). A comparison of binding studies shows that they all bind to the p150^{Glued} region spanning AA1049-1278 (Fig. 7E). If multiple cargo adaptors share this common binding domain, then they are expected to compete for binding to p150^{Glued}. To test this idea, we

transfected COS7 cells with fixed amounts of JIP1 and p150^{Glued} DNA and increasing amounts of SNX6 DNA. Communoprecipitations showed that at lower levels of SNX6 expression, p150^{Glued} predominantly binds to JIP1, but that at higher levels of SNX6 expression, p150^{Glued} predominantly binds to SNX6 (Fig. 7F). This competitive binding between SNX6 and JIP1 suggests that they share a binding site on C-terminal p150^{Glued}.

Next, we performed a series of coimmunoprecipitations using COS7 cells co-transfected with full-length p150^{Glued} and truncated JIP1. These experiments show that the interaction between p150^{Glued} and JIP1 is KLC-independent, because FLAG-p150^{Glued} robustly binds myc-JIP1[307-700], which lacks the C-terminal KLC-BD. Interestingly, FLAG-p150^{Glued} binds to both myc-JIP1[441-565] and myc-JIP1[554-711] (Fig. 7G). The myc-JIP1[441-565] fragment contains the SH3 dimerization domain of JIP1 (Kristensen et al., 2006) and thus may bind to endogenous full-length JIP1.

Anterograde and Retrograde JIP1 Motile Complexes Are Mutually Exclusive

In addition to the known interaction of JIP1 with KLC, we have now identified three novel interactions of JIP1 with KHC stalk, KHC tail, and p150^{Glued}-CBD (Fig. 8A). These interactions establish JIP1 as a scaffolding protein that binds to both anterograde and retrograde motor complexes; other proteins with this ability include the huntingtin/HAP1 complex (Caviston et al., 2007; Engelender et al., 1997; McGuire et al., 2006; Twelvetrees et al., 2010), JIP3 (Arimoto et al., 2011; Cavalli et al., 2005; Sun et al., 2011), and Milton/TRAK (Glater et al., 2006; van Spronsen et al., 2013).

However, it is unclear whether anterograde and retrograde motor complexes interact with scaffolding proteins simultaneously or alternatingly. Since KHC stalk and p150^{Glued} share a binding domain at the C-terminal PTB region of JIP1 (Figs. 3F and 7G), we hypothesized that KHC and p150^{Glued} compete for binding to JIP1. Thus, we asked whether p150^{Glued} and KHC stalk can simultaneously bind to JIP1 by co-expressing myc-JIP1, FLAG-p150^{Glued}, and GFP-KHC-stalk in COS7 cells. Immunoprecipitated GFP-KHC-stalk pulls down myc-JIP1, but no associated FLAG-p150^{Glued} (Fig. 8B); in the complementary experiment, immunoprecipitated FLAG-p150^{Glued} robustly pulled down myc-JIP1, but no associated GFP-KHC-stalk (Fig. 8D). This suggests that KHC stalk and p150^{Glued} cannot form a tripartite complex with JIP1, consistent with KHC stalk and p150^{Glued} sharing a binding domain at the PTB region in JIP1.

A similar triple transfection was performed using GFP-KHC-tail; coimmunoprecipitation against KHC tail also revealed no co-eluted FLAG-p150^{Glued} (Fig. 8C). Likewise, the complementary immunoprecipitation against FLAG-p150^{Glued} pulled down myc-JIP1, but no associated KHC tail (Fig. 8D). Though p150^{Glued} and KHC tail do not share a common binding domain, KHC tail binding to JIP1 may sterically hinder p150^{Glued} binding in the three dimensional structure of full-length JIP1, which remains unsolved. The results of these experiments are consistent with the exclusion of p150^{Glued} from the JIP1-KHC complex and the exclusion of KHC from the JIP1-p150^{Glued} complex.

Since the KLC-BD and the p150^{Glued}-binding domain on JIP1 do not overlap, we hypothesized that KLC and p150^{Glued} would be able to form a tripartite complex with JIP1. To address this, we performed triple transfections in COS7 cells with HA-KLC,

FLAG-p150^{Glued}, and myc-JIP1 and immunoprecipitated against the tags for KLC and p150^{Glued}. While HA-KLC and FLAG-p150^{Glued} do not coimmunoprecipitate in control lysates lacking exogenous JIP1, co-transfection of myc-JIP1 leads to formation of a tripartite complex containing KLC, p150^{Glued} , and JIP1 (Fig. 8E), which is consistent with the colocalization of KLC and dynein on APP vesicles in neurons (Szpankowski et al., 2012).

Taken together, these binding experiments suggest that the JIP1 motile complex exists in two mutually exclusive states. In one conformation, JIP1 binds directly to both KHC stalk and tail and excludes p150^{Glued} from binding to JIP1. This JIP1 complex likely mediates anterograde transport, consistent with the ability of JIP1 to activate full-length KHC motility. In another conformation, JIP1 binds directly to p150^{Glued} to mediate retrograde transport and can simultaneously bind to KLC (Fig. 8E). However, because KHC cannot directly bind to this p150^{Glued}-associated JIP1 complex, simultaneous binding of KLC may function to retain autoinhibited KHC on the vesicle. This model is consistent with previous studies showing that KLC is inhibitory to microtubule binding (Verhey et al., 1998) and KHC motility *in vitro* (Friedman and Vale, 1999), and that the JIP1 KLC-BD is sufficient for KHC recruitment to vesicles, but not for activation of motility (Kawano et al., 2012).

Furthermore, we affirmed that these JIP1 complexes indeed associate with APP. Immunoprecipitation of JIP1 and APP from mouse brain homogenate pulls down the expected set of associated motors, including KHC, p150^{Glued}, and dynein intermediate chain or DIC (Fig. 9A). Immunostaining of nontransfected cultured DRGs shows that endogenous APP and JIP1 colocalize on puncta along the axon (Fig. 9B). Moreover, these complexes are functional, as fluorescently tagged JIP1 and APP co-migrate on

both anterograde and retrograde moving vesicles along DRG axons (Figs. 9C and 9D).

p150^{Glued} Binding Competitively Inhibits Activation of KHC by JIP1 and Disrupts Anterograde APP Transport

Binding experiments show that KHC and p150^{Glued} cannot bind simultaneously to JIP1 and likely compete for binding to JIP1. Thus, we hypothesized that p150^{Glued} binding to JIP1 will functionally disrupt KHC activation *in vitro*. To this end, we performed motility experiments in which p150^{Glued}-CBD lysates were mixed first with JIP1 lysates then KHC-Halo lysates. The addition of p150^{Glued}-CBD severely disrupted the ability of JIP1 to activate KHC motility and only rare short runs can be observed (Fig. 10A). When normalized to KHC-Halo motility in the presence of JIP1, addition of p150^{Glued}-CBD significantly decreases both the relative frequency of stationary microtubule-binding events and runs as well as run length with no significant changes in speed (Fig. 10B). Moreover, at constant levels of JIP1, addition of increasing amounts of p150^{Glued}-CBD resulted in incremental decreases in KHC run frequency (Fig. 10C), suggesting that inhibition of JIP1-mediated KHC motility by p150^{Glued} occurs in a competitive manner.

To detect whether p150^{Glued} binding to JIP1 also disrupts motility in neurons, we imaged APP-DsRed transport in DRGs co-transfected with a bicistronic vector co-expressing p150^{Glued}-CBD and a GFP transfection marker. The overall number of APP-positive vesicles in the axon did not change significantly upon p150^{Glued}-CBD expression (control: 0.37 ± 0.05 per μm; p150^{Glued}-CBD: 0.42 ± 0.08 per μm). However, neurons expressing p150^{Glued}-CBD showed dramatic inhibition of APP

transport in both anterograde and retrograde directions, with a majority of arrested APP-positive vesicles (Figs. 10D and 10E). Moreover, $p150^{Glued}$-CBD expression in DRGs also decreased the run lengths and speeds of both anterograde and retrograde APP-positive vesicles (Fig. 10F and 10G). In the retrograde direction, $p150^{Glued}$-CBD likely acts as a dominant negative by competing against endogenous full-length $p150^{Glued}$ for JIP1 binding while in the anterograde direction, $p150^{Glued}$-CBD likely prevents formation of the anterograde JIP1 motile complex by disrupting the binding of KHC to JIP1.

JIP1 Phosphorylation Enhances KHC Activation *in vitro* and Promotes Anterograde APP Transport

To further validate the mechanism regulating switching between the anterograde and retrograde JIP1 motile complexes, we endeavored to identify a regulatory mechanism controlling JIP1 binding activity. Previous studies in *Drosophila* suggest a role for JNK in the regulation of JIP1-mediated transport of synaptic vesicles (Horiuchi et al., 2007). Immunoprecipitation of KHC from mouse brain homogenate preferentially pulls down a ~120kDa JIP1 band (Fig. 3A). This ~120-kDa JIP1 band as well as a lower molecular weight JIP1 band are phospho-proteins, as they are dephosphorylated upon lambda phosphatase treatment (Fig. 11A). These observations suggest that phospho-JIP1 preferentially binds to KHC. In addition, expression of truncated JIP1[307-554], which overlaps with JIP1-TBD, results in an additional phosphorylated band, which selectively binds to KHC tail; further, this binding is significantly disrupted in the absence of phosphatase inhibitors (Fig. 11B).

Thus, in order to identify JIP1 phosphorylation sites that enhance binding to KHC tail, we superimposed a map of known JIP1 phosphorylation sites (D'Ambrosio et al., 2006; Nihalani et al., 2003) onto our map of motor binding domains (Fig. 11C). Though no known phosphorylation sites are in C-terminal JIP1 where KLC and KHC stalk, the minimal KHC-tail-binding domain of JIP1 (AA391-440) contains a proline-directed site previously demonstrated *in vitro* to be directly phosphorylated by JNK – S421 (Nihalani et al. 2003). This region of JIP1 is heavily conserved in humans and rodents (Fig. 11D) and may represent a conserved KHC-tail-binding motif, as a similar region is found within the KHC-tail-binding domain of JIP3 (Fig. 11E).

Because the minimal KHC-tail-binding domain of JIP1 contains a high percentage of negatively charged residues (Fig. 4C), we hypothesized that phosphorylation in this region would further strengthen the interaction of JIP1 with the positively charged IAK region of KHC tail responsible for autoinhibition. Initially, we tested the ability of JIP1 phosphomutants to bind to KHC tail in COS7 lysates; while phosphodeficient JIP1-S421A binds weakly to KHC tail, phosphomimetic JIP1-S421D binds more robustly to KHC tail than wildtype JIP1 (Fig. 12A). Next, we confirmed that JIP1-S421 phosphomutants also have altered ability to activate full-length KHC motility *in vitro* (Fig. 12B). Relative to wildtype JIP1, JIP1-S421A activated fewer KHC runs with shorter run lengths and no change in speed while JIP1-S421D activated more runs with faster speed and no change in run length (Figs. 12C-12E).

Finally, we tested the effect of JIP1 phosphorylation on APP transport in DRGs by knockdown of endogenous JIP1 and rescue with a bicistronic vector co-expressing human wildtype or mutant JIP1 and a BFP transfection marker (Fig. 12F). When compared to neurons rescued with wildtype JIP1, neurons expressing JIP1-S421D

have increased anterograde APP transport. Conversely, neurons rescued with JIP1-S421A have decreased anterograde and increased retrograde APP transport (Fig. 12G). These shifts in direction of APP transport are consistent with the association of phospho-JIP1 in the anterograde JIP1 motile complex and of nonphosphorylated JIP1 in the retrograde JIP1 motile complex.

When compared to neurons rescued with wildtype JIP1, neurons expressing JIP1-S421A exhibited decreased anterograde run length while JIP1-S421D exhibited decreased retrograde run length (Fig. 12H). This indicates that nonphosphorylated JIP1 cannot sustain long anterograde runs while phospho-JIP1 cannot sustain long retrograde runs. Though no significant changes in APP speed were observed when rescuing with either JIP1 phosphomutant (Fig. 12I), rescue with JIP1-S421D doubled the percentage of anterograde APP runs with speeds higher than 2.5 μm/s (Fig. 8F). Interestingly, anterograde APP motility trends in neurons closely parallel KHC activation measurements *in vitro* (Figs. 12C-12E), consistent with our model that facilitation of an anterograde motile complex by JIP1 phosphorylation may underlie these observed changes in APP axonal transport.

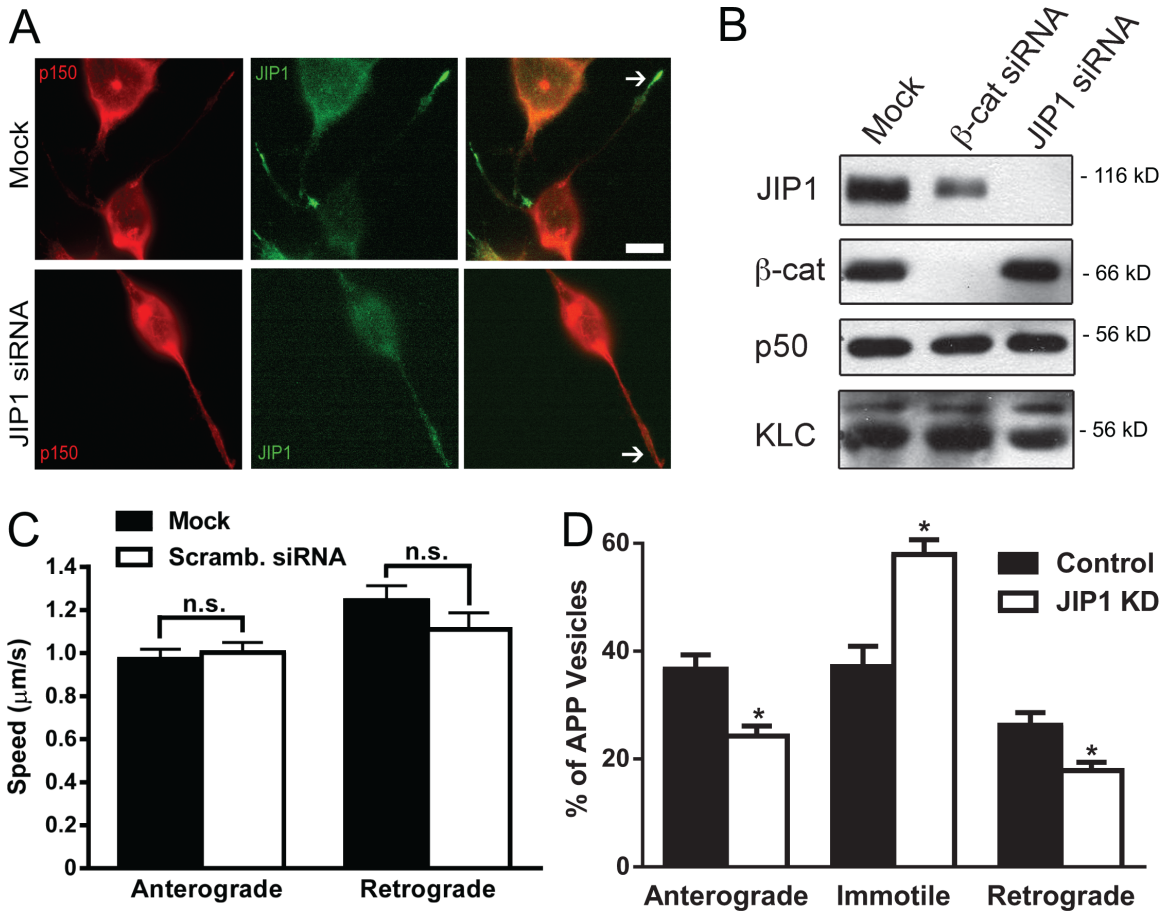

Figure 1. JIP1 knockdown disrupts transport of APP-positive vesicles in neuronal CAD cells.

(A) Immunostaining of CAD cells with anti-JIP1 antibody shows efficient knockdown with JIP1 siRNA 48 hours after transfection. Anti-p150 staining is shown as a reference of cell contour. Arrows point to distal neurites, where JIP1 accumulates under control conditions.

(B) Western blot of CAD cells 48 hours after transfection with JIP1 siRNA. β-catenin siRNA is shown as a control. No compensatory changes are observed in expression of motor proteins p50 (a subunit of dynactin) and KLC upon JIP1 knockdown.

(C) Sequence-specific scrambled siRNA showed no changes in anterograde (p=0.65) or retrograde (p=0.20) speed of APP-YFP transport in CAD cells (n=19-27 cells). In Figs. S1C and S1D, only JIP1 knockdown experiments assessed by immunofluorescence staining of parallel cover slips with greater than 90% knockdown were imaged and analyzed.

(D) JIP1 knockdown decreased the percentage of anterograde and retrograde APP-YFP vesicles in CAD cells (n=27-31 cells).

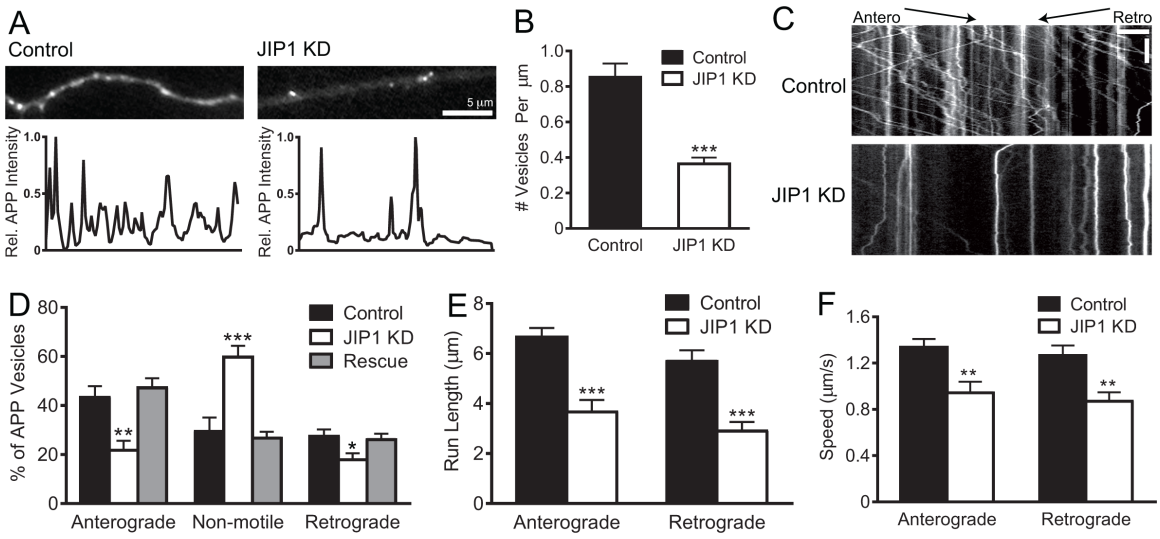

Figure 2. JIP1 knockdown disrupts both anterograde and retrograde transport of APP-positive vesicles.

(A) Representative images and linescans of APP-YFP intensity show that JIP1-knockdown DRGs contain fewer APP-positive vesicles in the axon than control DRGs. Scale bar = 5 μm.

(B) JIP1 knockdown in DRGs significantly decreased the number of APP-positive vesicles in the axon. Control: 0.85 ± 0.08 per μm; JIP1 siRNA: 0.36 ± 0.04 per μm. Data from Figs. 1B-1F represent 3 independent experiments (n = 15-23 neurons).

(C) Kymographs of APP-YFP motility in DRG transfected with siRNA against JIP1. Kymographs represent cumulative organelle movement (displacement on the x-axis) over time (y-axis). Arrested vesicles appear as vertical lines while motile vesicles appear as diagonal lines toward either the right (anterograde) or left (retrograde).

(D) JIP1 depletion significantly alters the directional distribution of APP-positive vesicles, causing decreases in the percentages of anterograde and retrograde vesicles and an increase in the percentage of arrested vesicles. Transport changes induced by JIP1 depletion are fully rescued by expression of a human JIP1 cDNA resistant to the siRNA.

(E, F) JIP1 depletion significant decreases average run lengths and speeds of APP-positive vesicles in both anterograde and retrograde directions. Means represent only vesicles categorized as motile (i.e. anterograde or retrograde in Fig. 1D).

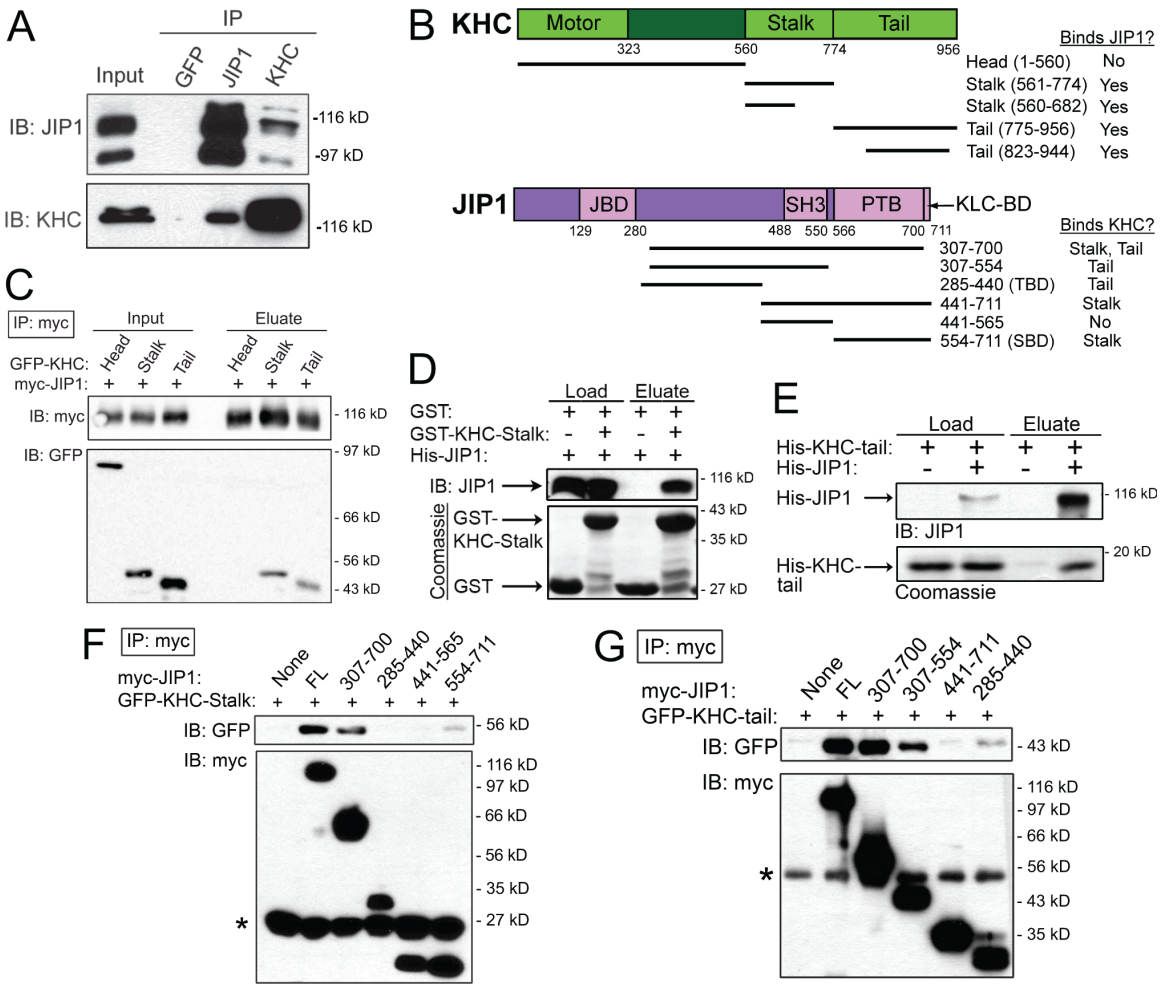

Figure 3. JIP1 binds directly to both stalk and tail domains of KHC independently of KLC.

(A) JIP1 coimmunoprecipitates with KHC in mouse brain homogenate. A monoclonal JIP1 antibody immunoprecipitates the expected 110-kDa band as well as a 90-kDa band that likely represents a splice isoform. Both bands are also recognized by multiple JIP1 monoclonal antibodies (R&D Systems, BD Transduction).

(B) Schematics of KHC (KIF5C) and JIP1 constructs and summary of mapping results. JIP1 contains JBD (JNK-binding domain), SH3 (src homology), and PTB (phosphotyrosine binding) domains.

(C) JIP1 binds to both stalk and tail domains of KHC. Lysates from COS7 cells co-transfected with myc-JIP1 and GFP-KHC fragments were immunoprecipitated with an anti-myc antibody.

(D) JIP1 binds directly to KHC stalk. Purified His-JIP1 incubated with glutathione beads bound to either GST or GST-KHC-stalk (AA560-682) selectively bound to GST-KHC-stalk but not GST.

(E) JIP1 binds directly to KHC tail. Purified His-KHC-tail (KIF5B AA823-944) with or without His-JIP1 was co-incubated with anti-JIP1 antibody, which specifically coimmunoprecipitated His-KHC-tail.

(F) KHC stalk binds to the C-terminus of JIP1 independently of KLC. Lysates from COS7 cells co-transfected with GFP-KHC-stalk and myc-JIP1 fragments were immunoprecipitated with an anti-myc antibody. KHC stalk coimmunoprecipitated with myc-JIP1[565-711] (myc-JIP1-SBD). * = antibody light chain bands.

(G) KHC tail binds to JIP1 independently of KLC. Lysates from COS7 cells transfected with GFP-KHC-tail and myc-JIP1 fragments were immunoprecipitated with an anti-myc antibody. KHC tail coimmunoprecipitated with myc-JIP1[285-440] (myc-JIP1-TBD). * = antibody heavy chain bands.

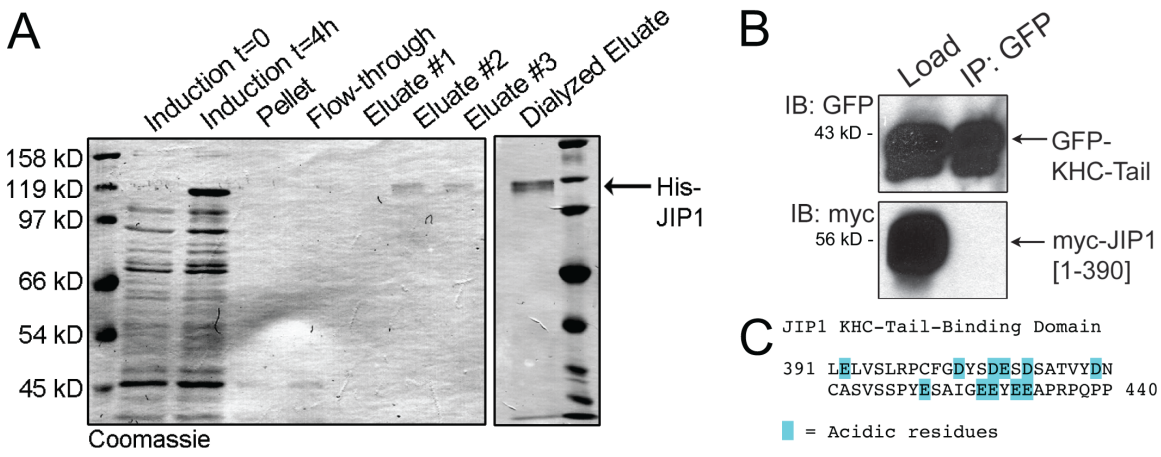

Figure 4. The minimal KHC-tail-binding domain of JIP1 (AA391-440) is highly acidic.

(A) Recombinant His-JIP1 was purified from *E. coli*. Coomasie-stained blot shows efficient induction of His-JIP1 in *E. coli* cultures with 1mM IPTG for 4 hours (Lanes 1 and 2). Pellets were denatured in 8M urea (Lane 3), purified using His-Bind Resin (Novagen) and eluted with 500mM imidazole (Lanes 4-7). Eluates were combined and concentrated by dialysis (Lane 8). Molecular weights (left) are shown in kDs.

(B) JIP1[1-390] does not bind to KHC tail. Lysates from COS7 cells co-transfected with myc-JIP1[1-390] and GFP-KHC-tail were immunoprecipitated with an anti-GFP antibody. No detectable myc-JIP1[1-390] coimmunoprecipitated with GFP-KHC-tail.

(C) The minimal KHC-tail-binding domain of JIP1 (AA391-440) contains 22% acidic residues.

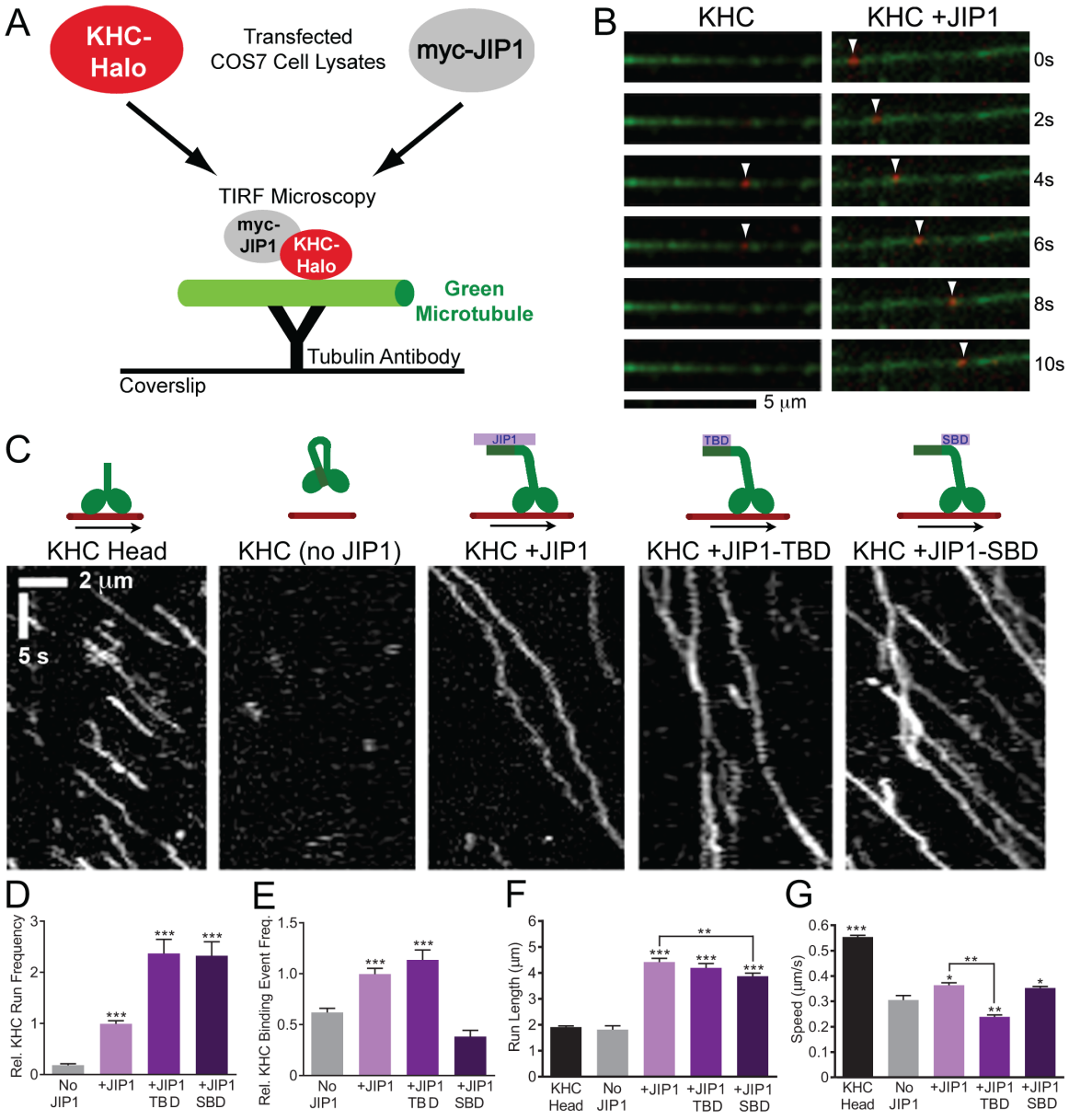

Figure 5. JIP1 binding relieves KHC autoinhibition in *in vitro* TIRF motility assays.

(A) Schematic of *in vitro* TIRF motility assay. Lysate from COS7 cells transfected with KHC-Halo and incubated with red fluorescent TMR ligand was combined with lysate from cells expressing myc-JIP1 constructs and applied to flow chambers containing green fluorescent microtubules, which were immobilized on glass coverslips with anti-tubulin antibody. KHC-Halo motility was imaged using a TIRF microscope.

(B) Time-lapsed images acquired from a flow chamber containing KHC-Halo (red) lysate alone (left) show a brief non-motile binding event (white arrowheads) to a microtubule (green). Images from a flow chamber containing KHC-Halo and myc-JIP1 lysates (right) show processive movement along the microtubule.

(C) Representative kymographs show activation of KHC-Halo by full-length JIP1, JIP1-TBD, or JIP1-SBD. 100 total frames (~33 seconds) are shown.

(D) Addition of full-length JIP1, JIP1-TBD, and JIP1-SBD increases the run frequency of full-length KHC-Halo. The absolute number of runs per 10 μm of microtubule was normalized to the KHC-Halo +JIP1 condition for each experiment. Data from Figs. 3D-3G represent 3 or more independent experiments per condition (n = 52-181 microtubules, n = 109-758 runs) and statistical comparisons were made relative to the KHC-Halo alone (no JIP1) condition unless otherwise indicated.

(E) Addition of full-length JIP1 or JIP1-TBD increases the relative frequency of non-motile microtubule-binding events by full-length KHC-Halo. The number of non-motile binding events per 10 μm microtubule length was normalized relative to the KHC-Halo +JIP1 condition for each independent experiment.

(F) Addition of full-length JIP1, JIP1-TBD or JIP1-SBD increases KHC-Halo run lengths.

(G) Addition of full-length JIP1 or JIP1-SBD but not JIP1-TBD increases speed of KHC-Halo runs.

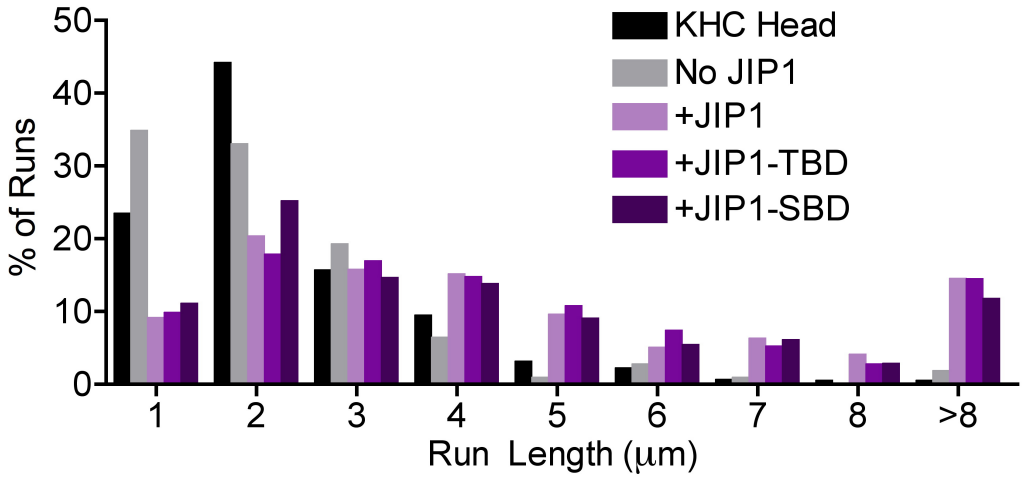

Figure 6. JIP1 binding to KHC increases run length *in vitro*.

Histograms of run length distributions for constitutively active KHC-head-Halo or KHC-Halo in the presence of JIP1, JIP1-TBD or JIP1-SBD in i*n vitro* TIRF motility assays. Data shown are pooled from 3 or more independent experiments per condition (n = 52-181 microtubules, n = 109-758 runs).

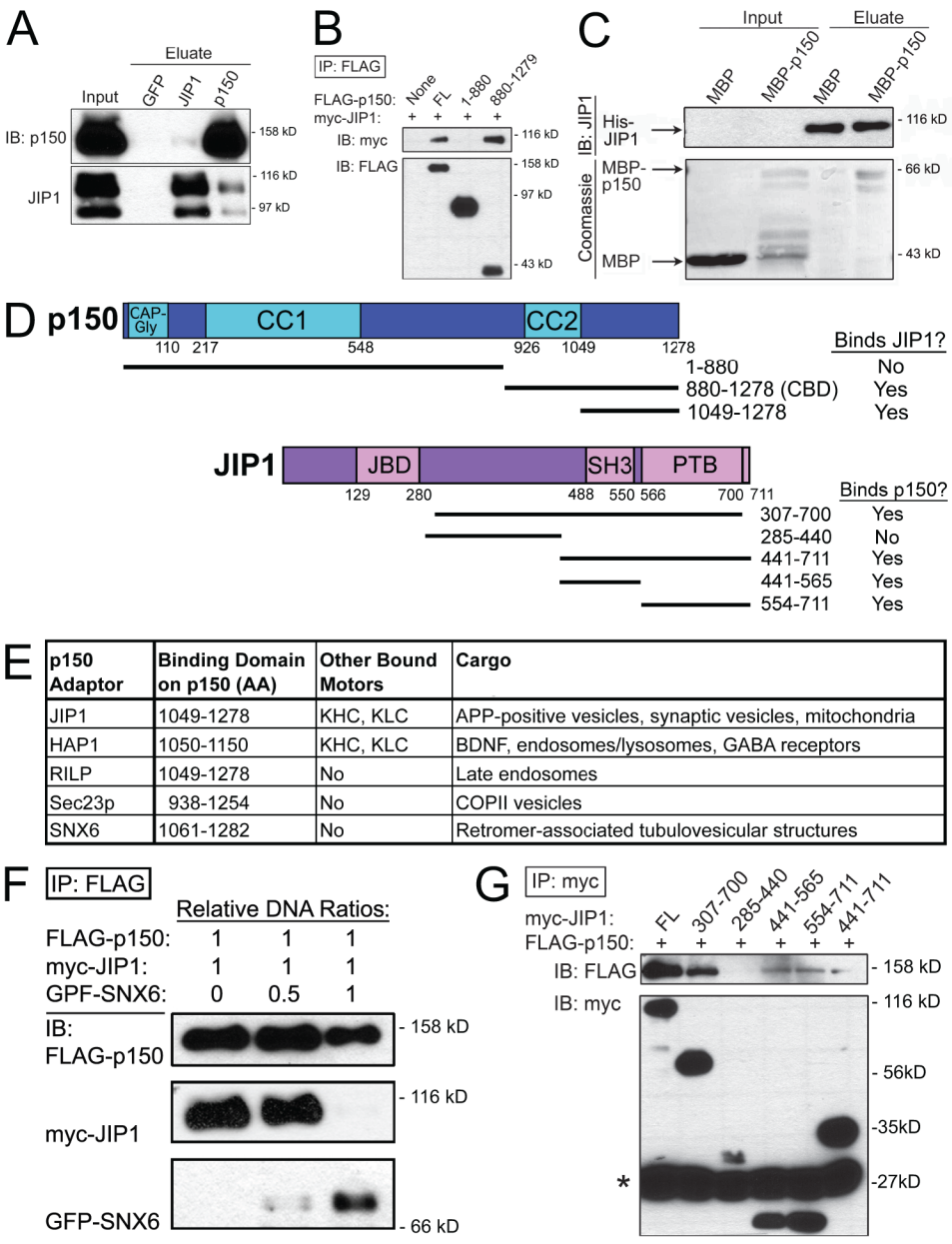

E

p150 Adaptor	Binding Domain on p150 (AA)	Other Bound Motors	Cargo
JIP1	1049-1278	KHC, KLC	APP-positive vesicles, synaptic vesicles, mitochondria
HAP1	1050-1150	KHC, KLC	BDNF, endosomes/lysosomes, GABA receptors
RILP	1049-1278	No	Late endosomes
Sec23p	938-1254	No	COPII vesicles
SNX6	1061-1282	No	Retromer-associated tubulovesicular structures

Figure 7. JIP1 binds directly to the p150^{Glued} subunit of dynactin.

(A) Endogenous JIP1 and p150^{Glued} co-immunoprecipitate from mouse brain homogenate.

(B) JIP1 binds to the C-terminal cargo-binding domain (CBD) of p150^{Glued}. Lysates from COS7 cells co-transfected with myc-JIP1 and FLAG-p150^{Glued} fragments were immunoprecipitated with an anti-FLAG antibody. JIP1 coimmunoprecipitated with C-terminal p150^{Glued}[880-1278], but not with N-terminal p150^{Glued}[1-880].

(C) JIP1 binds directly to C-terminal p150^{Glued}. When applied to His-Bind resin bound to His-JIP1, MBP-p150^{Glued}[1049-1278] selectively bound whereas MBP did not.

(D) Summary of $p150^{Glued}$ and JIP1 mapping results.

(E) A diverse set of cargo adaptors binds to $p150^{Glued}$-CBD.

(F) SNX6 and JIP1 bind competitively to $p150^{Glued}$. Lysates from COS7 cells transfected with fixed amounts of FLAG-p150 and myc-JIP1 DNA and progressively increasing amounts of GFP-SNX6 DNA were immunoprecipitated with anti-FLAG antibody. FLAG-p150 coimmunoprecipitates predominantly with myc-JIP1 in the low GFP-SNX6 condition, but mostly with GFP-SNX6 in the high GFP-SNX6 condition.

(G) C-terminal JIP1 binds to $p150^{Glued}$. Lysates from COS7 cells co-transfected with FLAG-$p150^{Glued}$ and myc-JIP1 fragments were immunoprecipitated with an anti-myc antibody. $p150^{Glued}$ coimmunoprecipitated with both myc-JIP1[441-565] and myc-JIP1[554-711]; the presence of both these domains in JIP1 (myc-JIP1[441-711]) did not strengthen the interaction. * = antibody light chain bands.

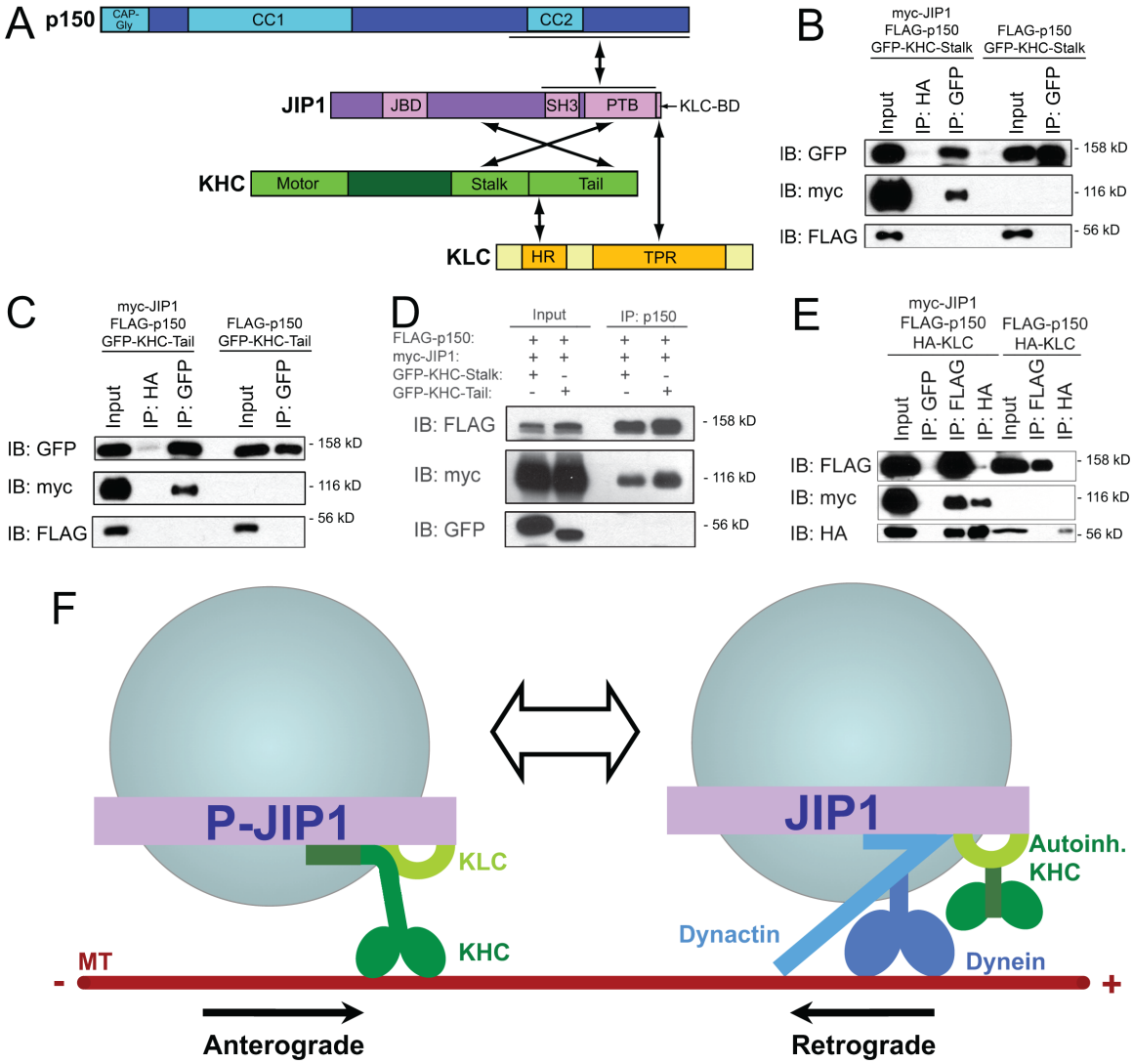

Figure 8. Anterograde and retrograde JIP1 motor complexes are mutually exclusive.

(A) Summary schematic of direct binding interactions between JIP1, Kinesin-1, and dynactin.

(B) JIP1 cannot bind simultaneously to both p150^{Glued} and KHC stalk. Lysates from COS7 cells triple transfected with myc-JIP1, FLAG-p150^{Glued} and GFP-KHC-stalk were immunoprecipitated with an anti-GFP antibody. FLAG-p150^{Glued} and GFP-KHC-stalk do not interact with each other either in the absence or presence of myc-JIP1.

(C) JIP1 cannot bind simultaneously to both p150^{Glued} and KHC tail. Lysates from COS7 cells triple transfected with myc-JIP1, FLAG-p150^{Glued} and GFP-KHC-tail were immunoprecipitated with an anti-GFP antibody. FLAG-p150^{Glued} and GFP-KHC-tail do not interact with each other either in the absence or presence of myc-JIP1.

(D) JIP1 cannot bind simultaneously to p150^{Glued} and KHC. Lysates from COS7 cells triple transfected with myc-JIP1, FLAG- p150^{Glued} and either GFP-KHC-tail or GFP-KHC-stalk were immunoprecipitated with an anti-p150^{Glued} antibody. Though robust levels of FLAG- p150^{Glued} and associated myc-JIP1 are co-immunoprecipitated, no interacting GFP-KHC-stalk or GFP-KHC-tail can be detected.

(E) JIP1 can bind simultaneously to both p150^{Glued} and KLC. Lysates from COS7 cells triple transfected with myc-JIP1, FLAG-p150^{Glued} and HA-KLC were immunoprecipitated with either an anti-FLAG or anti-HA antibody. In the absence of myc-JIP1, FLAG-p150^{Glued} and HA-KLC do not interact. The addition of myc-JIP1 facilitates the indirect interaction between p150^{Glued} and KLC as both FLAG and HA antibodies immunoprecipitate triple complexes of FLAG-p150^{Glued} myc-JIP1, and HA-KLC.

(F) Model of two mutually exclusive JIP1 motile complexes. The anterograde JIP1 complex activates KHC motility via direct binding to both stalk and tail domains (left) but cannot bind simultaneously to p150^{Glued}; KLC may remain bound via the C-terminal tail of JIP1 (Verhey et al., 2001). The retrograde JIP1 complex binds directly to p150^{Glued} to facilitate dynein-mediated transport and may retain autoinhibited KHC via simultaneous binding to KLC (right).

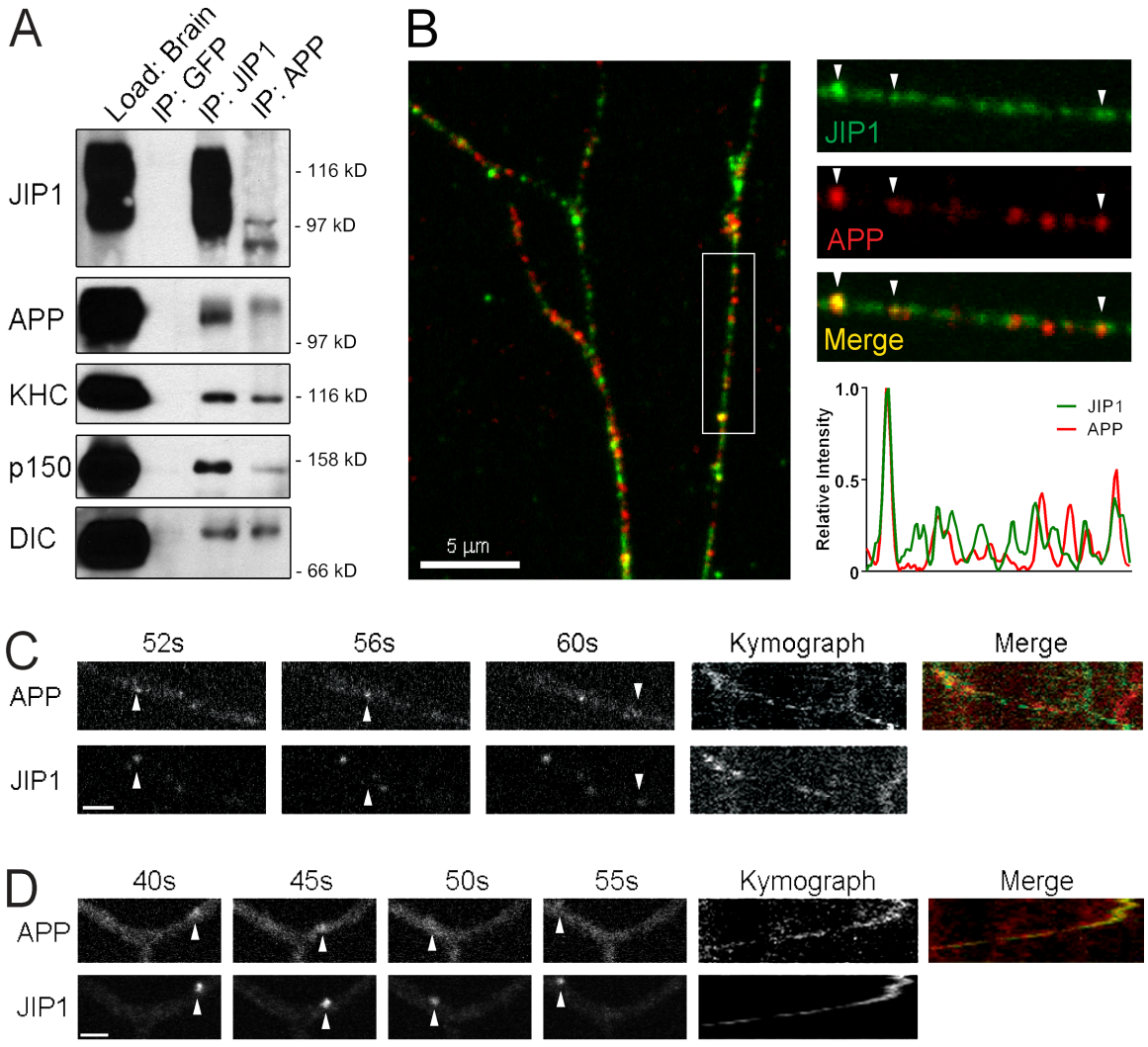

Figure 9. Endogenous APP and JIP1 form functional transport complexes with anterograde and retrograde motors.

(A) Endogenous JIP1 and APP coimmunoprecipitate with KHC, p150^{Glued} and DIC (dynein intermediate chain) in mouse brain homogenate. Interestingly, immunoprecipitation with a monoclonal APP antibody (Millipore 2C11) selectively co-immunoprecipitated the lower molecular weight band of JIP1.

(B) Endogenous JIP1 and APP colocalize on vesicles along axons in nontransfected DRGs. Representative images shows immunofluorescence staining of JIP1 (green) and APP (red). The boxed region is enlarged and analyzed by linescans to demonstrate individual vesicles on which JIP1 and APP are colocalized (arrowheads).

(C) Fluorescently tagged JIP1 and APP co-migrate on anterograde moving vesicles in DRGs. DRGs were transfected with APP-YFP and Halo-JIP1 and treated with red

HaloTag TMR ligand at 37˚C for 15 minutes and imaged at ~1 frame per second with a confocal microscope. Scale bar represents 2 μm.

(D) Fluorescently tagged JIP1 and APP co-migrate on retrograde moving vesicles in DRGs. DRGs were transfected with APP-dsRed and EGFP-JIP1 and imaged at 1 frame per second with a confocal microscope. Scale bar represents 2 μm.

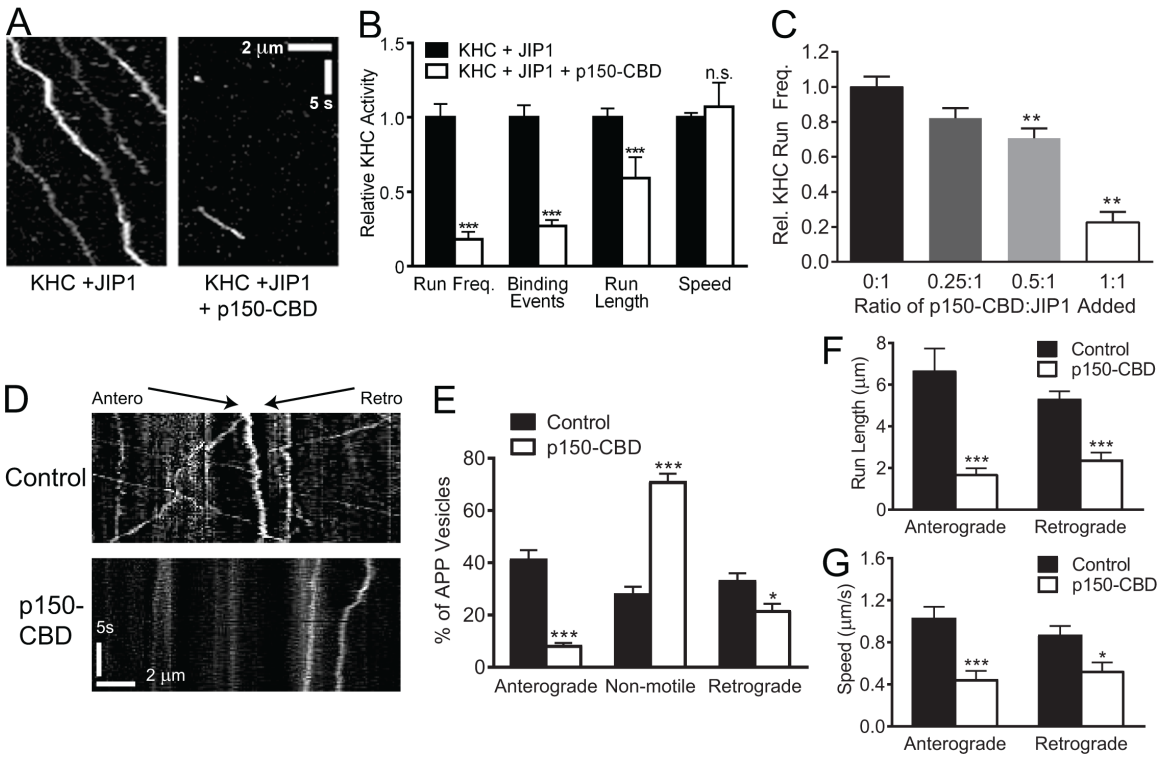

Figure 10. p150^{Glued}-CBD disrupts JIP1-mediated KHC motility *in vitro* and anterograde APP-positive vesicle transport in DRGs.

(A) Representative kymographs show that addition of p150^{Glued}-CBD disrupts enhancement of KHC-Halo motility by JIP1. Lysate from COS7 cells transfected with myc-JIP1 were combined with FLAG-p150^{Glued}-CBD lysate, then immediately combined with KHC-Halo lysate. This lysate mixture was applied to flow chambers containing immobilized fluorescent microtubules and imaged. 100 total frames (~33 seconds) are shown.

(B) Addition of p150^{Glued}-CBD decreases the number of motile KHC events mediated by JIP1. Motility measurements in the presence of FLAG-p150^{Glued}-CBD were normalized to the condition containing only myc-JIP1 and KHC-Halo and represent 3 independent experiments (n = 60-100 microtubules, n = 23-214 runs).

(C) p150^{Glued}-CBD competitively inhibits JIP1-mediated KHC motility *in vitro*. At constant levels of myc-JIP1 lysate, addition of incrementally higher levels of p150^{Glued}-CBD lysate leads to complementary decreases in relative KHC-Halo run frequency. Data represents 3 independent experiments (n = 6-52 microtubules).

(D) Kymographs of APP-DsRed motility in DRGs transfected with a bicistronic construct co-expressing FLAG-p150^{Glued}-CBD and GFP. ~80 total frames (~20 seconds) are shown.

(E) Expression of p150^{Glued}-CBD significantly decreases the percentage of anterograde APP-positive vesicles and correspondingly increases the percentage of arrested vesicles. Data from Figs. 10E-10G represent 4 independent experiments (n = 12-14 neurons).

(F, G) Expression of $p150^{Glued}$-CBD significantly decreases run length and speed of both anterograde and retrograde APP-positive vesicles. Means represent only vesicles categorized as motile (i.e. anterograde or retrograde in Fig. 10E).

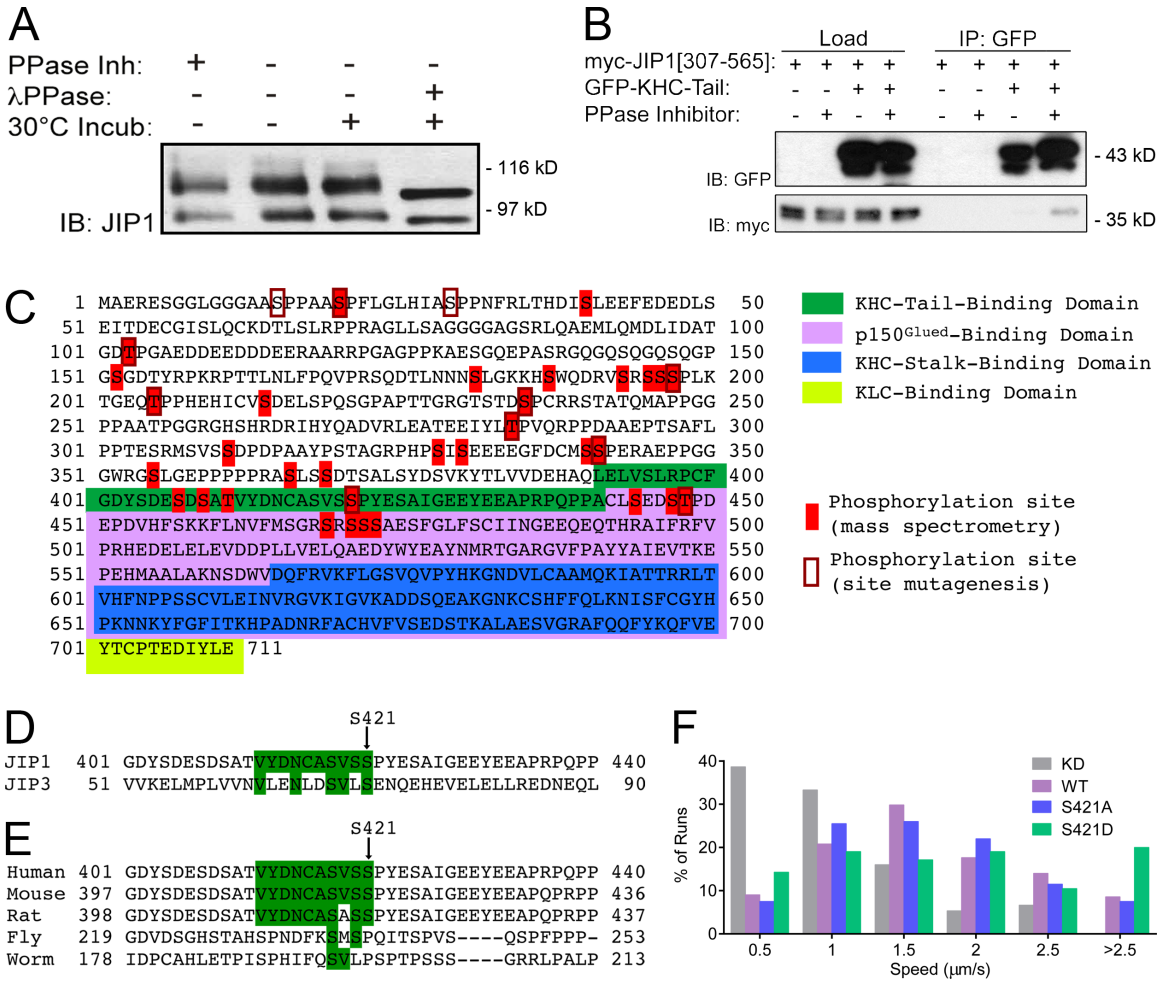

Figure 11. JIP1 Phosphorylation and KHC-Tail Binding

(A) JIP1 from mouse brain lysate is phosphorylated. Incubation of brain lysate at 30°C for 30 minutes with lambda phosphatase (200U per 100μg protein) dephosphorylates JIP1. Similar results were observed with alkaline phosphatase treatment (data not shown).

(B) KHC-tail preferentially binds to phosphorylated myc-JIP1[307-565]. Immunoprecipitation with an anti-GFP antibody of lysates of COS7 cells co-transfected with GFP-KHC-tail and myc-JIP1[307-565] selectively pulled down a phosphor-JIP1[307-565] band in the presence of phosphatase inhibitors.

(C) Summary of known phosphorylation sites in human JIP1. Phosphorylation sites identified by mass spectrometry (D'Ambrosio et a. 2005) are highlighted in red and those confirmed by site-directed mutagenesis to be directly phosphorylated by JNK *in vitro* (Nihalani et al. 2003) are boxed in red.

(D) The region around JIP1-S421 is heavily conserved in mammals.

(E) The region around JIP1-S421 may represent a 10-AA consensus motif for KHC binding, as it is 50% conserved in the minimal KHC-binding domain (AA50-80) of the motor adaptor protein JIP3.

(F) Histogram of APP speeds in neurons expressing JIP1 phosphomutants.
Data represents 3 independent experiments (n=7-9 neurons, n=78-224 runs).

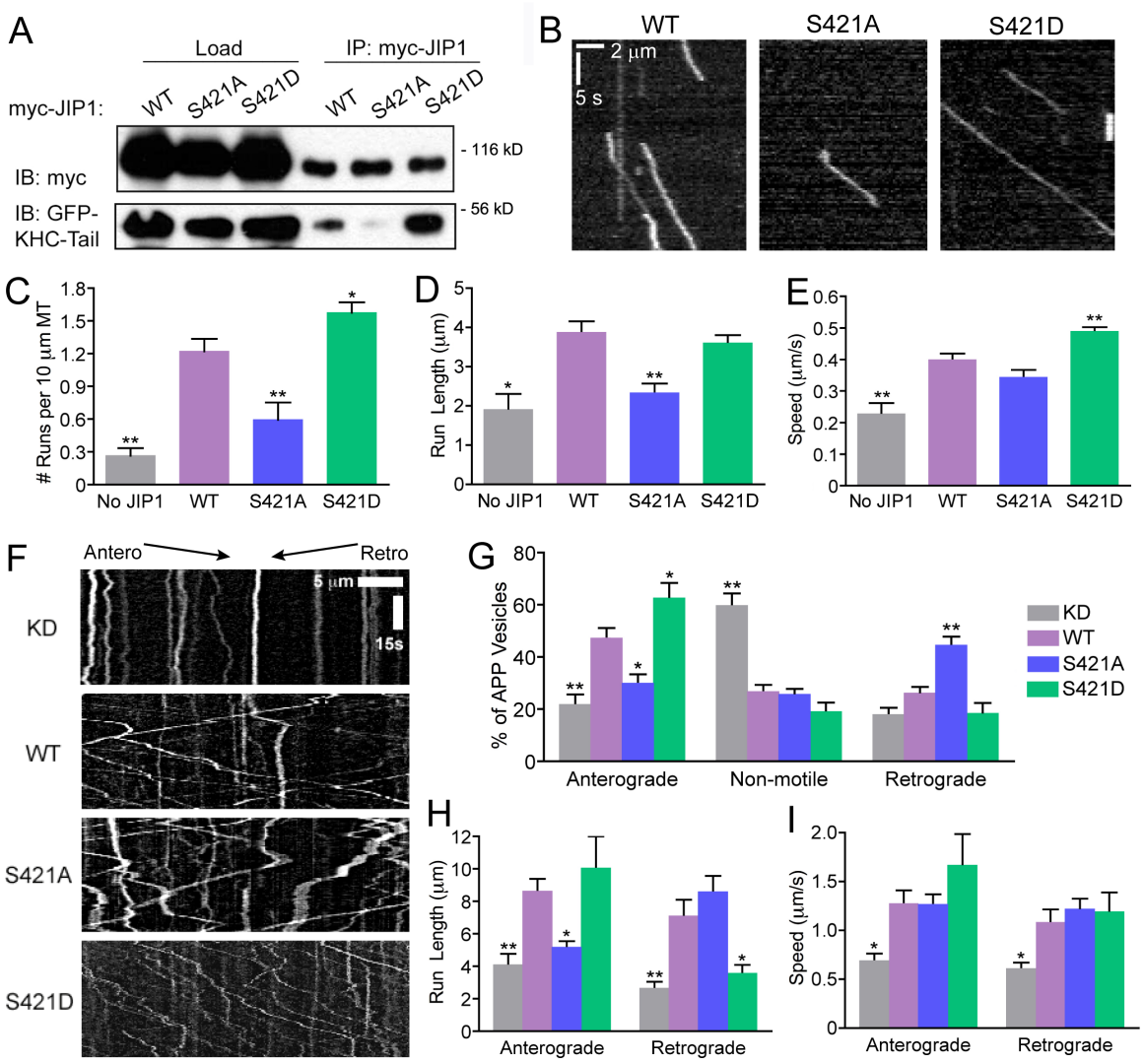

Figure 7. Mutations of the JNK phosphorylation site S421 in JIP1 alter KHC activation *in vitro* and APP directionality in neurons.

(A) Mutations at JIP1-S421 alter KHC tail binding ability. COS7 cells were co-transfected with GFP-KHC-tail and wildtype or mutant myc-JIP1 and immunoprecipitated with anti-myc antibody.

(B) Representative kymographs of KHC-Halo motility show weak activation by myc-JIP1-S421A and enhanced activation by myc-JIP1-S421D in *in vitro* motility assays. 100 total frames (~33 seconds) are shown.

(C) KHC-Halo run frequencies *in vitro* decrease in the presence of JIP1-S421A and increase in the presence of JIP1-S421D. Figs. 7C-7E represent data from 3 independent experiments (n=48-101 microtubules, n=18-254 runs) and statistical comparisons were made versus the wildtype JIP1 condition.

(D) KHC-Halo run length is decreased with addition of JIP1-S421A.

(E) KHC-Halo speed is increased with addition of JIP1-S421D.

(F) Representative kymographs of APP-YFP motility in DRGs transfected with siRNA targeted to mouse JIP1 and rescued with a bicistronic construct co-expressing human wildtype or mutant JIP1 as well as the fluorescent transfection marker BFP.

(G) DRGs expressing JIP1-S421D have increased percentages of anterograde APP vesicles while DRGs expressing JIP1-S421A have increased percentages of retrograde APP vesicles. Figs. 7G-7I represent data from 3 independent experiments (n=7-9 neurons, n=78-224 runs) with statistical comparisons made against the wildtype rescue condition.

(H) APP-positive vesicles in DRGs expressing JIP1-S421A have decreased anterograde run length while those expressing JIP1-S421D have decreased retrograde run length.

(I) No significant differences are observed in APP speeds in DRGs expressing JIP1-S421 phosphomutants.

DISCUSSION

Here, we examine the coordinated regulation of APP axonal transport by the scaffolding protein JIP1, which mediates the activity of both anterograde and retrograde motors via direct binding to KHC stalk and tail and the $p150^{Glued}$ subunit of dynactin. *In vitro* motility assays demonstrate that binding of JIP1 relieves autoinhibition of full-length KHC and enhances KHC processivity. Coimmunoprecipitations indicating that KHC and $p150^{Glued}$ cannot simultaneously bind to JIP1 led us to posit a model whereby JIP1 switches between two mutually exclusive conformations – an anterograde KHC-bound state and a retrograde $p150^{Glued}$-bound state. Indeed, binding of $p150^{Glued}$-CBD to JIP1 competitively disrupts enhancement of KHC motility by JIP1 *in vitro* and perturbs anterograde APP transport in neurons. Further, direct phosphorylation by JNK likely regulates the directional switching of JIP1, as phosphomimetic JIP1-S421D enhances KHC-tail binding and promotes anterograde APP axonal transport.

Direct binding of JIP1 to KHC stalk represents a novel mechanism for KHC activation by an adaptor protein. The flexibility of the stalk or hinge region of KHC was first observed in electron micrographs showing folding or bending of KHC (Hirokawa et al., 1989). A hingeless KHC mutant displays weak autoinhibition, moving with higher speeds than full-length KHC (Friedman and Vale, 1999), suggesting that the stalk is necessary for KHC bending and tail-to-head binding. Indeed, the minimal JIP1-binding domain that we identified for KHC stalk (AA560-682) overlaps with the truncated region in this hingeless KHC mutant (AA505-610). *In vitro*, binding of JIP1-SBD to KHC stalk enhances run frequency and speed. Thus, binding of JIP1 to

KHC stalk may conformationally restrain this flexible hinge region and hold KHC head and tail apart, effectively preventing KHC autoinhibition.

We find that both KHC stalk and tail interactions with JIP1 are necessary for maximal enhancement of KHC processivity, as addition of JIP1-TBD *in vitro* cannot increase KHC speed and JIP1-SBD does not enhance run lengths as efficiently as full-length JIP1. Consistent with the established stoichiometry that one KHC tail is sufficient to autoinhibit a motor head dimer (Hackney et al., 2009), the redundancy of multiple KHC binding sites on JIP1 may function to decrease the likelihood of full-length KHC returning to its autoinhibited conformation once bound to cargo. Moreover, the ability of JIP1 to dimerize via its SH3 domain (Kristensen et al., 2006) may allow recruitment of multiple Kinesin-1 motors onto a single APP-positive vesicle. This is consistent with the observation that long run lengths observed for APP in *Drosophila* are dependent on the activity of multiple KHCs (Reis et al., 2012) and with *in vitro* observations that increasing KHC motor number on a DNA scaffold correlates with increased run length (Derr et al., 2012; Furuta et al., 2013).

Though we have shown that direct binding of JIP1 to KHC is sufficient to activate motility *in vitro*, the majority of soluble Kinesin-1 in cells exists as a tetramer of KHC and KLC. Binding of KLC to KHC likely provides an additional layer of inhibition as addition of KLC decreases both microtubule binding (Blasius et al., 2007) and motility (Friedman and Vale, 1999) of KHC. In the presence of KLC, JIP1 is insufficient to activate KHC motility; activation of tetrameric Kinesin-1 requires an additional KHC-tail binding partner, FEZ1 (Blasius et al., 2007). JIP1 and FEZ1 may cooperate in a stepwise manner where initial binding of JIP1 to KLC and binding of FEZ1 to KHC tail overcomes KHC autoinhibition, thus priming KHC for binding to

JIP1, which then sustains anterograde transport via dual interactions with KHC stalk and tail.

Binding of JIP1 to KLC may also function to recruit Kinesin-1 to cargos. Several scaffolding proteins initially identified as KLC binding partners, including JIP3 (Bowman et al., 2000) and HAP1 (McGuire et al., 2006), also bind directly to KHC (Sun et al., 2011; Twelvetrees et al., 2010). Our biochemical observation that KLC and $p150^{Glued}$ can bind simultaneously to JIP1 is consistent with colocalization of KLC and dynein on APP vesicles in neurons (Szpankowski et al., 2012). Thus we propose that KLC may function to retain autoinhibited KHC on the organelle during retrograde transport (Fig. 5F), fitting recent experiments that show JIP1 KLC-BD can recruit Kinesin-1 to vesicles, but cannot activate transport (Kawano et al., 2012). The positioning of oppositely directed motors on the same scaffolding protein complex may function as a primed state that is poised for rapid transitions between retrograde and anterograde transport.

Together, our data support a model in which JIP1 phosphorylation regulates transport by switching between two distinct motile states. In contrast to an unregulated tug-of-war between opposing motors, mutually exclusive JIP1 motile complexes allow only one motor type to be active at any given time. Advantages to this regulatory scheme are twofold and particularly relevant in the extended axon. First, by avoiding frequent back-and-forth saltatory movement that is characteristic of the tug-of-war model, JIP1-coordinated transport can be sustained over long distances. Second, distinct anterograde and retrograde complexes confer directional bias for JIP1-associated cargos, promoting efficient transport in both directions.

These attributes are fully consistent with the observed transport of APP, as this cargo moves quickly for long distances in both anterograde and retrograde directions.

Previous studies have also correlated post-translational modifications of scaffolding proteins with directional transport changes, including phosphorylation of huntingtin in brain-derived neurotrophic factor (BDNF)-containing vesicles (Colin et al., 2008) and sumoylation of La in mRNA transport (van Niekerk et al., 2007). Here, we propose that direct phosphorylation of JIP1 by JNK acts as a molecular switch at the cargo level and affects changes in directionality of transport via direct alteration of motor binding affinities. Indeed, phosphomimetic JIP1-S421D shows enhanced binding to KHC tail and promotes anterograde APP transport while phosphodeficient JIP1-S421A has reduced binding to KHC tail and likely associates with the $p150^{Glued}$ to promote retrograde APP transport. Surprisingly, JIP1-S421A, which has an intact SBD, is unable to increase KHC run frequency and run length, in marked contrast to the robust effects of JIP1-SBD on KHC activation. This suggests phosphorylation of S421 may also indirectly regulate availability of C-terminal JIP1 for binding to KHC stalk, perhaps by inducing a conformation change that reveals the SBD. Though JIP1 S421 is directly phosphorylated by JNK *in vitro* (Nihalani et al., 2003) and synaptic vesicle transport in *Drosophila* relies on JNK and upstream kinases such as DLK (Horiuchi et al., 2007), further work will be required to directly correlate changes in JNK activity with changes in APP transport.

Finally, multiple levels of regulation may modulate APP transport *in vivo*. JIP1 can oligomerize and co-transport with JIP3 (Hammond et al., 2008), which does not directly bind to APP, but may facilitate APP transport by enhancing APP phosphorylation (Muresan and Muresan, 2005a), which in turn enhances the binding

of APP to JIP1 (Muresan and Muresan, 2005b). Furthermore, reduction of endogenous GSK3 levels can enhance both anterograde and retrograde APP transport, likely via changes in microtubule acetylation and stability (Weaver et al., 2013).

The molecular mechanism described here for the regulation of APP transport by JIP1 raises many further questions. Does JIP1 regulate the transport of other cargos along the axon? How might the mechanism for JIP1-mediated transport of APP described here affect Aβ production and Alzheimer's Disease pathology? While further work will be required to address these questions, our observations at both cellular and single molecule levels establish JIP1 as a coordinator of axonal transport that regulates transport directionality by alternating between anterograde and retrograde motile states. These new mechanistic insights further support a critical role for scaffolding proteins in the coordination of kinesin and dynein motor activity in the cell.

CHAPTER 3

JIP1 Facilitates Retrograde Autophagosome Transport in Axons via Associations with LC3 and Dynactin

Meng-meng Fu wrote this chapter and performed all experiments.

ABSTRACT

Autophagy is an essential function in neurons as disruption of autophagosome formation in transgenic animals leads to selective neurodegeneration. Neurons are highly polarized cells with axons that extend up to one meter in humans. In the axon, autophagosomes undergo unidirectional retrograde transport with <1% anterograde motility, yet the mechanism for this robust directional bias is unknown. We previously demonstrated that the motor scaffolding protein JIP1 (JNK-interacting protein 1) regulates both anterograde and retrograde transport of APP by alternatingly binds to either the anterograde motor kinesin or to the dynactin activator of the retrograde dynein motor in a phosphorylation dependent manner. We now describe the association of autophagosomes with the motor scaffolding protein JIP1 using coimmunoprecipitation, immunostaining, and organelle purification techniques. Preliminary studies indicate that the mechanism for JIP1 association with autophagosomes is via binding to the autophagosome adaptor LC3, likely through a conserved LIR motif in JIP1. Live-cell imaging of primary neurons shows that JIP1 knockdown does not disrupt autophagosome formation at the distal tips of axons. However, in wildtype neurons expressing mCherry-JIP1, newly formed autophagosomes are initially negative for JIP1 but become JIP1-positive and then move out of the distal axon tip, suggesting that recruitment of JIP1 is necessary for retrograde transport initiation. Thus, to determine whether JIP1 facilitates retrograde autophagosome transport, we knocked down JIP1 and observed in the mid-axon that the percentage of stationary autophagosomes doubled while the percentage of retrograde autophagosomes decreased from 72% to 39%, concurrent with significant deficits in retrograde speed and run length. Next, we performed rescue experiments with our previously characterized mutants at the JNK-dependent

phosphorylation site S421. Phosphodeficient JIP1-S421A robustly rescued retrograde autophagosome transport. In contrast, neurons expressing phosphomimetic JIP1-S421D, which enhances kinesin binding, increased the percentage of anterograde autophagosomes tenfold. Collectively, these experiments indicate that an interaction with LC3 may recruit JIP1 to autophagosomes, where JIP1 regulates retrograde motor function. Moreover, misregulation of JIP1 phosphorylation can lead to aberrant changes in the direction of autophagosome transport in the axon, which may be a precursor to neurodegeneration.

INTRODUCTION

Protein quality control plays an important role in cellular homeostasis; in addition to the ubiquitin-proteasome pathway, it also involves macroautophagy, or "bulk eating", the process by which misfolded or aggregated proteins and defective organelles are selectively targeted for degradation. Macroautophagy (henceforth referred to as autophagy) differs from chaperone-mediated autophagy (CMA), a substrate-specific mechanism for the degradation of select proteins. Autophagy is a constitutive process, but can be regulated in response to cellular cues such as starvation (Yorimitsu and Klionsky, 2005).

The fidelity of the autophagic process may be particularly relevant in the neuron for two reasons. First, as a post-mitotic cell, accumulation of misfolded proteins and organelles can become toxic. Second, neurons are highly polarized cells with extended axons and this extreme cell morphology may present a spatial challenge in the clearance of proteins and organelles from these extremities. Indeed, transgenic knockout animals for the Atg7 (autophagy-related 7) gene accumulate polyubiquitinated proteins and inclusion bodies in the brain and develop selective neurodegeneration (Komatsu et al., 2006), suggesting that autophagy is an essential function in neurons. Moreover, defects in autophagy have been observed in many neurodegenerative diseases, including Alzheimer's disease, Parkinson's disease, Huntingtin's disease and amyotrophic lateral sclerosis (ALS) or Lou Gehrig's disease (Wolfe et al., 2013).

Recently, two studies characterized the axonal transport of autophagosomes in primary neurons. Autophagosomes form in the distal axon tip, where they undergo

bidirectional transport in the distal axon and then move in a unidirectional retrograde manner in the mid-axon. The recruitment of the late endosome and lysosome markers Rab7 and LAMP1 may underlie this switch to processive motility. In the mid-axon, autophagosomes rarely experience pauses or switches in direction and move quickly with speeds of ~0.4 um/s toward the cell body (Maday et al., 2012). This characteristic unidirectional retrograde transport is unlike the movement of other vesicles in the axon, such as LAMP1-positive lysosomes, APP-positive vesicles, and mitochondria, which all move in both anterograde and retrograde directions (Fu and Holzbaur, 2013; Morris and Hollenbeck, 1993; Moughamian and Holzbaur, 2012).

Nevertheless, the mechanism for the robust retrograde motility of autophagosomes in axons has not been established. What is known in term of motor association to autophagosomes is that the microtubule motor kinesin can associate with authophagosomes via the adaptor protein FYCO1 (Pankiv et al., 2010). Additionally, several autophagy receptors are able to link myosin VI to autophagosomes in a process that is important for subsequent autophagosome maturation and fusion with lysosomes (Tumbarello et al., 2012). Though a role for FYCO1 or optineurin in regulating axonal transport of autophagosomes has not been shown, the motor likely responsible for retrograde transport is the minus-end directed microtubule motor dynein.

A candidate mediator between autophagosomes and the retrograde motor dynein is the scaffolding protein JIP1. We have previously shown that JIP1 can bind directly to the $p150^{Glued}$ subunit of the dynein activator dynactin. Though JIP1 has the

additional ability to bind KHC stalk and tail to activate motor activity, it exists either as an anterograde motor complex or a retrograde motor complex. Indeed, binding to $p150^{Glued}$ disrupts the ability of JIP1 to activate KHC, which is a robust mechanism for sustaining retrograde transport.

Here, we demonstrate JIP1 association with autophagosomes via immunostaining, live-cell colocalization, and organelle purification techniques. Preliminary experiments indicate that JIP1 may associate with autophagosomes by binding to the autophagosome adaptor LC3 via a conserved LIR motif. While knockdown of JIP1 does not affect autophagosome formation in the distal axon tip, it severely disrupts retrograde transport of autophagosomes in the mid-axon. Moreover, we previously demonstrated that phosphorylation of JIP1 at S421 enhances KHC tail binding and robustly promotes anterograde transport. Knockdown and rescue experiments with these mutants indicate that while the phosphodeficient JIP1-S421A robustly rescues retrograde autophagosome transport, the phosphomimetic JIP1-S421D leads to aberrant movement of autophagosomes in the anterograde direction. These results suggest that JIP1 association to autophagosomes is important in sustaining retrograde transport of autophagosomes and that this is likely a regulated process.

MATERIALS AND METHODS

Cell culture and transfection

Dissected adult mouse dorsal root ganglion (DRGs) were treated with papain, collagenase, and dispase II then centrifuged through a 20% Percoll gradient (Perlson et al., 2009). Isolated DRGs were transfected using Amaxa Nucleofector SCN Program 6 (Lonza) and plated on glass-bottom microwell dishes (FluoroDish, World Precision Instruments) that were pre-coated with poly-L-lysine and laminin. DRGs were maintained in F-12 media (Invitrogen) with 10% FBS, 2 mM L-glutamine, 100 U/mL penicillin, and 100 µg/mL streptomycin. For co-migration assays, DRGs were transfected with mCherry-JIP1. For JIP1 knockdown and rescue experiments, neurons from GFP-LC3 mice were transfected with DY-547-conjugated siRNA and pBI-CMV2(BFP)-JIP1(WT, S421A, or S421D).

Live-cell imaging

Cultured DRGs were imaged at 2 DIV in Hibernate A low-fluorescence medium (Brain Bits) inside a 37°C imaging chamber. Double- or triple-fluorescent neurons were observed at 63x using a Leica DMI6000B microscope with a CTR7000 HS control box run by Leica AF6000 software and a Hamamatsu C10600 Orca-R2 camera. Images of autophagosome transport and biogenesis were acquired at 1–3 s per frame for 3–5 minutes.

Vesicle tracking and analysis

Transport of LC3-positive vesicles in the mid-axon were analyzed by generating 75-µm kymographs (at least 100 µm away from the soma or the distal axon tip) using Metamorph software. Motile particles (e.g. anterograde or retrograde) were defined

as particles with net displacement greater than 10 μm. Speed and run length are defined as net velocity and displacement of a single autophagosome. The neuron was defined as the biologically relevant unit and motility parameters were averaged for each neuron and subject to subsequent statistical analysis.

Immunofluorescence

Culture DRGs were grown on glass coverslips and fixed with 4% paraformaldehyde, permeabilized with 0.1% Triton X-1000, incubated for 1 hour in blocking solution (5% goat serum and 1% BSA), and then incubated with primary monoclonal antibodies against JIP1 (B-7 Santa Cruz), and LC3 (MBL Japan) followed by incubation with species-specific fluorescent secondary antibodies.

Co-immunoprecipitations

COS7 cells transfected using Fugene6 (Roche) according to manufacturer's instructions were harvested 18-24 hours post-transfection and lysed using 0.5% Triton X-100 (in HEM buffer). Lysates were incubated with Protein-G Dynabeads (Invitrogen) and co-immunoprecipitations were performed following manufacturer's instructions using a monoclonal anti-myc antibody (Invitrogen). All coimmunoprecipitations represent at least 2 independent experiments.

Organelle Purification

Autophagosome-enriched fractions were prepared from wildtype adult mouse brains following previously described protocol (Maday et al., 2012). BCA assays were performed on all resulting fractions to ensure equal loading. Fractions were separated on 7% SDS-PAGE (15% for LC3) and immunoblotted with antibodies directed against LC3 (Abcam), JIP1 (B-7 Santa Cruz), $p150^{Glued}$ (BD Transduction),

and DIC (Chemicon).

Statistical analysis

Statistical analysis was performed using Student's t-test or one-way ANOVA with post-hoc Tukey's test. For JIP1 mutant experiments, we used post-hoc Dunnett's Test, comparing against the control wildtype JIP1 rescue condition. Bar graphs were plotted as mean ± SEM and the following denotations for statistical significance were used: * $p<0.05$, ** $p<0.01$, *** $p<0.001$, n.s. (not significant).

RESULTS

JIP1 Knockdown Disrupts Transport of Rab7-Positive Vesicles

Previously, we characterized the role of JIP1 in regulating the anterograde and retrograde transport of APP-positive vesicles. In immunostaining experiments of wildtype primary dorsal root ganglion (DRG) neurons, we observed that JIP1 puncta colocalize with APP puncta. However, a number of large JIP1-positive puncta did not co-localize with APP (Fu and Holzbaur, 2013), leading to our initial hypothesis that JIP1 serves as a scaffolding protein that mediates the axonal transport of other organelles as well.

To address this question, we took the initial approach of knocking down endogenous expression of mouse JIP1 using a targeted siRNA that we previously confirmed to deplete >90% of JIP1 in 48 hours with no detectable off-target effects. We electroporated red fluorescently tagged siRNA and a construct expressing EGFP-Rab7, a marker for late endosomes and lysosomes, and imaged motility in the mid-axon of doubly fluorescent neurons for 3 minutes (Fig. 1A). First, we quantified the number of Rab-positive vesicles in the mid-axon and found that JIP1 knockdown did not affect the number of Rab7-positive vesicles (Fig. 1B).

Next, we generated kymographs in order to analyze the motion of Rab7-positive vesicles in axons. In control neurons, the majority of Rab7-positive vesicles exhibit stationary or bidirectional motility, which we define here as having net displacement less than 10 um, while the remaining ~25% of Rab7-positive vesicles move in the

retrograde direction, defined by net displacement greater than 10um. By the same definition for motility, few Rab7-positive vesicles move in the anterograde direction. Upon JIP1 depletion, the percentage of retrograde-moving vesicles decreased significantly by about threefold ($p<0.001$), concurrent with an increase in the percentage of stationary or bidirectional vesicles ($p<0.001$, Fig. 1C).

Further analysis of the motile fraction of Rab7-positive vesicles revealed that average run length and speed did not change significantly following JIP1 knockdown (Fig. 1D and 1E). These unaltered measures of motility suggest that a sub-population of retrograde Rab7-positive vesicles are unaffected by JIP1 knockdown and likely associate with the retrograde motor complex via a JIP1-independent mechanism. This is consistent with the existence of alternate scaffolding proteins known to associate with Rab7-positive vesicles and with retrograde motors, including Rab7-positive lysosomal protein (RILP) and Snapin. Thus, these results indicate that JIP1 depletion arrests the retrograde transport of a sub-population of Rab7-positive vesicles.

JIP1 Associates with Autophagosomes

Previous work from our lab has demonstrated that retrograde-moving axonal autophagosomes co-localize with lysosomal-assoiated membrane protein 1 (LAMP1), a marker for late endosomes and lysosomes (Maday et al., 2012). Moreover, autophagosomes move in characteristically unidirectional retrograde manner, similar to the observed motility of retrograde Rab7-positive vesicles. Thus, we hypothesized that the subpopulation of Rab7-positive vesicles affected by JIP1 knockdown are autophagosomes. As a preliminary step, we stained non-transfected wildtype DRGs

for endogenous JIP1. We observed that large JIP1-positive puncta co-localized with LC3-positive puncta along the axon as well as at the distal axonal tip (Fig. 2A), indicating that JIP1 associates with autophagosomes in nontransfected neurons. Moreover, live-cell imaging of DRGs co-transfected with mCherry-LC3 and EGFP-JIP1 shows that LC3 and JIP1 co-migrate on autophagosomes that move in the retrograde direction (Fig. 2B), suggesting that JIP1 associates with retrograde-moving autophagosomes.

In addition, we purified autophagosomes from wildtype adult mouse brains using a three-step differential centrifugation protocol (Maday et al., 2012). We verified that this fraction indeed contains autophagosomes by blotting against LC3, which either exists as a membrane-bound lipidated LC3-II that resolves at a lower molecular weight (~14 kDa) or cytoplasmic LC3-I that resolves at a higher molecular weight (~16 kDa). We found that the final concentrated autophagosome fraction is preferentially enriched in both lipidated LC3-II. Moreover, when compared to crude homogenates (total starting material) and cytosol, purified autophagosomes also contain elevated levels of high-molecular-weight JIP1 (~110 kDa), while lower-molecular-weight JIP1 is not enriched (Fig. 2C, Lane 2). This result suggests that differentially spliced isoforms of JIP1 may perform different functions in the cell. Consistent with this idea, we previously characterized in coimmunoprecipitatons from crude brain homogenate that APP preferentially associates with the lower molecular weight band of JIP1 (Chapter 2, Figure 9A).

In mice, JIP1 has three isoforms. Isoform 1 is the longest with 707 AAs; Isoform 2 (698 AAs) and Isoform 3 (673 AAs) differ from Isoform 1 in the 5′ UTR, resulting in a different transcription initiation site and distinct and shorter N-termini. Alignment of

all three isoforms shows that they are identical after the first 77 amino acids of Isoform 1 (Figure 2C). These splice sites are consistent with antibody mapping experiments, which show that monoclonal antibodies directed against regions of JIP1 beyond the first 77 amino acids all recognize at least two distinct JIP1 bands (Fig. 2D). Interestingly, the CAD neuronal cell line predominantly expresses higher molecular weight JIP1 (Chapter 2, Fig. 1B), suggesting that this may be a neuronally enriched form of JIP1.

Moreover, motif scanning of JIP1 Isoform 1 identified four predicted myristoylation sites, all of which are absent in Isoform 3 and two of which are absent in Isoform 2 (Fig. 2E). Consistent with defined properties of myristoylation, these motifs are heavily enriched in glycines, which are the points of attachment for myristoyl groups, and located at the N-terminus of protein that likely relies on methionine-initiated translation. This suggests that high-molecular-weight JIP1 may undergo myristoylation, perhaps as a mechanism for vesicular membrane attachment. To confirm these myristoylation sites, we will like pursue a mass spectrometry approach to initially determine whether any or all sites are modified.

Purification of autophagosomes involved excluding mitochondrial fractions, which surprisingly contained very little JIP1, dynein intermediate chain (DIC) and the $p150^{Glued}$ subunit of dynactin. Previously, *Drosophila* embryos expressing a mutant form of the JIP1 homolog APLIP1 (APP-like interacting protein 1) displayed marked reduction in unidirectional retrograde mitochondrial transport (Horiuchi et al., 2005). Thus, our result that mitochondria lack JIP1 may indicate that the pool of mitochondria displaying retrograde transport defects in *Drosophila* may actually be mitochondria-containing autophagosomes (mitophagosomes). In order to address

whether JIP1 is involved in transport of mitophagosomes, I plan to knockdown JIP1 expression in DRGs with red fluorescent siRNA and then image the co-transport of Mito-SBFP in GFP-LC3 mice. Currently, our lab is in the process of generating and testing the Mito-SBFP construct, which is a derivative of the commonly used Mito-DsRed marker.

JIP1 Binds to the Autophagosome Adaptor LC3

JIP1 associates with APP-positive vesicles via direct binding to APP, which is a transmembrane protein. However, it is unclear how JIP1 may specifically associate with autophagosomes. Previously, the autophagosome adaptor FYCO1 was demonstrated to mediate transport of autophagosomes by binding to kinesin and to LC3 via a conserved LIR (LC3 interaction region) motif (Pankiv et al., 2010).

Thus, to detect whether JIP1 associates with autophagosomes via an interaction with LC3, we performed coimmunoprecipitations in COS7 cells co-transfected with GFP-LC3 and myc-JIP1 fragments. In cell lysates, the majority of GFP-LC3 is cytoplasmic, though a lower-molecular-weight band that likely represents lipidated GFP-LC3 is also visible. An anti-myc antibody pulled down full-length myc-JIP1 as well as GFP-LC3. The C-terminal fragments myc-JIP1[445-565] and myc-JIP1[554-711] did not coimmunoprecipitate GFP-LC3. However, the N-terminal truncation myc-JIP1[307-711] robustly co-immunoprecipitated GFP-LC3, as did the C-terminal truncation myc-JIP1[1-390], though to a lesser extent (Fig. 3A). These two constructs overlap in a ~80-AA region spanning JIP1[307-390], indicating that this may be a putative LC3-binding domain.

Indeed, this region of JIP1 contains a well-conserved predicted LIR motif (Fig. 3B). LIR motifs are short and follow the convention X_3-X_2-X_1-W/F-X_1-X_2-L, where X typically represents acidic residues (von Muhlinen et al., 2012). Because the putative JIP1 LIR motif contains the aromatic residue phenylalanine, it is an F-type LIR motif, which is often flanked by serines, as is the case here. The biochemistry underlying the ability of the LIR motif to bind to LC3 is well characterized. The acidic residues of the LIR motif interact with basic residues (R10 and R11) in N-terminal LC3 while the aromatic residue and lysine bind to hydrophobic pockets in LC3. These elements, including four consecutive acid residues, are all well-conserved in the putative mammalian JIP1 LIR.

To definitively prove that JIP1 binds directly to LC3, I plan to express GST-LC3 in *E. coli* and perform binding assays with purified protein. In addition, we are currently generating a LIR-deletion mutant to determine whether this area is necessary for LC3 transport; if this is the case, I will perform JIP1 knock down and rescue experiments in primary DRGs to characterize the effect of the LIR-deletion mutant on autophagosome transport.

Biogenesis of Autophagosomes Does Not Require JIP1

Previous work from our lab demonstrated that biogenesis of axonal autophagosomes in primary DRGs occurs in the distal axonal tips. Since we demonstrated that JIP1 associates with LC3 (Fig. 3A), we initially wanted to determine whether this interaction is necessary for autophagosome formation. Using time-lapse live-cell confocal microscopy of primary DRGs cultured from GFP-LC3 mice and transfected with JIP1 siRNA, we observed many autophagosome formation and enlargement

events in the distal axon tip. Initially, small punctate LC3-positive structures become visible and then gradually enlarge to form a ring-like structure, perhaps indicative of the double-membrane architecture of autophagosomes. These events occur on the timescale of several minutes (Fig. 4A), consistent with published data.

A static indicator of autophagosome formation is the total number of autophagosomes present in the distal axon tip, which we measured and normalized to the surface area of each axon tip. We found that JIP1 depletion did not significantly alter the distribution of autophagosomes in the axon tip (Fig. 4B), further confirming that initial formation of autophagosomes does not depend on JIP1.

Processive Retrograde Autophagosome Transport in the Mid-Axon Requires JIP1

Finally, we addressed whether the role of JIP1 in autophagy is to sustain robust retrograde transport in the mid-axon. We used targeted red fluorescent siRNA to knock down endogenous mouse JIP1 in primary DRGs dissected from GFP-LC3 mice and rescued with a bicistronic construct co-expressing resistant human JIP1 cDNA as well as a BFP transfection marker. Live-cell confocal imaging in the mid-axon of triple-fluorescent neurons ensured that every cell analyzed was indeed knocked down and rescued. We subsequently generated 75-μm kymographs (Fig. 5A) and categorized motile autophagosomes as those having net displacement greater than 10 μm and stationary or bidirectional autophagosomes as those having less than 10 μm of net displacement in a three-minute movie.

We found that knockdown of JIP1 significantly decreased the percentage of

retrograde autophagosomes from ~70% to ~40%, concurrent with a significant increase in the percentage of stationary or bidirectional autophagosomes from ~30% to 60% (Fig. 5B). Moreover, characterization of autophagosomes that continued to move in the retrograde direction in JIP1-depleted neurons indicates that they have significantly shorter net displacements and slower net speeds than autophagosome from control neurons (Fig. 5C and 5D). These reductions indicate that almost half of autophagosomes requires JIP1 for robust retrograde transport and that autophagosomes continuing to move in the retrograde direction in absence of JIP1 display slow speeds and short run lengths.

In addition, we tested the effects of rescuing with our JNK phosphomutants. Previously, we showed that the phosphomimetic JIP1-S421D increases binding to KHC tail in order to preferentially enhance anterograde APP axonal transport while the phosphodeficient JIP1-S421A preferentially enhances retrograde APP axonal transport. In autophagosome axonal transport, JIP1-S421A sufficiently rescued the percentage of retrograde autophagosomes as well as restored their net run lengths and speeds (Figs. 5B–D). This suggests that nonphosphorylated JIP1 likely regulates retrograde transport of autophagosomes. In contrast, JIP1-S421D expression decreased the percentage of retrograde autophagosomes to ~20% (Fig. 5B) and these retrograde-moving autophagosomes move with reduced net displacement (Fig. 5C). Moreover, typically <1% of autophagosomes move in the anterograde direction in the mid-axon, but neurons expressing JIP1-S421D displayed an unusually high percentage (~10%) of anterograde autophagosome transport. Moreover, the majority of autophagosomes in the JIP1-S421D-expressing neurons (~70%) are stationary or bidirectional (Fig. 5B). This suggests that phosphorylation of JIP1 at S421 not only disrupts normal retrograde autophagosome transport but also may

aberrantly activate kinesins, resulting in a high incidence of anterograde autophagosome transport.

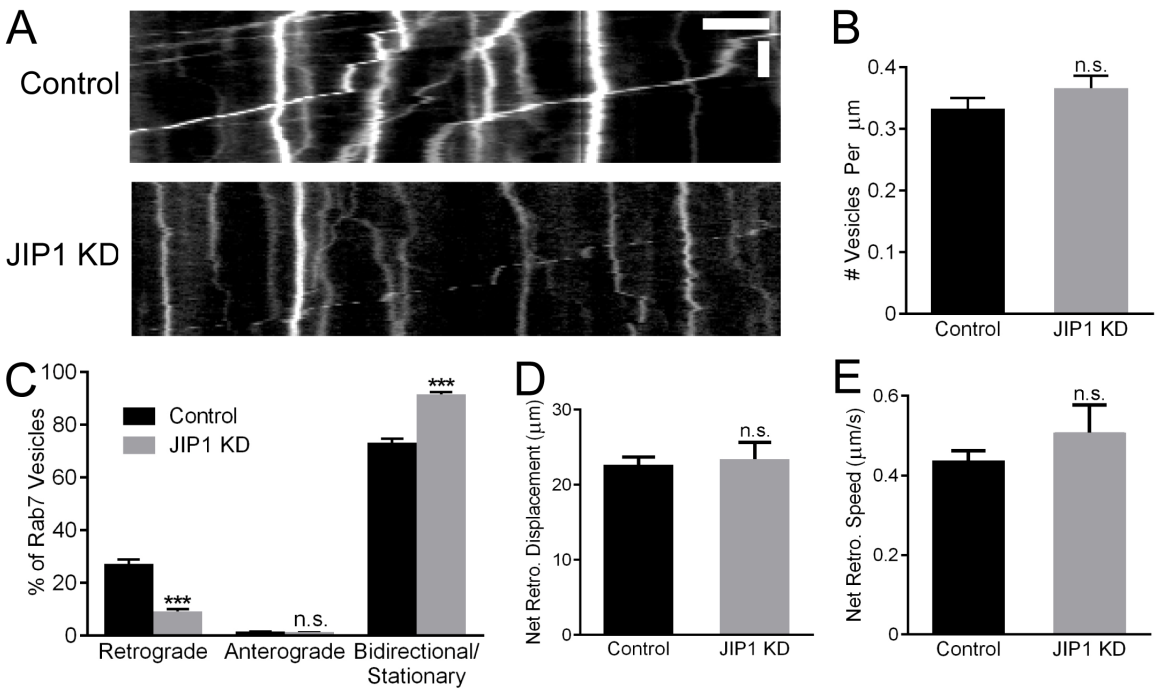

Figure 1. JIP1 Knockdown Disrupts Transport of Rab7-Positive Vesicles

(A) Representative kymographs of EGFP-Rab7-positive late endosome and lysosome motility in DRGs transfected with JIP1 siRNA. Kymographs represent motion as displacement along the axon (x-axis) over time (y-axis). Data represents three independent experiments (n = 13–16 neurons).

(B) JIP1 knockdown did not affect the number of EGFP-Rab7-positive vesicles in the axons of DRGs.

(C) JIP1 knockdown significantly alters the retrograde motility of EGFP-Rab7-positive vesicles and concurrently increases the percentage of bidirectional and stationary Rab7-positive vesicles in the axons of DRGs.

(D and E) JIP1 knockdown did not affect the net retrograde displacement or speed of EGFP-Rab7-positive vesicles that remained motile.

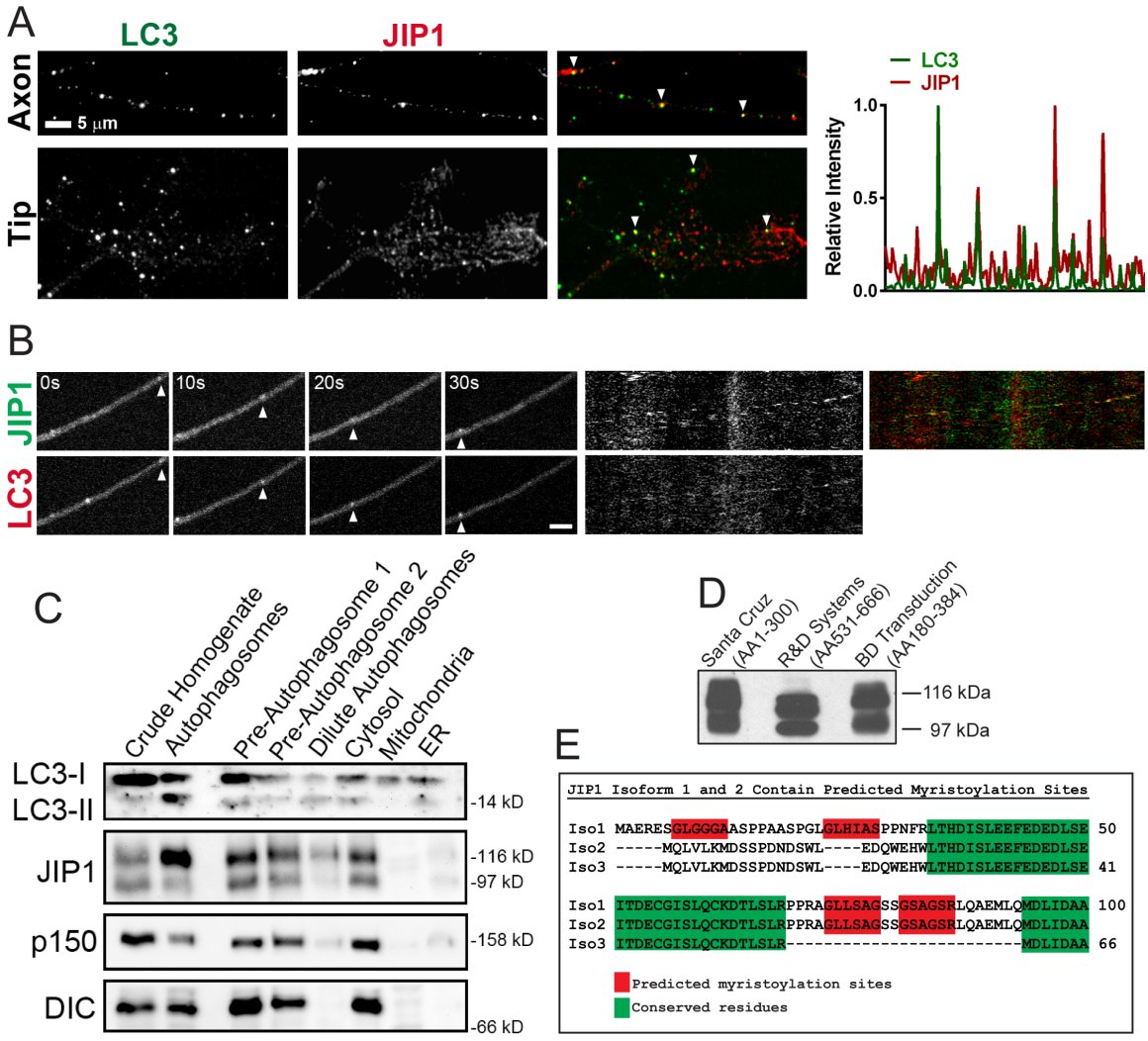

Figure 2. JIP1 Associates with Autophagosomes.

(A) Endogenous JIP1 and LC3 colocalize on vesicles along axons (top) and in distal axon tips (bottom) of nontransfected DRGs (arrowheads). Representative images show immunofluorescence staining of LC3 (green) and JIP1 (red).

(B) Fluorescently tagged mCherry-LC3 and EGFP-JIP1 co-migrate on retrograde moving autophagosomes in DRGs. DRGs co-transfected with EGFP-JIP1 and mCherry-LC3 were imaged on a confocal microscope.

(C) High-molecular-weight band of JIP1 is enriched in purified autophagosomes. Briefly, four mouse brains were homogenized, and subject to Nycodenz and Percoll gradient separations, which yielded “Pre-Autophagosome” fractions, then “Dilute Autophagosome” fractions, and finally

the purified “Autophagosome” fraction; discarded fractions enriched for cytosol, mitochondria and peroxisomes, and the endoplasmic reticulum (ER).

(D) Crude homogenate from mouse brains were subject to immunoblotting with three separate monoclonal antibodies generated against different epitopes of JIP1, which all detected two distinct bands.

(E) The longer isoforms of JIP1 contain 2-4 predicted myristoylation sites. JIP1 has 3 isoforms which are identical past the first 77 amino acids. However, at the N-terminus are 4 predicted myristoylation sites that are alternatively spliced.

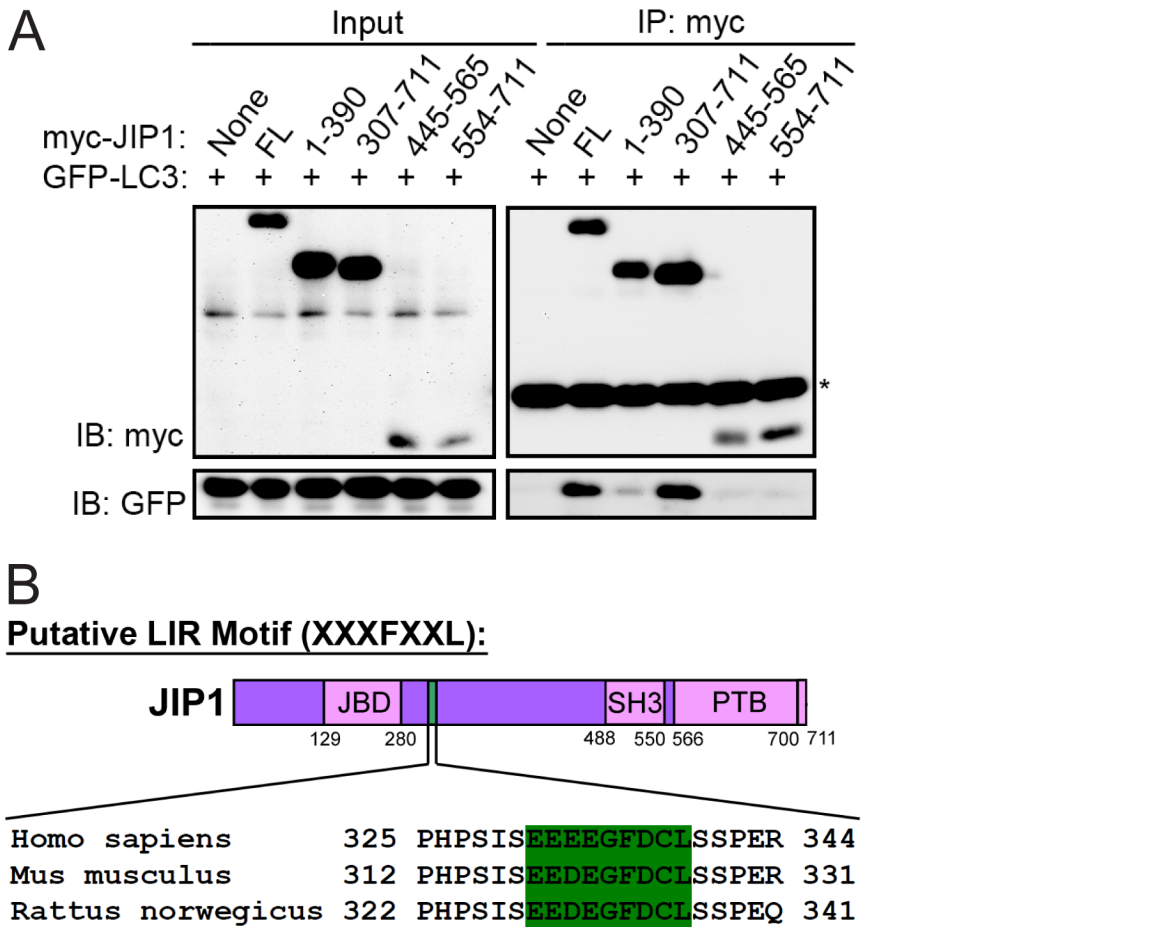

Figure 3. JIP1 Binds to the Autophagosome Adaptor LC3.

(A) JIP1 Binds to LC3. Lysates from COS7 cells co-transfected with GFP-LC3 and fragments of myc-JIP1 were immunoprecipitated with an anti-myc antibody. Both full length myc-JIP1 as well as myc-JIP1[1-390] and myc-JIP1[307-711] coimmunoprecipitated GFP-LC3. Asterisk denotes antibody light chain.

(B) JIP1 contains a predicted LIR (LC3-interaction region) motif. This EEEEGFDCL motif is conserved in mammalian JIP1 and has contains the three components that define LIR motifs and function to mediate binding to LC3 – a central aromatic phenylalanine residue, a lysine residue at the C-terminus and a high density of acidic residues.

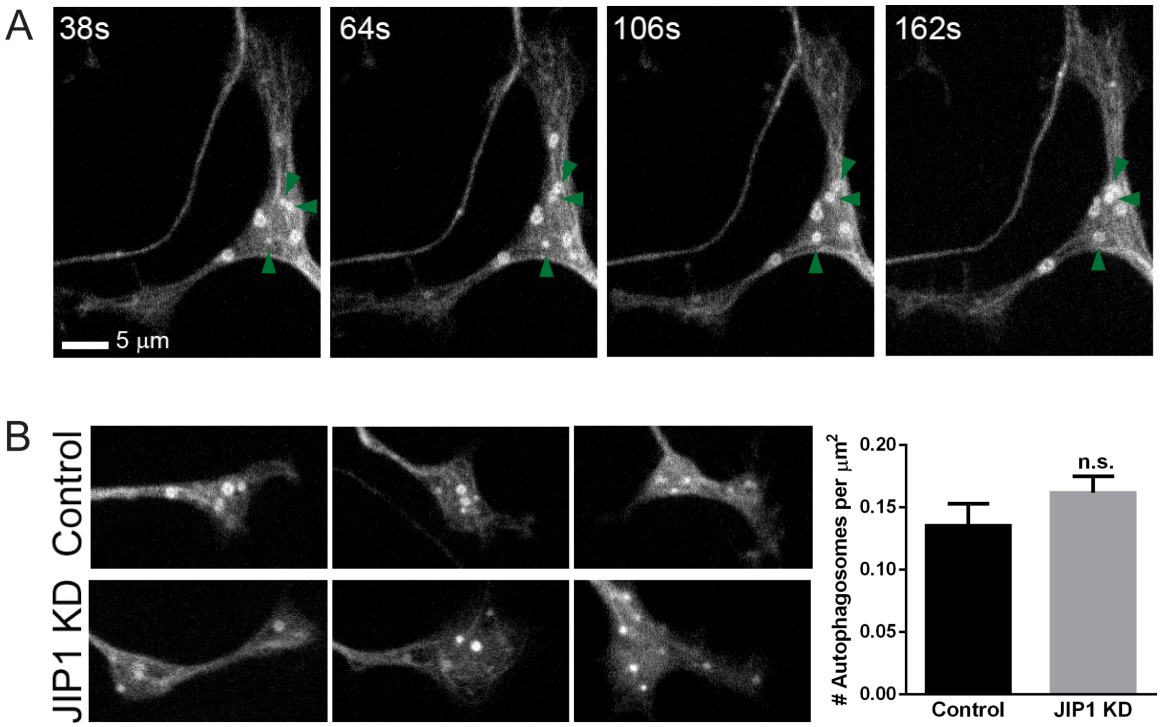

Figure 4. Biogenesis of Autophagosomes Does Not Require JIP1.

(A) Time-lapse imaging of autophagosome formation in the distal axon tip of a DRG transfected with JIP1 siRNA. Autophagosome biogenesis proceeds from a small punctate structure and gradually enlarges into a ring-like structure (arrowheads).

(B) JIP1 knockdown does not perturb the number of autophagosomes in the distal axon tip. The density of autophagosomes in DRGs transfected with JIP1 siRNA did not differ significantly ($p = 0.23$) from control neurons. Data represents three independent experiments (n = 18–22 neurons).

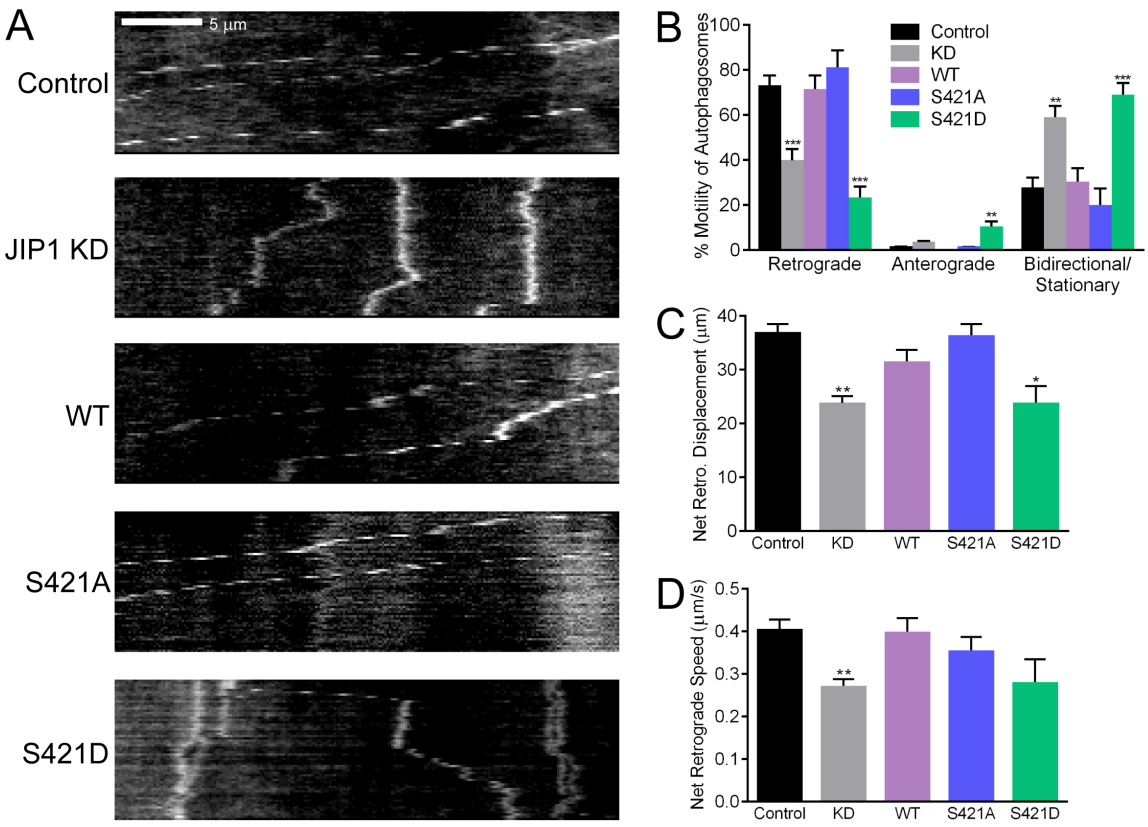

Figure 5. Processive Retrograde Autophagosome Transport in the Mid-Axon Requires JIP1.

(A) Representative kymographs of GFP-LC3 autophagosome motility in mouse DRGs transfected with JIP1 siRNA and rescued with resistant human cDNA. Kymographs represent motion as displacement along the axon (x-axis) over time (y-axis).

(B) JIP1 knockdown significantly decreased the percentage of retrograde-moving autophagosomes and increased the percentage of stationary or bidirectional autophagosomes. Rescue with both wildtype human JIP1 as well as with the S421A phosphodeficient mutant restores retrograde autophagosome transport, but the S421D phosphomimetic mutant does not and increases the percentage of anterograde autophagosome transport. Data represents three independent experiments (n = 7–16 neurons); statistical comparisons were made against the control condition.

(C and D) JIP1 knockdown decreased the net retrograde displacement and speed of autophagosomes that remained motile. Rescue with the S421D mutant also led to decreased net retrograde displacement.

DISCUSSION

We have characterized the association of JIP1 with autophagosomes using several different technique. While JIP1 knockdown does not disrupt autophagosome formation, it severely disrupts retrograde autophagosome transport in the mid-axon. Moreover, while the phosphodeficient JIP1-S421A mutant rescues retrograde autophagosome transport, the phosphomimetic JIP1-S421D actually results in aberrant anterograde transport of autophagosomes. These results suggest that dynein recruitment and activation proceeds through a regulated pathway.

Moreover, we present hypotheses and preliminary evidence suggesting that distinct sites in the JIP1 protein may play important roles in associating with autophagosomes. Confirmation that JIP1 binds to LC3 via a LIR motif will establish a direct link for JIP1 association to autophagosomes. Rather than recruiting cytosolic scaffolding proteins onto vesicular cargo, myristoylation sites at the N-terminus may function to tether a pool of JIP1s onto vesicular cargo. Pre-primed vesicular JIP1 may contribute to more efficient recruitment of cytosolic motors as it decreases the number of steps necessary for assembly of a full scaffolding complex.

Interestingly, autophagosomes purified from brains associate with both dyneins and kinesins. Because few anterograde runs normally are observed in the mid-axon, kinesins associated with autophagosomes are likely in an autoinhibited state. Coincidentally, JIP1 that is bound to $p150^{Glued}$ in the retrograde motor complex is able to bind simultaneously to KLC (Fu and Holzbaur, 2013) and this may be a mechanism for retaining autoinhibited kinesin on the autophagosome.

Biochemical quantization measurements indicate that multiple dyneins are found on a single endosome or lysosome (Hendricks et al., 2010). Moreover, in optical trapping experiments of phagosomes in a rodent macrophage cell line, robust retrograde transport correlates with high stall forces, consistent with high motor numbers of cargo-associated dynein (Hendricks et al., 2012; Rai et al., 2013).

Thus, recruitment of dynein to retrograde organelles, such as Rab7-positive vesicles and autophagosomes, likely involves multiple scaffolding proteins. In addition to JIP1, autophagosomes may also associate with the scaffolding protein Rab7-interacting lysosomal protein (RILP), which also recruits $p150^{Glued}$, as well as Snapin, which recruits dynein via dynein intermediate chain (DIC). In fact, Snapin-deficient neurons show dramatic disruption of Rab7-positive vesicle transport in the axon. In our experiments, Rab7-positive vesicles display mostly stationary or bidirectional transport (~75%) and only ~25% retrograde transport (Fig. 1C). In contrast, autophagosomes positive for GFP-LC3 display robust retrograde transport (~70%) with only ~30% stationary or bidirectional events (Fig. 5C). This difference suggests that autophagosomes have enhanced ability to recruit retrograde motors, perhaps via multiple associations to JIP1, RILP, and Snapin. Consistent with this idea that different scaffolding proteins cooperate to recruit many dyneins to each retrograde vesicle, knockdown of any one of these scaffolding proteins can lead to significant disruption of retrograde transport.

Many questions remain in the regulation of autophagosome transport. In addition to the role of retrograde scaffolding proteins in regulating dynein association to autophagosomes, kinesins as wells myosin can associate with autophagosomes as well (Pankiv et al., 2010; Tumbarello et al., 2012) and the interplay between these

different classes of motors and their corresponding adaptors has not been explored. Indeed further understanding of the molecular mechanisms underlying autophagosome transport may lead to clinical insights into why they fail in neurodegenerative diseases.

CHAPTER 4

Conclusions and Future Directions

THE CONTROVERSY BEHIND APP TRANSPORT

Several facets of APP transport have been and continue to be topics of controversy. A paper published over ten years ago demonstrated impaired APP transport in KLC-deficient mice, which lead to the suggestion that APP transport is mediated via direct binding to the tetratricopeptide repeat (TPR) domain of KLC (Kamal et al., 2000). However, a number of laboratories were unable to repeat this result, which has been attributed to nonspecific binding of recombinant proteins (Lazarov et al., 2005). Our current understanding supports a model whereby a complex of proteins, including JIP1, FEZ1, KLC, and KHC facilitate the anterograde transport of APP. The C-terminus of the transmembrane protein APP is exposed on the surface of vesicles, allowing it to attach to this complex via direct binding to JIP1 (Matsuda et al., 2001; Scheinfeld et al., 2002), which then indirectly links APP to KLC and KHC. Recent genetics evidence indicates that polymorphisms at the C-terminus of APP near its JIP1-binding site are protective against Alzheimer's Disease (Jonsson et al., 2012), though it is not understood whether this relates to APP transport.

Contrary to our findings, a recently published paper concluded that JIP1 knockdown does not affect APP axonal transport (Vagnoni et al., 2013). Several technical differences exist between our paper and this paper. First, we used primary adult mouse DRGs imaged at DIV3 while the Vagnoni et al. paper used embryonic rat cortical neurons imaged at DIV8. While we used electroporation to deliver siRNAs and DNAs, Vagnoni et al. used magnetic nanoparticles as their method of transfection. But perhaps most importantly, imaging parameters differed greatly. We imaged APP motility at 4 frames per second, or every 250 ms (with exposure durations of ~150 ms), while Vagnoni et al. imaged at 1 frame per second (with

unknown exposure time). We determined our frame rate to be optimal for capturing the motility of APP-positive vesicles, which are small and move quickly with speeds ~1 μm/s.

Most importantly, we observed vesicular APP transport while Vagnoni et al. observed tubular APP transport. Though small vesicular APP are visible in supplemental video from Vagnoni et al., we have never observed tubular APP in our DRG culture system, suggesting that tubules may be artifacts of fluorescent protein overexpression or unique to cortical neurons. Moreover, staining of endogenous APP in DRGs also shows punctate, not tubular staining (Chapter 2, Fig. 9B). Interestingly, these tubular APPs move at incredibly high speeds of >4 μm/s, making them the fastest tracked cargo in axons. This may have interesting mechanistic implications as kinesins move with maximum speeds ~1 μm/s *in vitro* and increasing motor number per cargo is not expected to increase speed (Derr et al., 2012; Furuta et al., 2013). Moreover, our vesicular APP speeds are consistent with vesicular APP speeds observed in primary hippocampal neurons (Stokin et al., 2005) whereas the higher APP speeds observed by Vagnoni et al. are consistent with published speeds of tubular APP transport using long exposures and slow frame rates (Kaether et al., 2000).

Furthermore, the connection between tubule intensity and imaging parameters is unclear. For example, a 5-μm long tubule moving at 4 μm/s will appear on a kymograph from one frame to the next as a 5-μm intensity in one frame followed by a 4-μm gap then a 5-μm intensity in the next frame, which could be visually difficult to resolve and analyze. Thus to follow up on the nature of tubulated APP, I plan to perform immunostaining of endogenous APP and to image APP-YFP dynamics in

primary cortical neurons.

KEY QUESTIONS IN CARGO-BASED TRANSPORT REGULATION

The Stoichiometry of Scaffolding Proteins and Motors

The majority of scaffolding proteins exists as dimers. This dimerization may serve two functions – to relieve autoinhibition efficiently via binding to both tails in the KHC dimer and/or to recruit two kinesin dimers. Careful biochemical determination of these binding relationships using full-length wildtype as well as dimerization-deficient mutant scaffolding proteins will indicate whether dimeric scaffolding proteins accomplish one or both of these functions.

However, these experiments present several technical challenges. First, scaffolding proteins are large and by definition have multivariate domains, making them difficult to express recombinantly, as discussed earlier. Second, generation of a dimerization-deficient mutant by taking a deletion approach would result in a much shorter protein and can lead to misfolding issues and result in nonfunctional proteins. This is a nuanced problem, as final demonstration of function necessitates the use of these dimerization-deficient proteins in *in vitro* motility assays, but it is nearly impossible to distinguish a null result (i.e. the mutant scaffolding protein does not affect motor function) from a nonfunctional misfolded protein.

An alternative approach of identifying key residues at the dimer interface and then generating point mutants may be difficult too. Previously, point mutations in the SH3 domain of JIP1 unambiguously abolished the ability of JIP1 to dimerize (Kristensen et al., 2006). Initially, we confirmed the result that the SH3 domain is necessary and sufficient for dimerization of JIP1 using coimmunoprecipitation of JIP1

truncations containing either myc or FLAG tags (data not shown). However, after several requests, we were unable to obtain these published mutant constructs. Thus, we generated one of the published dimerization-deficient mutants using site-directed mutagenesis of a wildtype JIP1 construct and showed that this does not alter JIP1 dimerization (data not shown).

Finally, direct demonstration that altering the number of scaffolding proteins on a vesicle or organelle results in motility changes in cellular cargos would resolve the decades-old question of why *in vitro* single molecule motor properties differ from organelle transport. This could be elegantly demonstrated using purified organelles *in vitro* motility assays as well as via direct demonstration in cells. Specifically, kinesins have run lengths of ~1–2 μm while most cargos have run lengths of >5 μm.

How Do Multiple Scaffolding Proteins on the Same Cargo Interact?

Certain cargos have multiple sets of adaptors. For mitochondria, Milton/Miro has been demonstrated to bind to kinesin as well as to $p150^{Glued}$ (Glater et al., 2006; van Spronsen et al., 2013). In addition, the syntaphilin anchoring protein has recently been demonstrated to also bind to kinesin. In this system, a model exists for how kinesin interaction with both Milton/Miro and syntaphilin results in observed changes in mitochondrial motility. However, this model has not incorporated the involvement of the retrograde motor.

In autophagosome transport, several adaptor proteins may be present. Snapin was demonstrated to bind to DIC and mediate lysosomal transport. It is possible that as

organelles transition from one identity to another, either via GTPase recruitment such as of Rab proteins or via vesicular fusion, that different scaffolding proteins predominate. For example, LAMP1-positive autolysosomes may rely heavily on Snapin whereas earlier less mature Rab7-positive autophagosomes may rely on JIP1. Certainly, as endosomes mature from Rab5-positive early endosomes to Rab7-positive late endosomes, they display marked changes in transport from bidirectional runs to sustained retrograde runs (Deinhardt et al., 2006), perhaps indicative of an enhanced ability to recruit RILP.

Do Scaffolding Proteins Play a Role in Circumnavigating Road Blocks?

One suggested function of bidirectional transport is to navigate around roadblocks. This may be particularly relevant in the axon, which is spatially crowded due to its cable-like structure. Single molecule experiments show that dynein is able to remain bound to the microtubule when it encounters patches of tau (Dixit et al., 2008). Thus, anterograde kinesin-associated cargos may benefit from having associated dyneins, which have the molecular toolkit of sidestepping onto adjacent protofilaments as well as reversing in direction. Moreover, if dyneins are spatially distant from kinesins on the vesicle, this would allow dyneins to associate with adjacent microtubules as well. Indeed, high resolution imaging of axonal transport revealed that cargos are capable of switching microtubule tracks (Mudrakola et al., 2009).

Another facet of this question is how retrograde transport is sustained on separate microtubule tracks. A single microtubule is unlikely to extend from the centrosome in the soma to the distal axon and this is supported by imaging of EB3 comet tails

that label growing microtubule plus ends, which are numerous and dynamic in the axon. Thus, many microtubules likely overlap and form from acentrosomal structures in the axon and a retrograde cargo that moves to the minus-end of a microtubule must re-initiate transport on another microtubule in order to sustain retrograde motion. This process has not been explicitly validated in axons and it is unclear whether scaffolding proteins play a role.

In conclusion, scaffolding proteins may play complex and pivotal roles in transport, many of which are not well understood at present. In order to dissect the molecular mechanisms underlying their facilitation of efficient transport, many technically advanced and multidisciplinary approaches must be considered. Elucidation of transport regulation from this perspective will not only improve our understanding of axonal transport, but may carry over to other specialized cells that rely on transport, such as pancreatic beta cells, podocytes in the kidney, and myelinating oligodendrocytes and Schwann cells.

BIBLIOGRAPHY

Abe, N., A. Almenar-Queralt, C. Lillo, Z. Shen, J. Lozach, S.P. Briggs, D.S. Williams, L.S. Goldstein, and V. Cavalli. 2009. Sunday driver interacts with two distinct classes of axonal organelles. *J Biol Chem*. 284:34628-34639.

Arimoto, M., S.P. Koushika, B.C. Choudhary, C. Li, K. Matsumoto, and N. Hisamoto. 2011. The Caenorhabditis elegans JIP3 Protein UNC-16 Functions As an Adaptor to Link Kinesin-1 with Cytoplasmic Dynein. *J Neurosci*. 31:2216-2224.

Baas, P.W., J.S. Deitch, M.M. Black, and G.A. Banker. 1988. Polarity orientation of microtubules in hippocampal neurons: uniformity in the axon and nonuniformity in the dendrite. *Proc Natl Acad Sci U S A*. 85:8335-8339.

Blasius, T.L., D. Cai, G.T. Jih, C.P. Toret, and K.J. Verhey. 2007. Two binding partners cooperate to activate the molecular motor Kinesin-1. *J Cell Biol*. 176:11-17.

Bowman, A.B., A. Kamal, B.W. Ritchings, A.V. Philp, M. McGrail, J.G. Gindhart, and L.S. Goldstein. 2000. Kinesin-dependent axonal transport is mediated by the sunday driver (SYD) protein. *Cell*. 103:583-594.

Bray, D., and M.B. Bunge. 1981. Serial analysis of microtubules in cultured rat sensory axons. *Journal of neurocytology*. 10:589-605.

Burton, P.R., and J.L. Paige. 1981. Polarity of axoplasmic microtubules in the olfactory nerve of the frog. *Proc Natl Acad Sci U S A*. 78:3269-3273.

Cai, D., K.J. Verhey, and E. Meyhofer. 2007. Tracking single Kinesin molecules in the cytoplasm of mammalian cells. *Biophysical journal*. 92:4137-4144.

Carter, A.P., C. Cho, L. Jin, and R.D. Vale. 2011. Crystal structure of the dynein motor domain. *Science*. 331:1159-1165.

Cavalli, V., P. Kujala, J. Klumperman, and L.S.B. Goldstein. 2005. Sunday Driver links axonal transport to damage signaling. *J Cell Biol*. 168:775-787.

Caviston, J.P., and E.L. Holzbaur. 2009. Huntingtin as an essential integrator of intracellular vesicular trafficking. *Trends Cell Biol*. 19:147-155.

Caviston, J.P., J.L. Ross, S.M. Antony, M. Tokito, and E.L. Holzbaur. 2007. Huntingtin facilitates dynein/dynactin-mediated vesicle transport. *Proc Natl Acad Sci U S A*. 104:10045-10050.

Caviston, J.P., A.L. Zajac, M. Tokito, and E.L. Holzbaur. 2011. Huntingtin coordinates the dynein-mediated dynamic positioning of endosomes and lysosomes. *Mol Biol Cell*. 22:478-492.

Chen, Y., and Z.H. Sheng. 2013. Kinesin-1-syntaphilin coupling mediates activity-dependent regulation of axonal mitochondrial transport. *J Cell Biol*. 202:351-364.

Colin, E., D. Zala, G. Liot, H. Rangone, M. Borrell-Pages, X.J. Li, F. Saudou, and S. Humbert. 2008. Huntingtin phosphorylation acts as a molecular switch for anterograde/retrograde transport in neurons. *EMBO J*. 27:2124-2134.

Courchet, J., T.L. Lewis, Jr., S. Lee, V. Courchet, D.Y. Liou, S. Aizawa, and F. Polleux. 2013. Terminal Axon Branching Is Regulated by the LKB1-NUAK1 Kinase Pathway via Presynaptic Mitochondrial Capture. *Cell*. 153:1510-1525.

D'Ambrosio, C., S. Arena, G. Fulcoli, M.H. Scheinfeld, D. Zhou, L. D'Adamio, and A. Scaloni. 2006. Hyperphosphorylation of JNK-interacting protein 1, a protein associated with Alzheimer disease. *Mol Cell Proteomics*. 5:97-113.

Dahlstrom, A.B. 2010. Fast intra-axonal transport: Beginning, development and post-genome advances. *Progress in neurobiology*. 90:119-145.

Dajas-Bailador, F., E.V. Jones, and A.J. Whitmarsh. 2008. The JIP1 scaffold protein regulates axonal development in cortical neurons. *Curr Biol*. 18:221-226.

Deinhardt, K., S. Salinas, C. Verastegui, R. Watson, D. Worth, S. Hanrahan, C. Bucci, and G. Schiavo. 2006. Rab5 and Rab7 control endocytic sorting along the axonal retrograde transport pathway. *Neuron*. 52:293-305.

Derr, N.D., B.S. Goodman, R. Jungmann, A.E. Leschziner, W.M. Shih, and S.L. Reck-Peterson. 2012. Tug-of-war in motor protein ensembles revealed with a programmable DNA origami scaffold. *Science*. 338:662-665.

Dickens, M., J.S. Rogers, J. Cavanagh, A. Raitano, Z. Xia, J.R. Halpern, M.E. Greenberg, C.L. Sawyers, and R.J. Davis. 1997. A cytoplasmic inhibitor of the JNK signal transduction pathway. *Science*. 277:693-696.

Dietrich, K.A., C.V. Sindelar, P.D. Brewer, K.H. Downing, C.R. Cremo, and S.E. Rice. 2008. The kinesin-1 motor protein is regulated by a direct interaction of its head and tail. *Proc Natl Acad Sci U S A*. 105:8938-8943.

Dixit, R., J.L. Ross, Y.E. Goldman, and E.L. Holzbaur. 2008. Differential regulation of dynein and kinesin motor proteins by tau. *Science*. 319:1086-1089.

Elie-Caille, C., F. Severin, J. Helenius, J. Howard, D.J. Muller, and A.A. Hyman. 2007. Straight GDP-tubulin protofilaments form in the presence of taxol. *Curr Biol*. 17:1765-1770.

Encalada, S.E., L. Szpankowski, C.H. Xia, and L.S. Goldstein. 2011. Stable kinesin and dynein assemblies drive the axonal transport of mammalian prion protein vesicles. *Cell*. 144:551-565.

Engelender, S., A.H. Sharp, V. Colomer, M.K. Tokito, A. Lanahan, P. Worley, E.L. Holzbaur, and C.A. Ross. 1997. Huntingtin-associated protein 1 (HAP1) interacts with the p150Glued subunit of dynactin. *Hum Mol Genet*. 6:2205-2212.

Fishman, R.S. 2007. The Nobel Prize of 1906. *Archives of ophthalmology*. 125:690-694.

Friedman, D.S., and R.D. Vale. 1999. Single-molecule analysis of kinesin motility reveals regulation by the cargo-binding tail domain. *Nat Cell Biol*. 1:293-297.

Friel, C.T., and J. Howard. 2012. Coupling of kinesin ATP turnover to translocation and microtubule regulation: one engine, many machines. *Journal of muscle research and cell motility*. 33:377-383.

Fu, M.M., and E.L. Holzbaur. 2013. JIP1 regulates the directionality of APP axonal transport by coordinating kinesin and dynein motors. *J Cell Biol*.

Furuta, K., A. Furuta, Y.Y. Toyoshima, M. Amino, K. Oiwa, and H. Kojima. 2013. Measuring collective transport by defined numbers of processive and nonprocessive kinesin motors. *Proc Natl Acad Sci U S A*. 110:501-506.

Gilbert, S.P., R.D. Allen, and R.D. Sloboda. 1985. Translocation of vesicles from squid axoplasm on flagellar microtubules. *Nature*. 315:245-248.

Gill, S.R., T.A. Schroer, I. Szilak, E.R. Steuer, M.P. Sheetz, and D.W. Cleveland. 1991. Dynactin, a conserved, ubiquitously expressed component of an activator of vesicle motility mediated by cytoplasmic dynein. *J Cell Biol*. 115:1639-1650.

Glater, E.E., L.J. Megeath, R.S. Stowers, and T.L. Schwarz. 2006. Axonal transport of mitochondria requires milton to recruit kinesin heavy chain and is light chain independent. *J Cell Biol*. 173:545-557.

Gross, S.P. 2004. Hither and yon: a review of bi-directional microtubule-based transport. *Phys Biol*. 1:R1-11.

Hackney, D.D., N. Baek, and A.C. Snyder. 2009. Half-site inhibition of dimeric kinesin head domains by monomeric tail domains. *Biochemistry*. 48:3448-3456.

Hackney, D.D., J.D. Levitt, and J. Suhan. 1992. Kinesin undergoes a 9 S to 6 S conformational transition. *J Biol Chem*. 267:8696-8701.

Hackney, D.D., and M.F. Stock. 2000. Kinesin's IAK tail domain inhibits initial microtubule-stimulated ADP release. *Nat Cell Biol*. 2:257-260.

Hammond, J.W., K. Griffin, G.T. Jih, J. Stuckey, and K.J. Verhey. 2008. Co-operative versus independent transport of different cargoes by kinesin-1. *Traffic*. 9:725-741.

Hendricks, A.G., E.L. Holzbaur, and Y.E. Goldman. 2012. Force measurements on cargoes in living cells reveal collective dynamics of microtubule motors. *Proc Natl Acad Sci U S A*. 109:18447-18452.

Hendricks, A.G., E. Perlson, J.L. Ross, H.W. Schroeder, 3rd, M. Tokito, and E.L. Holzbaur. 2010. Motor Coordination via a Tug-of-War Mechanism Drives Bidirectional Vesicle Transport. *Curr Biol*. 20:697-702.

Hirokawa, N., S. Niwa, and Y. Tanaka. 2010. Molecular motors in neurons: transport mechanisms and roles in brain function, development, and disease. *Neuron*. 68:610-638.

Hirokawa, N., K.K. Pfister, H. Yorifuji, M.C. Wagner, S.T. Brady, and G.S. Bloom. 1989. Submolecular domains of bovine brain kinesin identified by electron microscopy and monoclonal antibody decoration. *Cell*. 56:867-878.

Hirokawa, N., and R. Takemura. 2005. Molecular motors and mechanisms of directional transport in neurons. *Nat Rev Neurosci*. 6:201-214.

Holleran, E.A., L.A. Ligon, M. Tokito, M.C. Stankewich, J.S. Morrow, and E.L.F. Holzbaur. 2001. BetaIII spectrin binds to the Arp1 subunit of dynactin. *J Biol Chem*. 276:36598-36605.

Holzbaur, E.L., J.A. Hammarback, B.M. Paschal, N.G. Kravit, K.K. Pfister, and R.B. Vallee. 1991. Homology of a 150K cytoplasmic dynein-associated polypeptide with the Drosophila gene Glued. *Nature*. 351:579-583.

Hong, Z., Y. Yang, C. Zhang, Y. Niu, K. Li, X. Zhao, and J.J. Liu. 2009. The retromer component SNX6 interacts with dynactin p150(Glued) and mediates endosome-to-TGN transport. *Cell Res*. 19:1334-1349.

Horiuchi, D., R.V. Barkus, A.D. Pilling, A. Gassman, and W.M. Saxton. 2005. APLIP1, a kinesin binding JIP-1/JNK scaffold protein, influences the axonal transport of both vesicles and mitochondria in Drosophila. *Curr Biol*. 15:2137-2141.

Horiuchi, D., C.A. Collins, P. Bhat, R.V. Barkus, A. Diantonio, and W.M. Saxton. 2007. Control of a kinesin-cargo linkage mechanism by JNK pathway kinases. *Curr Biol*. 17:1313-1317.

Howard, J., and A.A. Hyman. 2009. Growth, fluctuation and switching at microtubule plus ends. *Nat Rev Mol Cell Biol*. 10:569-574.

Janke, C., and J.C. Bulinski. 2011. Post-translational regulation of the microtubule cytoskeleton: mechanisms and functions. *Nat Rev Mol Cell Biol*. 12:773-786.

Johansson, M., N. Rocha, W. Zwart, I. Jordens, L. Janssen, C. Kuijl, V.M. Olkkonen, and J. Neefjes. 2007. Activation of endosomal dynein motors by stepwise assembly of Rab7-RILP-p150Glued, ORP1L, and the receptor betalll spectrin. *J Cell Biol*. 176:459-471.

Jonsson, T., J.K. Atwal, S. Steinberg, J. Snaedal, P.V. Jonsson, S. Bjornsson, H. Stefansson, P. Sulem, D. Gudbjartsson, J. Maloney, K. Hoyte, A. Gustafson, Y. Liu, Y. Lu, T. Bhangale, R.R. Graham, J. Huttenlocher, G. Bjornsdottir, O.A. Andreassen, E.G. Jonsson, A. Palotie, T.W. Behrens, O.T. Magnusson, A. Kong, U. Thorsteinsdottir, R.J. Watts, and K. Stefansson. 2012. A mutation in APP protects against Alzheimer's disease and age-related cognitive decline. *Nature*. 488:96-99.

Jordens, I., M. Fernandez-Borja, M. Marsman, S. Dusseljee, L. Janssen, J. Calafat, H. Janssen, R. Wubbolts, and J. Neefjes. 2001. The Rab7 effector protein RILP controls lysosomal transport by inducing the recruitment of dynein-dynactin motors. *Curr Biol*. 11:1680-1685.

Kaan, H.Y., D.D. Hackney, and F. Kozielski. 2011. The structure of the kinesin-1 motor-tail complex reveals the mechanism of autoinhibition. *Science*. 333:883-885.

Kaether, C., P. Skehel, and C.G. Dotti. 2000. Axonal membrane proteins are transported in distinct carriers: a two-color video microscopy study in cultured hippocampal neurons. *Mol Biol Cell*. 11:1213-1224.

Kamal, A., G.B. Stokin, Z. Yang, C.H. Xia, and L.S. Goldstein. 2000. Axonal transport of amyloid precursor protein is mediated by direct binding to the kinesin light chain subunit of kinesin-I. *Neuron*. 28:449-459.

Kanai, Y., Y. Okada, Y. Tanaka, A. Harada, S. Terada, and N. Hirokawa. 2000. KIF5C, a novel neuronal kinesin enriched in motor neurons. *J Neurosci*. 20:6374-6384.

Kang, J.S., J.H. Tian, P.Y. Pan, P. Zald, C. Li, C. Deng, and Z.H. Sheng. 2008. Docking of axonal mitochondria by syntaphilin controls their mobility and affects short-term facilitation. *Cell*. 132:137-148.

Karki, S., and E.L. Holzbaur. 1995. Affinity chromatography demonstrates a direct binding between cytoplasmic dynein and the dynactin complex. *J Biol Chem*. 270:28806-28811.

Kawano, T., M. Araseki, Y. Araki, M. Kinjo, T. Yamamoto, and T. Suzuki. 2012. A Small Peptide Sequence is Sufficient for Initiating Kinesin-1 Activation Through Part of TPR Region of KLC1. *Traffic*.

Klopfenstein, D.R., M. Tomishige, N. Stuurman, and R.D. Vale. 2002. Role of phosphatidylinositol(4,5)bisphosphate organization in membrane transport by the Unc104 kinesin motor. *Cell*. 109:347-358.

Kollman, J.M., A. Merdes, L. Mourey, and D.A. Agard. 2011. Microtubule nucleation by gamma-tubulin complexes. *Nat Rev Mol Cell Biol*. 12:709-721.

Komatsu, M., S. Waguri, T. Chiba, S. Murata, J. Iwata, I. Tanida, T. Ueno, M. Koike, Y. Uchiyama, E. Kominami, and K. Tanaka. 2006. Loss of autophagy in the central nervous system causes neurodegeneration in mice. *Nature*. 441:880-884.

Konishi, Y., and M. Setou. 2009. Tubulin tyrosination navigates the kinesin-1 motor domain to axons. *Nat Neurosci*. 12:559-567.

Koushika, S.P. 2008. "JIP"ing along the axon: the complex roles of JIPs in axonal transport. *Bioessays*. 30:10-14.

Kreutzberg, G.W. 1969. Neuronal dynamics and axonal flow. IV. Blockage of intra-axonal enzyme transport by colchicine. *Proc Natl Acad Sci U S A*. 62:722-728.

Kristensen, O., S. Guenat, I. Dar, N. Allaman-Pillet, A. Abderrahmani, M. Ferdaoussi, R. Roduit, F. Maurer, J.S. Beckmann, J.S. Kastrup, M. Gajhede, and C. Bonny. 2006. A unique set of SH3-SH3 interactions controls IB1 homodimerization. *EMBO J*. 25:785-797.

Lasek, R.J. 1967. Bidirectional transport of radioactively labelled axoplasmic components. *Nature*. 216:1212-1214.

Lawrence, C.J., R.K. Dawe, K.R. Christie, D.W. Cleveland, S.C. Dawson, S.A. Endow, L.S. Goldstein, H.V. Goodson, N. Hirokawa, J. Howard, R.L. Malmberg, J.R. McIntosh, H. Miki, T.J. Mitchison, Y. Okada, A.S. Reddy, W.M. Saxton, M. Schliwa, J.M. Scholey, R.D. Vale, C.E. Walczak, and L. Wordeman. 2004. A standardized kinesin nomenclature. *J Cell Biol*. 167:19-22.

Lazarov, O., G.A. Morfini, E.B. Lee, M.H. Farah, A. Szodorai, S.R. DeBoer, V.E. Koliatsos, S. Kins, V.M. Lee, P.C. Wong, D.L. Price, S.T. Brady, and S.S. Sisodia. 2005. Axonal transport, amyloid precursor protein, kinesin-1, and the processing apparatus: revisited. *J Neurosci*. 25:2386-2395.

Letourneau, P.C. 1982. Analysis of microtubule number and length in cytoskeletons of cultured chick sensory neurons. *J Neurosci*. 2:806-814.

Lubinska, L., S. Niemierko, B. Oderfeld Nowak, and L. Szwarc. 1964. Behaviour of Acetylcholinesterase in Isolated Nerve Segments. *J Neurochem*. 11:493-503.

Ma, B., J.N. Savas, M.S. Yu, B.P. Culver, M.V. Chao, and N. Tanese. 2011. Huntingtin mediates dendritic transport of beta-actin mRNA in rat neurons. *Scientific reports*. 1:140.

MacAskill, A.F., and J.T. Kittler. 2010. Control of mitochondrial transport and localization in neurons. *Trends Cell Biol*. 20:102-112.

Macaskill, A.F., J.E. Rinholm, A.E. Twelvetrees, I.L. Arancibia-Carcamo, J. Muir, A. Fransson, P. Aspenstrom, D. Attwell, and J.T. Kittler. 2009. Miro1 is a calcium sensor for glutamate receptor-dependent localization of mitochondria at synapses. *Neuron*. 61:541-555.

Maday, S., K.E. Wallace, and E.L. Holzbaur. 2012. Autophagosomes initiate distally and mature during transport toward the cell soma in primary neurons. *J Cell Biol*. 196:407-417.

Mandelkow, E.M., R. Schultheiss, R. Rapp, M. Muller, and E. Mandelkow. 1986. On the surface lattice of microtubules: helix starts, protofilament number, seam, and handedness. *J Cell Biol*. 102:1067-1073.

Matsuda, S., T. Yasukawa, Y. Homma, Y. Ito, T. Niikura, T. Hiraki, S. Hirai, S. Ohno, Y. Kita, M. Kawasumi, K. Kouyama, T. Yamamoto, J.M. Kyriakis, and I. Nishimoto. 2001. c-Jun N-terminal kinase (JNK)-interacting protein-1b/islet-brain-1 scaffolds Alzheimer's amyloid precursor protein with JNK. *J Neurosci*. 21:6597-6607.

McGuire, J.R., J. Rong, S.H. Li, and X.J. Li. 2006. Interaction of Huntingtin-associated protein-1 with kinesin light chain: implications in intracellular trafficking in neurons. *J Biol Chem*. 281:3552-3559.

Mitchell, D.J., K.R. Blasier, E.D. Jeffery, M.W. Ross, A.K. Pullikuth, D. Suo, J. Park, W.R. Smiley, K.W. Lo, J. Shabanowitz, C.D. Deppmann, J.C. Trinidad, D.F. Hunt, A.D. Catling, and K.K. Pfister. 2012. Trk activation of the ERK1/2 kinase pathway stimulates intermediate chain phosphorylation and recruits cytoplasmic dynein to signaling endosomes for retrograde axonal transport. *J Neurosci*. 32:15495-15510.

Montagnac, G., J.B. Sibarita, S. Loubery, L. Daviet, M. Romao, G. Raposo, and P. Chavrier. 2009. ARF6 Interacts with JIP4 to control a motor switch mechanism regulating endosome traffic in cytokinesis. *Curr Biol*. 19:184-195.

Morfini, G., G. Pigino, G. Szebenyi, Y. You, S. Pollema, and S.T. Brady. 2006. JNK mediates pathogenic effects of polyglutamine-expanded androgen receptor on fast axonal transport. *Nat Neurosci*. 9:907-916.

Morfini, G.A., Y.M. You, S.L. Pollema, A. Kaminska, K. Liu, K. Yoshioka, B. Bjorkblom, E.T. Coffey, C. Bagnato, D. Han, C.F. Huang, G. Banker, G. Pigino, and S.T. Brady. 2009. Pathogenic huntingtin inhibits fast axonal transport by activating JNK3 and phosphorylating kinesin. *Nat Neurosci*. 12:864-871.

Morris, R.L., and P.J. Hollenbeck. 1993. The regulation of bidirectional mitochondrial transport is coordinated with axonal outgrowth. *J Cell Sci*. 104 (Pt 3):917-927.

Moughamian, A.J., and E.L. Holzbaur. 2012. Dynactin is required for transport initiation from the distal axon. *Neuron*. 74:331-343.

Mudrakola, H.V., K. Zhang, and B. Cui. 2009. Optically resolving individual microtubules in live axons. *Structure*. 17:1433-1441.

Muller, M.J., S. Klumpp, and R. Lipowsky. 2008. Tug-of-war as a cooperative mechanism for bidirectional cargo transport by molecular motors. *Proc Natl Acad Sci U S A*. 105:4609-4614.

Muresan, Z., and V. Muresan. 2005a. c-Jun NH2-terminal kinase-interacting protein-3 facilitates phosphorylation and controls localization of amyloid-beta precursor protein. *J Neurosci*. 25:3741-3751.

Muresan, Z., and V. Muresan. 2005b. Coordinated transport of phosphorylated amyloid-beta precursor protein and c-Jun NH2-terminal kinase-interacting protein-1. *J Cell Biol*. 171:615-625.

Nakata, T., S. Terada, and N. Hirokawa. 1998. Visualization of the dynamics of synaptic vesicle and plasma membrane proteins in living axons. *J Cell Biol*. 140:659-674.

Nihalani, D., H.N. Wong, and L.B. Holzman. 2003. Recruitment of JNK to JIP1 and JNK-dependent JIP1 phosphorylation regulates JNK module dynamics and activation. *J Biol Chem*. 278:28694-28702.

Nikolaev, A., T. McLaughlin, D.D. O'Leary, and M. Tessier-Lavigne. 2009. APP binds DR6 to trigger axon pruning and neuron death via distinct caspases. *Nature*. 457:981-989.

Niu, Y., C. Zhang, Z. Sun, Z. Hong, K. Li, D. Sun, Y. Yang, C. Tian, W. Gong, and J.J. Liu. 2013. PtdIns(4)P regulates retromer-motor interaction to facilitate dynein-cargo dissociation at the trans-Golgi network. *Nat Cell Biol*. 15:417-429.

Okada, Y., H. Yamazaki, Y. Sekine-Aizawa, and N. Hirokawa. 1995. The neuron-specific kinesin superfamily protein KIF1A is a unique monomeric motor for anterograde axonal transport of synaptic vesicle precursors. *Cell*. 81:769-780.

Ori-McKenney, K.M., L.Y. Jan, and Y.N. Jan. 2012. Golgi outposts shape dendrite morphology by functioning as sites of acentrosomal microtubule nucleation in neurons. *Neuron*. 76:921-930.

Pankiv, S., E.A. Alemu, A. Brech, J.A. Bruun, T. Lamark, A. Overvatn, G. Bjorkoy, and T. Johansen. 2010. FYCO1 is a Rab7 effector that binds to LC3 and PI3P to mediate microtubule plus end-directed vesicle transport. *J Cell Biol*. 188:253-269.

Perlson, E., G.B. Jeong, J.L. Ross, R. Dixit, K.E. Wallace, R.G. Kalb, and E.L. Holzbaur. 2009. A switch in retrograde signaling from survival to stress in rapid-onset neurodegeneration. *J Neurosci*. 29:9903-9917.

Rai, A.K., A. Rai, A.J. Ramaiya, R. Jha, and R. Mallik. 2013. Molecular adaptations allow dynein to generate large collective forces inside cells. *Cell*. 152:172-182.

Reis, G.F., G. Yang, L. Szpankowski, C. Weaver, S.B. Shah, J.T. Robinson, T.S. Hays, G. Danuser, and L.S. Goldstein. 2012. Molecular motor function in axonal transport in vivo probed by genetic and computational analysis in Drosophila. *Mol Biol Cell*. 23:1700-1714.

Rocha, N., C. Kuijl, R. van der Kant, L. Janssen, D. Houben, H. Janssen, W. Zwart, and J. Neefjes. 2009. Cholesterol sensor ORP1L contacts the ER protein VAP to control Rab7-RILP-p150 Glued and late endosome positioning. *J Cell Biol*. 185:1209-1225.

Ross, J.L., K. Wallace, H. Shuman, Y.E. Goldman, and E.L. Holzbaur. 2006. Processive bidirectional motion of dynein-dynactin complexes in vitro. *Nat Cell Biol*. 8:562-570.

Sahlender, D.A., R.C. Roberts, S.D. Arden, G. Spudich, M.J. Taylor, J.P. Luzio, J. Kendrick-Jones, and F. Buss. 2005. Optineurin links myosin VI to the Golgi complex and is involved in Golgi organization and exocytosis. *J Cell Biol*. 169:285-295.

Samuels, A.J., L.L. Boyarsky, R.W. Gerard, B. Libet, and M. Brust. 1951. Distribution exchange and migration of phosphate compounds in the nervous system. *The American journal of physiology*. 164:1-15.

Scheinfeld, M.H., R. Roncarati, P. Vito, P.A. Lopez, M. Abdallah, and L. D'Adamio. 2002. Jun NH2-terminal kinase (JNK) interacting protein 1 (JIP1) binds the cytoplasmic domain of the Alzheimer's beta-amyloid precursor protein (APP). *J Biol Chem*. 277:3767-3775.

Schroer, T.A. 2004. Dynactin. *Annu Rev Cell Dev Biol*. 20:759-779.

Schroer, T.A., and M.P. Sheetz. 1991. Two activators of microtubule-based vesicle transport. *J Cell Biol*. 115:1309-1318.

Scott, D.A., U. Das, Y. Tang, and S. Roy. 2011. Mechanistic logic underlying the axonal transport of cytosolic proteins. *Neuron*. 70:441-454.

Sheng, Z.H., and Q. Cai. 2012. Mitochondrial transport in neurons: impact on synaptic homeostasis and neurodegeneration. *Nat Rev Neurosci*. 13:77-93.

Soppina, V., A.K. Rai, A.J. Ramaiya, P. Barak, and R. Mallik. 2009. Tug-of-war between dissimilar teams of microtubule motors regulates transport and fission of endosomes. *Proc Natl Acad Sci U S A*. 106:19381-19386.

Stepanova, T., J. Slemmer, C.C. Hoogenraad, G. Lansbergen, B. Dortland, C.I. De Zeeuw, F. Grosveld, G. van Cappellen, A. Akhmanova, and N. Galjart. 2003. Visualization of microtubule growth in cultured neurons via the use of EB3-GFP (end-binding protein 3-green fluorescent protein). *J Neurosci*. 23:2655-2664.

Stiess, M., N. Maghelli, L.C. Kapitein, S. Gomis-Ruth, M. Wilsch-Brauninger, C.C. Hoogenraad, I.M. Tolic-Norrelykke, and F. Bradke. 2010. Axon extension occurs independently of centrosomal microtubule nucleation. *Science*. 327:704-707.

Stock, M.F., J. Guerrero, B. Cobb, C.T. Eggers, T.G. Huang, X. Li, and D.D. Hackney. 1999. Formation of the compact confomer of kinesin requires a COOH-terminal heavy chain domain and inhibits microtubule-stimulated ATPase activity. *J Biol Chem*. 274:14617-14623.

Stokin, G.B., C. Lillo, T.L. Falzone, R.G. Brusch, E. Rockenstein, S.L. Mount, R. Raman, P. Davies, E. Masliah, D.S. Williams, and L.S. Goldstein. 2005. Axonopathy and transport deficits early in the pathogenesis of Alzheimer's disease. *Science*. 307:1282-1288.

Sun, F., C. Zhu, R. Dixit, and V. Cavalli. 2011. Sunday Driver/JIP3 binds kinesin heavy chain directly and enhances its motility. *EMBO J*. 30:3416-3429.

Szpankowski, L., S.E. Encalada, and L.S. Goldstein. 2012. Subpixel colocalization reveals amyloid precursor protein-dependent kinesin-1 and dynein association with axonal vesicles. *Proc Natl Acad Sci U S A*. 109:8582-8587.

Tumbarello, D.A., B.J. Waxse, S.D. Arden, N.A. Bright, J. Kendrick-Jones, and F. Buss. 2012. Autophagy receptors link myosin VI to autophagosomes to mediate Tom1-dependent autophagosome maturation and fusion with the lysosome. *Nat Cell Biol*. 14:1024-1035.

Twelvetrees, A., A.G. Hendricks, and E.L. Holzbaur. 2012. SnapShot: axonal transport. *Cell*. 149:950-950 e951.

Twelvetrees, A.E., E.Y. Yuen, I.L. Arancibia-Carcamo, A.F. MacAskill, P. Rostaing, M.J. Lumb, S. Humbert, A. Triller, F. Saudou, Z. Yan, and J.T. Kittler. 2010. Delivery of GABAARs to synapses is mediated by HAP1-KIF5 and disrupted by mutant huntingtin. *Neuron*. 65:53-65.

Tytell, M., M.M. Black, J.A. Garner, and R.J. Lasek. 1981. Axonal transport: each major rate component reflects the movement of distinct macromolecular complexes. *Science*. 214:179-181.

Vagnoni, A., E.B. Glennon, M.S. Perkinton, E.H. Gray, W. Noble, and C.C. Miller. 2013. Loss of c-Jun N-terminal kinase-interacting protein-1 does not affect axonal transport of the amyloid precursor protein or Abeta production. *Hum Mol Genet*.

Vagnoni, A., L. Rodriguez, C. Manser, K.J. De Vos, and C.C. Miller. 2011. Phosphorylation of kinesin light chain 1 at serine 460 modulates binding and trafficking of calsyntenin-1. *J Cell Sci*. 124:1032-1042.

Vale, R.D., T.S. Reese, and M.P. Sheetz. 1985a. Identification of a novel force-generating protein, kinesin, involved in microtubule-based motility. *Cell*. 42:39-50.

Vale, R.D., B.J. Schnapp, T. Mitchison, E. Steuer, T.S. Reese, and M.P. Sheetz. 1985b. Different axoplasmic proteins generate movement in opposite directions along microtubules in vitro. *Cell*. 43:623-632.

Vale, R.D., B.J. Schnapp, T.S. Reese, and M.P. Sheetz. 1985c. Movement of organelles along filaments dissociated from the axoplasm of the squid giant axon. *Cell*. 40:449-454.

Vale, R.D., B.J. Schnapp, T.S. Reese, and M.P. Sheetz. 1985d. Organelle, bead, and microtubule translocations promoted by soluble factors from the squid giant axon. *Cell*. 40:559-569.

van Niekerk, E.A., D.E. Willis, J.H. Chang, K. Reumann, T. Heise, and J.L. Twiss. 2007. Sumoylation in axons triggers retrograde transport of the RNA-binding protein La. *Proc Natl Acad Sci U S A*. 104:12913-12918.

van Spronsen, M., M. Mikhaylova, J. Lipka, M.A. Schlager, D.J. van den Heuvel, M. Kuijpers, P.S. Wulf, N. Keijzer, J. Demmers, L.C. Kapitein, D. Jaarsma, H.C. Gerritsen, A. Akhmanova, and C.C. Hoogenraad. 2013. TRAK/Milton motor-adaptor proteins steer mitochondrial trafficking to axons and dendrites. *Neuron*. 77:485-502.

Verhey, K.J., and J.W. Hammond. 2009. Traffic control: regulation of kinesin motors. *Nat Rev Mol Cell Biol*. 10:765-777.

Verhey, K.J., D.L. Lizotte, T. Abramson, L. Barenboim, B.J. Schnapp, and T.A. Rapoport. 1998. Light chain-dependent regulation of Kinesin's interaction with microtubules. *J Cell Biol*. 143:1053-1066.

Verhey, K.J., D. Meyer, R. Deehan, J. Blenis, B.J. Schnapp, T.A. Rapoport, and B. Margolis. 2001. Cargo of kinesin identified as JIP scaffolding proteins and associated signaling molecules. *J Cell Biol*. 152:959-970.

Vershinin, M., B.C. Carter, D.S. Razafsky, S.J. King, and S.P. Gross. 2007. Multiple-motor based transport and its regulation by Tau. *Proc Natl Acad Sci U S A*. 104:87-92.

von Muhlinen, N., M. Akutsu, B.J. Ravenhill, A. Foeglein, S. Bloor, T.J. Rutherford, S.M. Freund, D. Komander, and F. Randow. 2012. LC3C, bound selectively by a noncanonical LIR motif in NDP52, is required for antibacterial autophagy. *Mol Cell*. 48:329-342.

Wang, X., and T.L. Schwarz. 2009. The mechanism of Ca2+ -dependent regulation of kinesin-mediated mitochondrial motility. *Cell*. 136:163-174.

Wassmer, T., N. Attar, M. Harterink, J.R. van Weering, C.J. Traer, J. Oakley, B. Goud, D.J. Stephens, P. Verkade, H.C. Korswagen, and P.J. Cullen. 2009. The retromer coat complex coordinates endosomal sorting and dynein-mediated transport, with carrier recognition by the trans-Golgi network. *Dev Cell*. 17:110-122.

Wasteneys, G.O., and J.C. Ambrose. 2009. Spatial organization of plant cortical microtubules: close encounters of the 2D kind. *Trends Cell Biol*. 19:62-71.

Waterman-Storer, C.M., S. Karki, and E.L. Holzbaur. 1995. The p150Glued component of the dynactin complex binds to both microtubules and the actin-related protein centractin (Arp-1). *Proc Natl Acad Sci U S A*. 92:1634-1638.

Watson, P., R. Forster, K.J. Palmer, R. Pepperkok, and D.J. Stephens. 2005. Coupling of ER exit to microtubules through direct interaction of COPII with dynactin. *Nat Cell Biol*. 7:48-55.

Weaver, C., C. Leidel, L. Szpankowski, N.M. Farley, G.T. Shubeita, and L.S. Goldstein. 2013. Endogenous GSK-3/shaggy regulates bidirectional axonal transport of the amyloid precursor protein. *Traffic*. 14:295-308.

Weiss, P., and H.B. Hiscoe. 1948. Experiments on the mechanism of nerve growth. *The Journal of experimental zoology*. 107:315-395.

Welte, M.A. 2004. Bidirectional transport along microtubules. *Curr Biol*. 14:R525-537.

Whitmarsh, A.J. 2006. The JIP family of MAPK scaffold proteins. *Bioessays*. 34:828-832.

Wolfe, D.M., J.H. Lee, A. Kumar, S. Lee, S.J. Orenstein, and R.A. Nixon. 2013. Autophagy failure in Alzheimer's disease and the role of defective lysosomal acidification. *Eur J Neurosci*. 37:1949-1961.

Wong, Y.L., K.A. Dietrich, N. Naber, R. Cooke, and S.E. Rice. 2009. The Kinesin-1 tail conformationally restricts the nucleotide pocket. *Biophysical journal*. 96:2799-2807.

Yang, G.Z., M. Yang, Y. Lim, J.J. Lu, T.H. Wang, J.G. Qi, J.H. Zhong, and X.F. Zhou. 2012. Huntingtin associated protein 1 regulates trafficking of the amyloid precursor protein and modulates amyloid beta levels in neurons. *J Neurochem*. 122:1010-1022.

Yorimitsu, T., and D.J. Klionsky. 2005. Autophagy: molecular machinery for self-eating. *Cell death and differentiation*. 12 Suppl 2:1542-1552.

Zala, D., M.V. Hinckelmann, H. Yu, M.M. Lyra da Cunha, G. Liot, F.P. Cordelieres, S. Marco, and F. Saudou. 2013. Vesicular glycolysis provides on-board energy for fast axonal transport. *Cell*. 152:479-491.

Zelena, J. 1970. Ribosome-like particles in myelinated axons of the rat. *Brain research*. 24:359-363.

Zelena, J., L. Lubinska, and E. Gutmann. 1968. Accumulation of organelles at the ends of interrupted axons. *Z Zellforsch Mikrosk Anat*. 91:200-219.